2019-01-11

Viscosity of Characterized Visbroken Heavy Oils

Marquez Socorro, Andres Alfonso

UNIVERSITY OF CALGARY

Viscosity of Characterized Visbroken Heavy Oils

by

Andres Alfonso Marquez Socorro

A THESIS

SUBMITTED TO THE FACULTY OF GRADUATE STUDIES

IN PARTIAL FULFILMENT OF THE REQUIREMENTS FOR THE

DEGREE OF MASTER OF SCIENCE

GRADUATE PROGRAM IN CHEMICAL ENGINEERING

CALGARY, ALBERTA

JANUARY, 2019

Abstract

The Expanded Fluid viscosity model was extended to visbroken heavy oils characterized into the following fractions: distillates and the residue SARA fractions (saturates, aromatics, resins and asphaltenes). To do so, a Western Canadian bitumen was visbroken at five different reaction conditions (temperature and residence time). Densities and viscosities were measured for each fraction and used to develop new property correlations based on conversion. The correlated fraction properties were then recombined to obtain the whole oil viscosity. The model matched the density and viscosity of all the visbroken oils in this dataset with average absolute deviations of 1.1 kg/m^3 and 8%, respectively. The model successfully predicted the properties of a visbroken product from a chemically similar bitumen feedstock but not for those from a chemically dissimilar oil. This method is suitable for implementation in process simulators but is only recommended for whole oil feeds chemically similar to Western Canadian bitumen.

Acknowledgements

This journey gave me the opportunity to meet and work with many remarkable people. First I would like to make a special acknowledgement to my supervisor, Dr. Harvey Yarranton, for the opportunity to be part of this amazing team. His teachings and guidance have significantly contributed in shaping the person I am today. You have my uttermost respect and admiration.

I would like to extent my gratitude to Glen Hay and Shawn Taylor for all the time and feedback provided to guide this project in the right direction. I also want to recognize Florian Schoeggl and Elaine Baydak for all their support and teachings.

I want to extend my gratitude to all the members of the HOPP research group, particularly to Franklin, John, Sandra, Yulman, Adel, Nicolay, Daniela, Jairo, Yoshi, Javier and Emilio. Other people that also deserved a place in this acknowledgement are Camilla, Pradeep, Diego, Karen and Anderson. Thank you for all the good times and all you taught me. Thanks to the NSERC Industrial Research Chair in Heavy Oil Properties and Processing, Schlumberger, CNRL, Suncor, Nexen, VMG and Ecopetrol for the funding of this project. I would also like to thank the Department of Chemical and Petroleum Engineering for their support.

Finally, I would like to thank my family for making me the person I am today. Special thanks to my sister Andrea for all her support and care. Undoubtedly I would not be here without them.

Dedication

To my family, in particular my aunts, uncles and sister.

To Fernando and Esperanza.

Table of Contents

Abstract 1
Acknowledgements 2
Dedication 3
Table of Contents 4
List of Tables 6
List of Figures and Illustrations 11
List of Symbols, Abbreviations and Nomenclature 14

Chapter 1: Introduction 18
1.1. Overview 18
1.2. Objectives 20
1.3. Outline 21

Chapter 2: Literature Review 22
2.1 Crude Oil Definition 22
2.2 Crude Oil Chemistry 22
2.3 Crude Oil Characterization 24
2.4 Crude Oil Viscosity Modeling 28
2.5 Heavy Oil Upgrading 34
2.5.1 Carbon Rejection 34
2.5.2 Hydrogen Addition Processes 38
2.6 Effect of Visbreaking on Crude Oils 39

Chapter 3: Experimental Methods 44
3.1 Materials 44
3.2 Visbreaking Lab-Scale Plant 45
3.2.1 Apparatus 45
3.2.2 Experimental Procedure 48
3.3 Fractionation Methods 49
3.3.1 Spinning Band Distillation (SBD) 49
3.3.2 Simulated Distillation (SimDist) 51
3.3.3 SARA Fractionation 51
3.4 Property Measurements 54
3.4.1 Viscosity and Density from a Capillary Viscometer Apparatus 54
3.4.2. Viscosity from Cone and Plate Rheometer 56
3.4.3. Density 57
3.4.4. Molecular Weight 57
3.4.5. Micro Carbon Residue 59

Chapter 4: Methodology 60
4.1. Oil Characterization 60
4.2. Viscosity and Density Prediction 61
4.2.1. Expanded Fluid (EF) Viscosity Model 61
4.2.2. Density 65

4.3. Data Processing 66

Chapter 5: Results and Discussion 70
5.1. Effect of Visbreaking on Oil Composition and Properties 70
5.1.1. Conversion and Oil Composition 70
5.1.2. Physical Properties 74
5.2. Density and Viscosity Correlations for Oil Fractions 81
5.2.1. Density 81
5.2.2. Viscosity 86
5.2.3. Model Evaluation with Development Dataset 92
5.2.4. Model Sensitivity 100
5.3. Model Evaluation with Test Dataset 103
5.3.1. Similar Oil (WC-B-A4) 103
5.3.2. Dissimilar Oil (ME-VR-A1) 111

Chapter 6: Conclusions and Recommendations 120
6.1. Conclusions 120
6.2. Recommendations 122

References 124

Appendix A: Whole Oil Data 135

Appendix B: Distillation Data 146

Appendix C: Measured Properties of Each Fraction 156

Appendix D: Density and Viscosity Parameters of Oil Fractions 165

List of Tables

Table 2.1 Crude oil classification 22

Table 3.1 Samples used in this project.....45

Table 4.1 Summary of what data are available for each fraction. 69

Table 5.1 Reaction conditions and conversions of the Development Dataset. 71

Table 5.2 Composition of the feedstock and visbroken products in the Development Dataset.....73

Table 5.3 EF model parameters for distillates from the Development Dataset. 88

Table 5.4 Average absolute relative deviations in the model for the residue viscosities from the Development Dataset.. 92

Table 5.5 Average absolute deviations (AAD) in SAR recombinations for maltene densities.....93

Table 5.6 Average absolute relative deviations in the model for the maltenes viscosity.. 94

Table 5.7 Average absolute deviations (AAD) in component recombination for whole oil density. 96

Table 5.8 Average absolute relative deviations in the model for the whole oil viscosity. 100

Table 5.9 Sensitivity of the predicted whole oil density to model input errors…….. 101

Table 5.10 Average absolute relative deviations in the model for the whole oil viscosity using fitted densities. 102

Table 5.11 Average absolute relative deviations in the model for the whole oil viscosity using predicted densities…… 102

Table 5.12 Comparison between the feedstocks for the Development Dataset (WC-B-A3(2) and Test Dataset (WC-B-A4 and ME-VR-A1).. 103

Table 5.13 Distillate content, specific gravity and viscosity of the WC-B-A4 feedstock and visbroken product.....104

Table 5.14 SARA content of the residues from the WC-B-A4 feedstock and visbroken product. 104

Table 5.15 Specific gravity of the distillates and saturate, aromatic, and resin fractions from the WC-B-A4 feedstock and visbroken product 105

Table 5.16 Measured viscosity of the saturate, aromatic, and resin fractions and distillation residue from the WC-B-A4 feedstock and visbroken product.....106

Table 5.17 Properties of ME-VR-A1 and its visbroken products.....112

Table 5.18 SARA contents of ME-VR-A1 and its visbroken products.....113

Table 5.19 Specific gravity of ME-VR-A1 feedstock and its visbroken products.....113

Table 5.20 Viscosity of the saturates, aromatics, and resins from the ME-VR-A1 feedstock and its visbroken products 114

Table A.1 Whole oil density and viscosity for WC-B-A3(1).....135

Table A.2 Whole oil density and viscosity for WC-B-A3(2).....136

Table A.3 Whole oil density and viscosity for WC-B-A3(1)-VIS5.1. 137

Table A.4 Whole oil density and viscosity for WC-B-A3(2)-VIS4.9. 138

Table A.5 Whole oil density and viscosity for WC-B-A3(2)-VIS8.1. 139

Table A.6 Whole oil density and viscosity for WC-B-A3(2)-VIS19.3. 140

Table A.7 Whole oil density and viscosity for WC-B-A3(2)-VIS38.1. 141

Table A.8 Whole oil density and viscosity for WC-B-A4.....142

Table A.9 Whole oil density and viscosity for WC-B-A4-VIS1 142

Table A.10 Whole residue density and viscosity for ME-VR-A1.....143

Table A.11 Whole residue density and viscosity for ME-VR-A1-VIS12.5. 144

Table A.12 Whole residue density and viscosity for ME-VR-A1-VIS18.8. 145

Table B.1 Spinning Band Distillation data for WC-B-A3(1) feedstock.....146

Table B.2 Spinning Band Distillation data of WC-B-A3(2) feedstock. 147

Table B.3 Spinning Band Distillation data of WC-B-A3(1)-VIS5.1.....147

Table B.4 Spinning Band Distillation data of WC-B-A3(2)-VIS4.9.....148

Table B.5 Spinning Band Distillation data of WC-B-A3(2)-VIS8.1.....149

Table B.6 Spinning Band Distillation data of WC-B-A3(2)-VIS19.3.....150

Table B.7 Spinning Band Distillation data of WC-B-A3(2)-VIS38.1. 151

Table B.8 Spinning Band Distillation data of WC-B-A4. 152

Table B.9 Spinning Band Distillation data of WC-B-A4-VIS1. 152

Table B.10 Extended Simulated Distillation assays for WC-B-A3 and its visbroken products. 153

Table B.11 Extended Simulated Distillation assays for WC-B-A4 and its visbroken product. 154

Table B.12 Extended Simulated Distillation assays for ME-VR-A1 and its visbroken products. 155

Table C.1 Distillate densities of the WC-B-A3 feed and products for the Development Dataset. 156

Table C.2 Distillate viscosities of the WC-B-A3 feed. 156

Table C.3 Residue viscosities of the WC-B-A3 feed and products for the Development Dataset. 157

Table C.4 Maltene densities of the WC-B-A3 feed and products for the Development Dataset. 157

Table C.5 Maltene viscosities of the WC-B-A3 feed and products for the Development Dataset. 157

Table C.6 Saturate densities of the WC-B-A3 feed and products for the Development Dataset. 158

Table C.7 Saturate viscosities of the WC-B-A3 feed and products for the Development Dataset. 158

Table C.8 Aromatic densities of the WC-B-A3 feed and products for the Development Dataset. 158

Table C.9 Aromatic viscosities of the WC-B-A3 feed and products for the Development Dataset. 159

Table C.10 Resin viscosities of the WC-B-A3 feed and products for the Development Dataset. 159

Table C.11 Distillate densities of the WC-B-A4 feedstock and product for the Test Dataset. 159

Table C.12 Residue viscosities of the WC-B-A4 feedstock and product for the Test Dataset.....160

Table C.13 Maltene densities of the WC-B-A4 feedstock and product for the Test Dataset.....160

Table C.14 Maltene viscosities of the WC-B-A4 feedstock and product for the Test Dataset.....160

Table C.15 Saturate densities of the WC-B-A4 feedstock and product for the Test Dataset.....161

Table C.16 Saturate viscosities of the WC-B-A4 feedstock and product for the Test Dataset.....161

Table C.17 Aromatic densities of the WC-B-A4 feedstock and product for the Test Dataset.....161

Table C.18 Aromatic viscosities of the WC-B-A4 feedstock and product for the Test Dataset.....162

Table C.19 Resin viscosities of the WC-B-A4 feedstock and product for the Test Dataset. 162

Table C.20 Maltene densities of the ME-VR-A1 feedstock and products for the Test Dataset.....162

Table C.21 Maltene viscosities of the ME-VR-A1 feedstock and products for the Test Dataset.....163

Table C.22 Saturate densities of the ME-VR-A1 feedstock and products for the Test Dataset.....163

Table C.23 Saturate viscosities of the ME-VR-A1 feedstock and products for the Test Dataset.....163

Table C.24 Aromatic densities of the ME-VR-A1 feedstock and products for the Test Dataset.....164

Table C.25 Aromatic viscosities of the ME-VR-A1 feedstock and products for the Test Dataset.....164

Table C.26 Resin viscosities of the ME-VR-A1 feedstock and products for the Test Dataset.....164

Table D.1 Distillate parameters of the WC-B-A3 feed and products for the Development Dataset.....165

Table D.2 Saturate parameters of the WC-B-A3 feed and products for the Development Dataset.....165

Table D.3 Aromatic parameters of the WC-B-A3 feed and products for Development Dataset.....166

Table D.4 Resin parameters of the WC-B-A3 feed and products for Development Dataset.....166

Table D.5 Asphaltene parameters of the WC-B-A3 feed and products for the Development Dataset.....166

Table D.6 Distillate parameters of the WC-B-A4 feed and products for the Test Dataset....167

Table D.7 Saturate parameters of the WC-B-A4 feed and products for the Test Dataset. 167

Table D.8 Aromatic parameters of the WC-B-A4 feed and products for the Test Dataset. ..167

Table D.9 Resin parameters of the WC-B-A4 feed and products for the Test Dataset. 168

Table D.10 Asphaltene parameters of the WC-B-A4 feed and products for the Test Dataset.....168

Table D.11 Saturate parameters of the ME-VR-A1 feed and products for the Test Dataset.168

Table D.12 Aromatic parameters of the ME-VR-A1 feed and products for the Test Dataset.....169

Table D.13 Resin parameters of the ME-VR-A1 feed and products for the Test Dataset.....169

Table D.14 Asphaltene parameters of the ME-VR-A1 feed and products for the Test Dataset.....169

List of Figures and Illustrations

Figure 2.1 Relationship between carbon number, boiling point, and structure of chemical compounds in crude oil. 24

Figure 2.2 Comparison between TBP and SimDist for a Western Canadian bitumen (WC-B-A3). 27

Figure 2.3 Coil visbreaking process schematic. 36

Figure 2.4 Soaker visbreaking process schematic. 36

Figure 2.5 Thermal conversion reaction paths of SARA fractions 41

Figure 3.1 Schematic of the in-house visbreaking lab scale plant. 46

Figure 3.2 Schematic of spinning band distillation apparatus 50

Figure 3.3 Capillary viscometer apparatus schematic 56

Figure 3.4 Cone and Plate Rheometer schematic. 57

Figure 4.1 Oil fractions used in characterization methodology. 61

Figure 4.2 Methodology to obtain density and EF parameters for each fraction. 66

Figure 5.1 Comparison between distillation assays of both Development Dataset feeds. 70

Figure 5.2 Comparison between SBD and ASTM 7169 for: a) WC-B-A3 feedstock; b) WC-B-A3(2)-VIS19.3 visbroken sample. 71

Figure 5.3 Extended SimDist (ASTM D7169) of the feedstock and visbroken products in the Development Dataset. 72

Figure 5.4 Effect of conversion on the Development Dataset feedstock and visbroken product composition: a) distillate content in whole oil; b) saturate, aromatic, resin, and asphaltene contents in the residue. 74

Figure 5.5 Effect of conversion on the properties of feedstock and visbroken products from the Development Dataset: a) relative viscosity; b) specific gravity; c) molecular weight; d) microcarbon residue. 76

Figure 5.6 Effect of conversion on the specific gravity of distillates from the Development Dataset. 77

Figure 5.7 Effect of conversion on the properties of the saturates from the Development Dataset: a) specific gravity; b) viscosity 78

Figure 5.8 Effect of conversion on the properties of the aromatics from the Development Dataset: a) specific gravity; b) viscosity 79

Figure 5.9 Effect of conversion on the properties of the resins from the Development Dataset: a) specific gravity; b) viscosity 80

Figure 5.10 Effect of conversion on the specific gravity of the asphaltenes from the Development Dataset 81

Figure 5.11 Effect of conversion on normalized distillate density parameters from the Development Dataset: a) reference density; b) slope.....83

Figure 5.12 Effect of conversion on normalized saturate density parameters from the Development Dataset: a) reference density; b) slope.....84

Figure 5.13 Effect of conversion on normalized aromatic and resin density parameters from the Development Dataset: a) reference density; b) slope.....85

Figure 5.14 Effect of conversion on normalized asphaltene density parameters from the Development Dataset: a) reference density; b) slope.....86

Figure 5.15 Effect of conversion on the viscosity parameters of the feedstock and visbroken products from the Development Dataset: a) C_2, b) $\rho_s°$; c) C_3. 87

Figure 5.16 Effect of conversion on the EF model parameters for saturates from the Development Dataset: a) C_2; b) $\rho_s°$.....89

Figure 5.17 Effect of conversion on the EF model parameters for aromatics and resins from the Development Dataset: a) C_2; b) $\rho_s°$.....90

Figure 5.18 Asphaltenes EF parameters estimation approach. 91

Figure 5.19 Asphaltenes EF parameters against conversion. 91

Figure 5.20 Measured and modeled density of maltenes versus temperature at atmospheric pressure: a) WC-B-A3(1)-VIS5.1; b) WC-B-A3(2)VIS38.1. 93

Figure 5.21 Measured and modeled viscosity of maltenes versus temperature at atmospheric pressure: a) WC-B-A3(2); b) WC-B-A3(1)-VIS5.1; c) WC-B-A3(2)VIS38.1. 95

Figure 5.22 Measured and modeled density of whole oils versus temperature at atmospheric pressure: a) WC-B-A3(1)-VIS5.1; b) WC-B-A3(2)-VIS38.1. 96

Figure 5.23 Measured and modeled viscosity of whole oils versus temperature at atmospheric pressure: a) WC-B-A3(1); b) WC-B-A3(1)-VIS5.1; c) WC-B-A3(2)VIS38.1 98

Figure 5.24 Distillates-asphaltenes BIP increments for the visbroken samples in the Development Dataset. 99

Figure 5.25 Correlated whole oil viscosity for WC-B-A3(1)-VIS5.1 (a) and WC-B-A3(2)-VIS38.1 (b) using fitted densities 100

Figure 5.26 Extended SimDist (ASTM D7169) of the WC-B-A4 feedstock and visbroken product. 104

Figure 5.27 Measured and modeled atmospheric pressure viscosity of maltenes from: a) WC-B-A4; b) WC-B-A4-VIS1 108

Figure 5.28 Measured and modeled atmospheric pressure viscosity of whole oils: a) WC-B-A4; b) WC-B-A4-VIS1 108

Figure 5.29 Measured and predicted atmospheric pressure properties of WC-B-B4-VIS1 maltenes: a) density; b) viscosity. 109

Figure 5.30 Measured and predicted atmospheric pressure viscosity of WC-B-B4-VIS1 residue. 110

Figure 5.31 Measured and predicted atmospheric pressure properties of WC-B-B4-VIS1 whole oils: a) density; b) viscosity. 110

Figure 5.32 Extended SimDist (ASTM D7169) of dissimilar oil test dataset 112

Figure 5.33 Measured and modeled atmospheric pressure viscosity of maltenes from: a) ME-VR-A1; b) ME-VR-A1-VIS12.5; c) ME-VR-A1-VIS18.8 116

Figure 5.34 Measured and predicted atmospheric pressure properties of WC-VR-A1-VIS12.5 maltenes: a) density; b) viscosity. 118

Figure 5.35 Measured and predicted atmospheric pressure properties of WC-VR-A1-VIS18.8 maltenes: a) density; b) viscosity. 118

Figure 5.36 Measured and predicted properties of WC-B-B4-VIS12.5 whole oil at 2.5 MPa. 119

List of Symbols, Abbreviations and Nomenclature

Symbols

A_0	Yaws viscosity fluid specific parameters
B	Absorption energy of the molecular collisions
B_0	Yaws viscosity fluid specific parameters
b	Temperature dependency for density
b_1	Walther model fluid specific parameters
b_2	Walther model fluid specific parameters
c	Walther model fluid specific parameters
C_0	Yaws viscosity fluid specific parameters
c_2	Viscosity response to expansion (EF fluid specific parameter)
c_3	Viscosity response to pressure (EF fluid specific parameter)
C_n	Normal alkane with carbon number n
D_0	Yaws viscosity fluid specific parameters
dv_x/dy	Shear rate
H/C	Hydrogen to carbon ratio
K	Calibration constant
M	Molecular weight
P	Pressure
P_0	Atmospheric pressure
ΔP	Differential pressure
ρ_s^o	Compressed state density (EF fluid specific parameter)

Q	Flow rate
T	Temperature
τ_{yx}	Shear stress
V	Volume
V_0	Intrinsic volume
ΔV	Voltage differential
v_x	Velocity in x coordinate
w	Weight fraction
X	Conversion

Abbreviations

AAD	Average absolute deviation
AARD	Average absolute relative deviation
AET	Atmospheric equivalent temperature
ASTM	American Society for Testing Materials
API	American Petroleum Institute
B	Bitumen
BIP	Binary interaction parameter
CCR	Conradson carbon residue
EF	Expanded fluid model
GC	Gas chromatography
LPG	Liquefied petroleum gas
MCR	Micro carbon residue
ME	Middle East

OF	Objective function
SAFT	Statistical associating fluid theory
SAGD	Steam-assisted gravity drainage
SAR	Saturates, aromatics and resins
SARA	Saturates, aromatics, resins and asphaltenes
SBD	Spinning band distillation
SG	Specific gravity
SimDist	Simulated distillation
TBP	True boiling point
TI	Toluene insolubles
VPO	Vapour pressure osmometer
VR	Vacuum residue
WC	Western Canada

Greek letter

$\propto$	EF binary interaction parameter
ϑ	Kinematic viscosity
ρ	Density
μ	Dynamic viscosity

Subscripts

0	Feedstock property
37.7	Property at 37.7 °C
Asph	Asphaltenes
B	Boiling point

Dist	Distillates
f	Residual property
G	Dilute gas property
i	Component
j	Component
me	Measured
pr	Predicted
ref	Reference condition (0 °C)

Chapter 1: Introduction

1.1. Overview

Crude oils are the most commonly used source of energy, particularly as the source of liquid fuels. The worldwide demand for crude oil is continuously increasing but the supply of conventional crude oil is limited (BP, 2018). The average quality of the crude oil supply has decreased in recent years with a progressive decrease in API gravity and viscosity (Speight, 2007). Therefore, an efficient exploitation of the available reserves of lower API heavy oils, extra heavy oils, and bitumens will likely be required to meet the increasing energy demand in the long term. One of the defining characteristics of these fluids is their high viscosity. By definition (Gray, 1994), the viscosity of a heavy oil is between 100 and 10,000 mPa·s and bitumen viscosity exceeds 10,000 mPa·s and can be as high as 1 million mPa·s at atmospheric conditions.

The high viscosity of these fluids presents considerable challenges for recovery, transport and refining operations. To be accepted by pipeline carriers, crude oils must achieve density and viscosity specifications. For example, Enbridge's pipeline specifications are a minimum API gravity of 19° and a maximum viscosity of 329 mPa.s at a delivery temperature from 5 to 38°C (Gray, 2015). The two main methods to achieve these specifications in heavy oils and bitumen systems are dilution and upgrading. Dilution involves blending these materials with solvents such as natural gas condensate, producing a mixture with an overall lower viscosity. The capital costs for dilution related facilities are relatively low; however, the volume of diluent reduces the pipeline capacity for crude oil by 25 to 35% and a return pipeline for the diluent is required (De Klerk *et al.,* 2014).

Field upgrading usually involves visbreaking. Visbreaking is the mild liquid-phase thermal cracking of a heavy oil or bitumen, resulting in an increased yield of more valuable middle distillates and a viscosity decrease of the residue. Viscosity reduction and conversion of heavy fractions to distillates increases with increasing process severity (residence time and temperature) up to the point where coke forms. Coke formation occurs at higher severity when the residue becomes unstable (asphaltene material becomes insoluble in the medium), followed by asphaltene

flocculation and ultimately coke formation (Joshi *et al.,* 2008). To design and optimize a visbreaking process, it is necessary to predict the composition and viscosity of the reacted fluid and this prediction requires oil characterization, visbreaking reaction modeling and viscosity modeling.

Oil characterization involves dividing the oil into a number of components and pseudo-components that represent its distribution of properties. These characterizations are typically based on gas chromatography or distillation assays. Gas chromatography provides a molecular weight distribution for the pseudo-components and correlations are used to calculate other properties. However, GC does not allow the direct measurement of the pseudo-component viscosities. Distillation assays provide a boiling point distribution for the pseudo-components and correlations are again applied to obtain other properties. In addition, physical cuts can be obtained and their properties measured directly, including viscosity. However, distillation assays are limited to a maximum temperature of 300 °C to avoid thermally cracking the sample. For heavy oils and bitumens the distillation residue is significant and can be up to 75 wt% of the oil (Riazi, 2005). Hence, this residue must be characterized by another method.

One of the most common methods to assay and characterize heavy oils and residues is SARA fractionation; that is the separation of the sample into four solubility and adsorption fractions: saturates, aromatics, resins and asphaltenes (known as SARA). Saturates include paraffins and naphthenes. Aromatics, resins and asphaltenes are a continuum of aromatic and polynuclear aromatic species of increasing density, molecular weight and heteroatom content. By grouping the residue components into these chemically similar fractions, variations in physical properties during visbreaking reactions become easier to track.

Once the feed is characterized, a reaction model is used to predict the distribution of the pseudo-components in the product. Several lumped kinetic models are available in the literature based on either boiling point fractions or SARA (Singh *et al.,* 2012). A more recent approach taken by process simulation tools such as Symmetry (Hay, 2018) is to assign a series of representative molecules into the pseudo-components determined from both TBP and SARA assays. A reaction

scheme is applied to these molecules to obtain a distribution of molecules in the visbroken product. Then the product TBP and SARA distributions are calculated based on the properties of the product molecules. This characterization methodology provides a realistic number of fractions where physical properties can be measured and remains consistent with current process simulation characterization trends.

The final step is to model the viscosity of the products. There are currently no generalized models to predict the viscosity of visbroken products (Rueda-Velásquez *et al.*, 2017). This thesis addresses this knowledge gap. There are currently five models available for the viscosity of characterized native heavy oils and bitumen: Corresponding States, Friction Theory, Free Volume Theory, the Walther Model, and the Expanded Fluid model. The Expanded Fluid model developed by Yarranton and Satyro (2009) was chosen for this thesis because it: 1) designed for heavy oils; 2) has a small number of adjustable parameters; 3) is continuous through the entire phase diagram; 4) has easily determined parameters from incomplete or estimated data; 5) is computationally efficient.

1.2. Objectives

The main objective of this thesis is to extend the Expanded Fluid model to predict the viscosity of visbroken oils based on the feedstock characterization and reaction conditions. The specific objectives are as follows:

1. Visbreak a bitumen sample at five different severity conditions to produce reacted oils using an in-house lab scale plant.
2. Characterize and measure the properties of the native and reacted oils based on the following methodology:
    a. Perform a spinning band distillation to obtain a distillable fraction characterized by boiling point distributions as well as a residual fraction. Carry out a SARA analysis on the residual fraction.
    b. Measure the density of the distillable fraction.
    c. Measure the viscosity and density of the whole residue, the de-asphalted residue, saturates, aromatics, resins and asphaltenes fractions.

3. Adapt the EF model for reacted samples:
    a. Fit the EF model to the distillate and SARA cut viscosities.
    b. Develop correlations for the viscosity model parameters as a function of conversion.
    c. Adapt the model mixing rules to match the viscosity of the de-asphalted residue, whole residue, and whole oil.
4. Test the model and correlations on the viscosity of visbroken samples provided by the University of Alberta and Sinopec Research Institute of Petroleum Processing (RIPP).

1.3. Outline

This thesis is divided into five chapters which are briefly described below.

- *Chapter Two* is a literature review of the nature of crude oils, crude oil chemistry, oil characterization, viscosity modeling, and upgrading. Changes in crude oil chemistry and properties during visbreaking reactions are also discussed.
- *Chapter Three* presents the experimental apparatus and methodology used to visbreak oil samples, characterize the feedstock and products, and measure their density and viscosity.
- *Chapter Four* presents the methodology used to apply the EF model to visbroken products. First, the characterization methodology is outlined. Then, the Expanded Fluid model is discussed in detail. Finally, the processing of measured data into the required inputs is described.
- *Chapter Five* presents the results obtained in this thesis. The results for the visbroken products generated in this thesis are discussed including the effects of visbreaking on product composition, density, and viscosity. Correlations for the density and viscosity with conversion are presented where conversion is the percent change in the mass of the 524°C+ fraction from the reaction. Finally, these correlations are tested on a similar oil and an oil from a different geographical location.
- *Chapter Six* summarizes the conclusions from the thesis and provides recommendations for future work.

Chapter 2: Literature Review

This chapter provides a review of the background material required to understand viscosity changes in crude oil during visbreaking. Crude oil chemistry, oil characterization, viscosity modeling, and upgrading are reviewed with an emphasis on heavy oils. Then, the effects of visbreaking on crude oil are discussed.

2.1 Crude Oil Definition

Crude oil is a complex mixture of hundreds of thousands, or perhaps millions, of hydrocarbon based molecules with varying amounts of oxygen, nitrogen, sulfur, and heavy metals such as nickel and vanadium. Other compounds found in crude oils include hydrogen, helium, nitrogen, carbon dioxide, and sulfur dioxide. Crude oils can be classified as conventional oil, heavy oil, or extra heavy oil based on their API gravity and viscosity, as shown in Table 2.1 (Gray, 1994). An extra heavy oil is commonly termed a bitumen when it is immobile at reservoir conditions.

Table 2.1 Crude oil classification (Gray 1994).

Classification	Density kg/m^3	API Gravity	Viscosity MPa·s
Conventional Oil	<900	>20°	$<10^2$
Heavy Oil	900-1000	10°-19°	10^2-10^5
Extra Heavy Oil	>1000	<10°	$>10^5$

2.2 Crude Oil Chemistry

Crude oils can be classified as paraffinic, naphthenic, or aromatic (Speight, 2007) depending on which of these chemical classes predominates. These classes are defined as follows:

- Paraffins are straight or branched chains of saturated hydrocarbons (referred to as normal and isoparaffins, respectively).
- Naphthenes are saturated hydrocarbons with at least one ring structure. Most naphthenic molecules present in crude oil have more than one ring and paraffinic side chains.

- Aromatics are hydrocarbons compounds with at least one benzene ring. These molecules in crude oil are usually linked with paraffinic side chains or naphthenic rings. Thus, their complexity increases significantly with the number of rings due to a larger amount of possible configurations of linked rings and side chains.

Most crude oil molecules are heterocompounds; that is, they are molecules from the previous groups that also contain one or more heteroatoms (S, O, N, Ni, V, Fe).

Crude oils, particularly heavy oils, are sometimes described with a different set of chemical classes; that is, saturates, aromatics, resins, and asphaltenes (Speight, 2007). The saturates, aromatics, and resins are adsorption classes. The asphaltenes are a solubility class and are defined as the fraction of the oil soluble in an aromatic solvent (usually toluene) but insoluble in an *n*-alkane (usually *n*-pentane or *n*-heptane). The saturates are composed of paraffinic and naphthenic compounds. The aromatics, resins and asphaltenes are a continuum of aromatic and polynuclear aromatic species of increasing molecular weight, density, aromaticity and heteroatom content. The asphaltenes are known to self-associate into nano-aggregates consisting of 5-10 molecules per aggregate on average (McKenna *et al.,* 2013; Yarranton *et al.,* 2013).

The complexity of crude oils components is illustrated in Figure 2.1 (Altgelt and Boduszynsky, 1994). The left boundary of this figure represents the *n*-alkanes (paraffins), while the right boundary represents the more complex multi-aromatic and polyfunctional molecules. As boiling point increases, the carbon number range broadens due to a larger variety of possible chemical families. The aromaticity, heteroatom content, and overall complexity of the oil also increase. In general, saturates predominate at the lowest carbon numbers. The aromatic species progress from the aromatic to the resin to the asphaltene class as the carbon number increases.

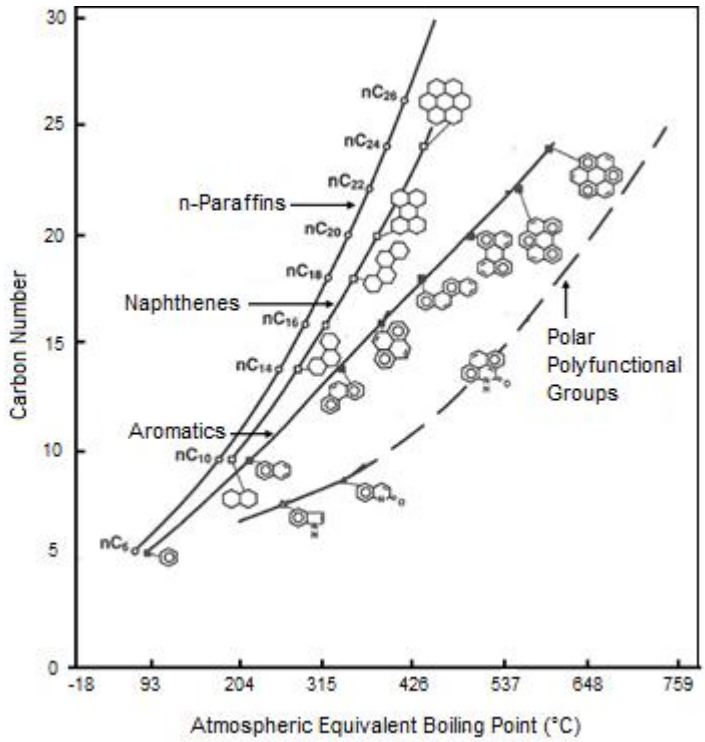

Figure 2.1 Relationship between carbon number, boiling point, and structure of chemical compounds in crude oil. Adapted from Altgelt and Boduszynsky (1994).

2.3 Crude Oil Characterization

Crude oil characterization is the first step in modeling thermodynamic behaviour, reaction kinetics, and physical properties such as density and viscosity. Characterization is the representation of the oil as a set of real and pseudo-components that reflect the property distributions within the oil. It is required because the number and complexity of the components in crude oil are too great and too ill-defined to create a complete molecular description. Crude oil characterization is generally based on one of more of the following three types of assay: chromatography, distillation, and solubility. Selecting the appropriate assay depends on the type of oil and application required. Each type is described below.

Gas Chromatography

Gas chromatography (GC) is based on the retention time of components in a fluid passing through a packed column. The retention time is related to the molecular weight of the component. Hence,

GC provides a molecular weight distribution for the components (or pseudo-components). Correlations are applied to obtain other properties such as density and critical properties. However, GC does not allow the direct measurement of viscosity and other pertinent properties of the pseudo-components to determine how they change with reaction.

Physical Distillation

Distillation measures the mass fraction that distills from the oil as temperature is ramped. Hence, distillation assays fractionate the crude oil into components and pseudocomponents representing boiling point intervals. This fractionation narrows the range of molecular weight (and therefore the variation in molecular size and structure) within each interval (Altgelt and Boduszynsky, 1994). Existing correlations are applied to obtain other properties such as specific gravity, molecular weight, hydrogen to carbon ratio, and viscosity (Ramos-Pallares *et al.,* 2017; Riazi, 2005). In addition, physical cuts can be obtained and their properties can be directly measured.

The physical distillation assays most relevant for crude oils are listed below.

- ASTM D86 is one of the oldest and simplest methods, the assay is performed at atmospheric conditions. It is not suitable for heavy oils because very little of the oil will distill at atmospheric pressure.
- ASTM D1160 is similar to ASTM 86 but is performed at sub-atmospheric pressures, typically 1, 2, 10, or 50 mm Hg. The data are converted to atmospheric equivalent boiling temperatures (AET) using the Maxwell and Bonnell (1957) correlation. This assay extends the ASTM D86 method to heavier petroleum fractions.
- True boiling point (ASTM D2892) is considered the most reliable method to determine the boiling temperature of a petroleum fraction (Riazi, 2005). True boiling point (TBP) data are obtained from a column with 14 to 18 theoretical plates at a reflux ratio above 1 to 5, producing a more efficient component separation and increasing reproducibility between laboratories. The distillation is initially performed at atmospheric pressure but can be decreased to 2 mmHg. Therefore, this method has limited applicability to heavy oil where the sample can only be distilled to approximately 400°C AET. Correlations are available to convert ASTM D86 data into TBP (Riazi, 2005).

- ASTM D5236 is similar to ASTM D2892 but is performed at pressures from 0.1 to 50 mmHg. Samples with low boiling point material must be previously topped for example by performing an atmospheric pressure ASTM D2892. The Maxwell and Bonnell correlation (1957) is used to convert the reduced pressure boiling temperatures to AET. This assay extends the ASTM D2892 method to heavier petroleum fractions with an initial boiling temperature above 150ºC.
- The Spinning Band Distillation (SBD) method consist of a column with a rotating spiral band increasing vapor-liquid equilibrium by providing over 100 theoretical plates, at a typical reflux ratio of 5:1. This approach provides boiling points equivalent to TBP (ASTM D2892). For heavy petroleum fractions, the distillation is performed at pressures as low as 1 mmHg. The Maxwell and Bonnell correlation (1957) is again used to convert the data to TBP.

Distillation assays are only applicable up to an actual distillation temperature of approximately 300 °C, the temperature at which the sample may begin to crack (Carbognani *et al.*, 2007). For heavy oils and bitumens, there is a significant distillation residue (approximately 75 wt% of the oil) even with a vacuum distillation (Riazi, 2005). Hence, the distillation residue must be characterized by another method.

Simulated Distillation (SimDist)

SimDist or Simulated Distillation (ASTM D2887) is a distillation assay obtained by gas chromatography. Correlations are used to convert retention times to boiling points. This method can be applied to petroleum fractions with a boiling range between 55 to 538°C. Some variations are also available depending on the type of sample, such as ASTM D5307, D6352 and D7169. ASTM D7169 is applicable up to 720°C and is commonly used to determine the boiling temperature distribution of heavier crude oils and residues.

SimDist assays have been found to provide fast and reliable results at TBP below 375°C, as shown in Figure 2.2 for a Western Canadian bitumen. This agreement is to be expected because the correlations used in SimDist were based on physical distillation data measured at these conditions.

Sanchez-Lemus *et al.* (2015) used a deep vacuum fractionation apparatus to measure the properties of heavier crude oil cuts than obtained with conventional distillation. They demonstrated that the TBP from a conventional physical distillation follow a Gaussian extrapolation to higher TBP. Figure 2.2 shows that the SimDist TBP increasingly deviate from the TBP extrapolated from the physical distillation. Hence, the reliability of SimDist data above 375°C is uncertain. As with other GC methods, SimDist does not provide physical cuts with which to perform direct measurements.

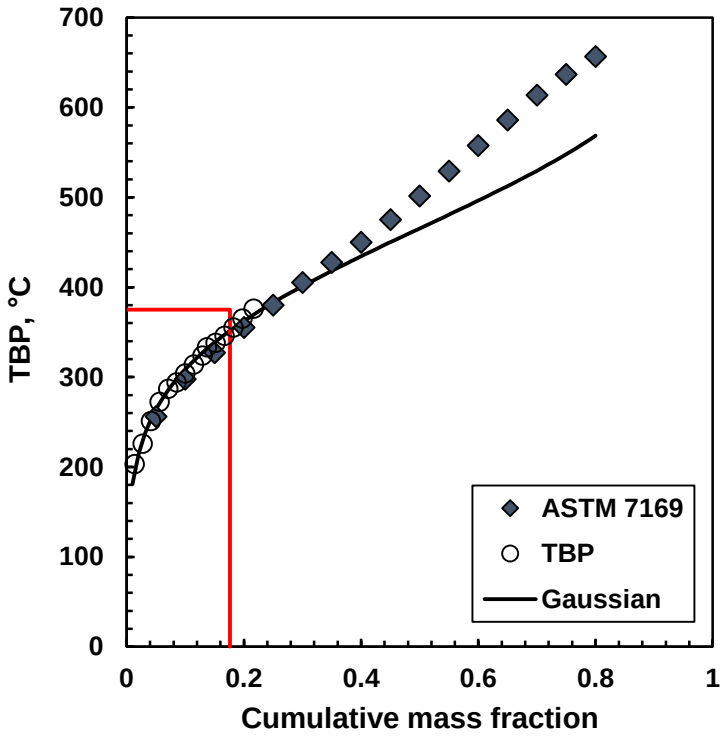

Figure 2.2 Comparison between TBP and SimDist for a Western Canadian bitumen (WC-B-A3).

SARA Fractionation

SARA fractionation is a combination of solubility and liquid chromatographic separations that separate the oil into four fractions: saturates, aromatics, resins and asphaltenes (SARA). The methodology is described in detail in ASTM D2007 and ASTM D4124. Asphaltenes are fractionated first by precipitation with *n*-pentane. The remaining fractions are separated by liquid chromatography using two columns. The first column contains attapulgus clay which adsorbs the

resins. The second one is packed with either silica gel or alumina which adsorbs the aromatics. Saturates elute through both columns without being absorbed.

SARA is applicable to non-volatile samples. Light components must be removed first either by topping or distillation. The asphaltenes obtained from SARA will also contain some non-asphaltene material; that is, any toluene insoluble components from the crude oil such as sand, clay, and some heavy organics. The toluene insoluble material can be separated from the asphaltenes by dilution with toluene and centrifugation. If this step is taken, the final assay will include the toluene insoluble content along with the SARA content.

2.4 Crude Oil Viscosity Modeling

Viscosity is the resistance of a fluid to flow. It can also be thought as the proportionality factor between the conductive momentum transfer and its velocity gradient as shown by Newton's Law of Viscosity, which in one dimensional flow is given by (Bird *et al.*, 2002):

$$\tau_{yx} = -\mu \frac{dv_x}{dy} \qquad (2.1)$$

where τ_{yx} is the shear stress generating momentum transfer, μ is the viscosity of the fluid, v_x, is the velocity in the x coordinate, y is the distance in the y coordinate. The gradient dv_x/dy is the shear rate. Fluids following this law have a constant viscosity at a given temperature, pressure and composition, and are referred to as Newtonian fluids. When the viscosity is a function of not only these variables, but also of the shear stress or shear rate, they are considered to be non-Newtonian fluids. Crude oils have been found to be non-Newtonian fluids at temperatures below approximately 30°C but are Newtonian fluids at higher temperatures (Abivin *et al.*, 2012; Soto-Castruita *et al.*, 2015). For most practical applications they can be considered Newtonian fluids and are modeled as such.

Newtonian viscosity models for crude oils must quantify the change in fluid viscosity with changes in conditions including temperature, pressure, and composition. For example. the viscosity of liquid petroleum and its fractions decreases as the temperature increases, as pressure decreases, and as the boiling point, molar mass, and density of the fraction increases (Gray, 2015). It is also

necessary to consider the physical state of the fluids. Some viscosity models are only applicable in the gas or liquid region while others encompasses all of the phases. Finally, some models treat the oil as a single component fluids while others can accommodate an oil characterized into pseudo-components. Only the latter type of model is suitable for predicting the viscosity of separated crude oil fractions (such as distillation cuts or deasphalted oils) or of reacted oils based on the feedstock properties.

The following models are applicable to characterized crude oils: the modified Walther model, Corresponding States, Friction Theory, Free Volume Theory, and the Expanded Fluid model. The Walther model is applicable only to the liquid region. The other models are full phase models. Corresponding States and Friction Theory are built on correlations based on critical properties. Free Volume Theory and the Expanded Fluid model relate viscosity to density. The Expanded Fluid model was designed specifically for heavy oils and is used in this thesis; it is presented in detail in Chapter 4. The other models are described below.

Modified Walther Model

The empirical method originally proposed by Walther (1931) relates the double log of viscosity to the double log of temperature for liquids. This expression was adapted by ASTM D431 to relate kinematic viscosity to temperature as follows:

$$\log(\log(\vartheta + c)) = b_1 + b_2 \log(T) \qquad (2.2)$$

where ϑ is the fluid kinematic viscosity, T is temperature, b_1 and b_2 are fluid specific parameters and c usually ranges from 0.7 to 1. Several authors have fitted this equation to match viscosity data of crude oils and mixtures from specific geographical locations, including Athabasca and Peace River bitumen (Badamchi-Zadeh *et al.,* 2009a; Badamchi-Zadeh *et al.,* 2009b; Mehrotra *et al.,* 1986; Svrcek *et al.,* 1988), Cold Lake bitumen (Eastick *et al.,* 1990; Mehrotra 1990a), Lloydminster heavy oils (Li *et al.,* 2013) and Middle East oils (Mehrotra 1990b).

Yarranton *et al.* (2013) included a third fluid specific parameter in the correlation to account for viscosity changes with pressure. The model was used to predict the viscosity of characterized crude oils using a GC assay. Correlations were developed for the fluid specific parameters based on the

molecular weight of the pseudo-components. This approach was tested using crude oils from the Gulf of Mexico, Middle East, Asia and Europe obtaining an average relative deviation of 44%. However, the GC assay must be extrapolated to account for the C_{30}+ fraction. For heavy oils and bitumen, this fraction accounts for more than 70 wt% of the oil, making the viscosity prediction highly sensitive to the extrapolation procedure (Ramos-Pallares *et al.*, 2017).

Ramos-Pallares *et al.* (2017) modified this approach to predict the fluid specific parameters based on a distillation assay. This model inputs are the temperature, pressure, C5 asphaltene content, maltene distillation curve, and the bulk fluid specific gravity and molecular weight. The model predicted the viscosity of fourteen heavy oils and bitumen from different geographical locations with an average relative deviation of 57% without tuning and 8% if a single viscosity point was used to tune the model. This method is only applicable in the liquid phase up to a reduced temperature (temperature / critical temperature) of approximately 0.75.

Corresponding States

This semi-theoretical method is based on the principle that the properties of fluids vary consistently in reference to their critical point. A reduced property is then defined as the property divided by its value at the critical point. The reduced properties of corresponding fluids are expected to map onto each other when plotted in reduced temperature and pressure (or density) coordinates. Based on this principle, the properties of a fluid can be determined from the known properties of a reference fluid.

Hanley (1976) applied this principle to relate the reduced viscosity of low molecular weight hydrocarbons and LNG to the reduced viscosity of methane at the same reduced temperature and density by introducing two shape factor terms to account for non-correspondence. Ely and Hanley (1981) later extended this approach to hydrocarbons of molecular weights up to C_{20} and their binary mixtures. The mixture was assumed to behave as a hypothetical single component fluid and a set of mixing rules were established to calculate the mixture parameters from those of the pure components. This model predicted the viscosity of all the components and binary mixtures in the

dataset with an average relative deviation of 8%. Baltatu (1982) developed a characterization approach to apply this model to light petroleum fractions (minimum API gravity of 39.4°).

Tham and Gubbins (1970) developed a corresponding states formulation for the viscosity of polyatomic non-polar compounds based on reduced temperature and pressure, using a rotational coupling coefficient to account for non-conformity. This coefficient was treated as an adjustable parameter and was fitted to experimental liquid viscosity data. Pedersen *et al.* (1984) applied this approach to characterized crude oils from GC data using methane as the reference fluid and the correlation developed by Hanley *et al.* (1975) as the reference viscosity. The rotational coupling coefficient was empirically related to molecular weight and reduced density. The method provided reliable results for pure hydrocarbons, carbon dioxide, binary mixtures and light crude oils.

Pedersen and Fredenslund (1987) further extended the applicability of this approach to heavier oil fractions. Methane, the reference fluid, has a reduced freezing point that can lie above the reduced temperatures and pressure of many of the heavier fractions. Therefore the reference model Hanley *et al*. (1975) and rotational coupling coefficient were modified by applying an additional term based on oil mixtures and fractions data below reduced temperatures of 0.4. However, below a reference temperature of 60 K the density and viscosity remained almost unaltered with pressure changes (Lindeloff *et al.,* 2004). Hence, methane is not a suitable reference fluid for oil viscosities above 10 mPa·s. Lindeloff *et al.* (2004) modified the reference function below 60 K based on crude oil data instead of methane. This method predicted the viscosity of 8 heavy oils with a deviation of a factor of 2-3 from the experimental data. Tuning is required in order to capture the viscosity of these fluids over a wide range of temperatures.

Friction Theory

This semi-empirical approach relates the viscosity of a fluid to the friction forces between layers arising from the molecular attractive and repulsive forces. Quinones-Cisneros *et al.* (2000) developed this concept to determine viscosity from the contributions of a dilute gas term (μ_G) and a residual viscosity term (μ_f) as follows:

$$\mu = \mu_G + \mu_f \qquad (2.3)$$

The dilute gas viscosity is calculated from the correlation developed by Chung *et al.* (1988). The residual viscosity is determined as a function of the attractive and repulsive van der Waals pressure terms as well as three fluid specific parameters. The attractive and repulsive terms are calculated from a cubic equation of state. The fluid specific parameters were fitted to experimental data, where a temperature dependency was found. This dependency was "captured" using three exponential series and the resultant model required a total of seven adjustable parameters. The model was capable of fitting the viscosity of *n*-paraffins up to *n*-decane and six binary mixtures with an average relative deviation of 3%.

To reduce the number of adjustable parameters, Quiñones-Cisneros *et al.* (2001a) applied the corresponding states principle to develop generalized correlations for the friction theory parameters. These parameters were considered to be the sum of a temperature independent critical friction term and a temperature dependent residual friction term. Thirteen parameters must be determined to calculate both terms. A dataset of *n*-paraffins up to *n*-octadecane was fitted to obtain generalized values for these parameters. This correlation required only a single tuning parameter, the characteristic critical viscosity of the fluid. This approach was capable of modeling the viscosity of nine additional hydrocarbons, nitrogen, carbon dioxide and mixtures with an average relative deviation of 4%.

Quiñones-Cisneros *et al.* (2001b) extended this approach to crude oils characterized by GC and introduced an equation to estimate the characteristic critical viscosity of the plus fraction and required a single adjustable parameter to be tuned with data above the saturation pressure. Quiñones-Cisneros *et al.* (2003) further extended this methodology by modifying the characterization approach based on GC, dividing the C_{11}+ fraction into pseudo-components based on a molecular weight chi-squared distribution. The characteristic viscosity of each pseudo-component could then be determined as a function of molecular weight, critical properties, and an adjustable parameter. This parameter introduced the possibility of tuning with atmospheric viscosity data instead. Using this methodology the viscosity of lighter oils could be modeled (molecular weights below 200 g/mol). However, significant deviations were obtained for heavier

oil systems (Quinones-Cisneros *et al.*, 2003; Quiñones-Cisneros *et al.*, 2004) attributed to limitations of cubic type equations of state in predicting the repulsive terms.

Quinones-Cisneros *et al.* (2004) introduced a volume translation term to improve the performance for heavy oil systems that required an additional adjustable compressibility parameter. The two adjustable parameters were capable of modeling the high pressure viscosity of six live heavy oils within the error of the measurements. However higher deviations were encountered below the saturation pressure. Kumar *et al.* (2011) introduced a pressure dependence in the mixing rules to account for the effect of component asymmetry. Two adjustable parameters must be tuned to two experimental viscosity values, one above and one below the saturation pressure. This methodology captured the viscosity below saturation pressure with an average relative deviation of 4%.

Free Volume Theory

This theory considers the fluid as a mixture of occupied and free volumes. When there is free volume, molecules can diffuse into the free volume allowing the fluid to move (Cohen and Turnbull, 1959). The greater the free volume, the more readily the fluid can move, and the lower the viscosity. If there is no free volume, the viscosity becomes infinite. Hildebrand (1971) applied this theory to relate the fluidity (inverse of viscosity) with an expansion from an intrinsic volume, as follows:

$$\frac{1}{\mu} = B\frac{(V - V_0)}{V_0} \qquad (2.4)$$

where V_o is the intrinsic volume at which the molecules are too crowded to allow flow (leading to an infinite viscosity), V is the volume at the given conditions, and B is the absorption energy of the molecular collisions.

Allal *et al.* (2001) developed a viscosity correlation consisting on a dilute gas term and a perturbation free volume fraction term. The required inputs are dilute gas viscosity, molecular weight, density, and three fluid specific parameters as inputs. This approach was capable of fitting the viscosity data of eight hydrocarbons with an average relative deviation of 3.5%. Tan *et al.* (2005) used this approach, coupled with densities from the SAFT equation of state, to model the

viscosity of *n*-alkanes up to *n*-dodecane. Six generalized parameters were fitted to the data, resulting in an average relative deviation below 2%.

De La Porte and Kossack (2014) applied the free volume model to long branched *n*-alkanes (up to C_{14}), using the modified Tait equation to model high pressure density data. An average relative deviation of 5.3% was obtained for the correlated viscosity dataset. De la Porte *et al.* (2014) extended this methodology to heavy oils characterized into pseudo-components by lumping resins and asphaltenes in one fraction. The properties of this heavy fraction were calculated by fitting the model to the experimental viscosity data.

2.5 Heavy Oil Upgrading

Crude oils are refined to obtain products such as LPG, gasoline, diesel, jet fuel, solvents, kerosene and asphalt. The refining process can be classified into three general stages: separation where crude oil is physically divided into distinct streams typically by distillation, conversion in which some streams are chemically altered to produce more valuable constituents, and finishing where product streams are purified (Speight, 2007). For heavy oils and bitumen in particular, the boiling point and molecular weight of the heavier streams must be reduced to achieve product specifications. The conversion processes that can be applied to these streams are classified as either carbon rejection or hydrogen addition.

2.5.1 Carbon Rejection

Carbon rejection processes involve transferring hydrogen from large to small molecules by means of thermal cracking (Rana *et al.*, 2007; Speight, 1986). These reactions generate light paraffinic components and an increasingly aromatic and denser heavy fraction. If the cracking reaction progresses sufficiently, the heavy fraction will eventually phase separate and form coke. Carbon rejection technologies include visbreaking, delayed coking, fluid coking and flexicoking. This thesis focuses on visbreaking.

Visbreaking

Visbreaking is a mild liquid-phase thermal cracking process taking place at low temperatures and residence times (Joshi *et al.,* 2008; Speight, 2012). While no carbon is rejected from the oil, like other carbon rejection technologies, this process involves hydrogen transfer from the heavier more aromatic structures to the smaller compounds. Visbreaking increases the yield of the more valuable distillates and decreases the viscosity of the residue. This technology is commonly used for vacuum residue processing; however, its applicability for field upgrading has been gaining attention due to simplicity and low cost (Gray, 2015). Refineries focus mainly on thermally cracking vacuum distillation bottoms to produce distillate fractions, as well as reduce residue viscosity to decrease the amount of light blend required to meet fuel oil specifications (Speight, 2007). With field upgrading applications, the target is to reduce raw heavy oil or bitumen viscosity enough to decrease, or even eliminate, the quantity of diluent necessary to achieve pipeline specifications (Wang *et al.,* 2014). Light distillate production is undesirable for this application.

Visbreaking is typically performed in either a coil or a soaker configuration. A schematic of a coil visbreaker process is shown in Figure 2.3. Coil visbreaking is a high temperature, short residence time process. The feedstock is pumped to a pre-heater to achieve a temperature of 300-330°C. The fluid proceeds to the coil reactor operating at temperatures from 460-500°C for a residence time of 1-5 minutes (Gray, 2015; Joshi *et al.,* 2008). The reacted product is then quenched to a temperature below 350°C and fractionated into the desired product streams.

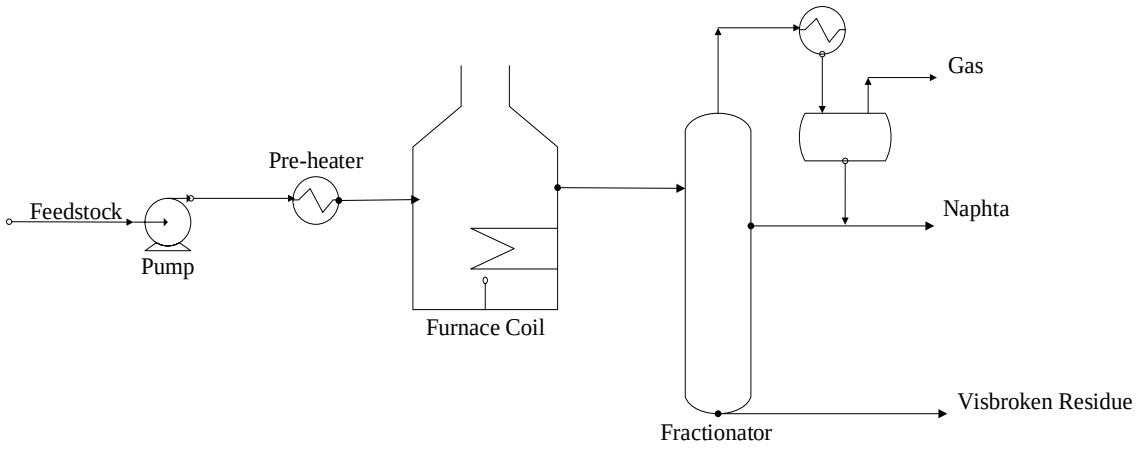

Figure 2.3 Coil visbreaking process schematic.

A schematic of a soaker visbreaker process is provided in Figure 2.4. Soaker visbreaking is a low temperature, high residence time process. The main difference between soaker and coil visbreaking is the addition of an adiabatic soaker drum between the furnace coil and the fractionator. The furnace temperature is reduced to 430-460°C. Most of the reaction takes place in the soaker drum, achieving residence times from 15-25 minutes (Gray, 2015; Joshi *et al.*, 2008). While soaker visbreaking provides lower energy consumption and slower coke build up, soaker drum de-coking is more complex and requires longer shut-down times.

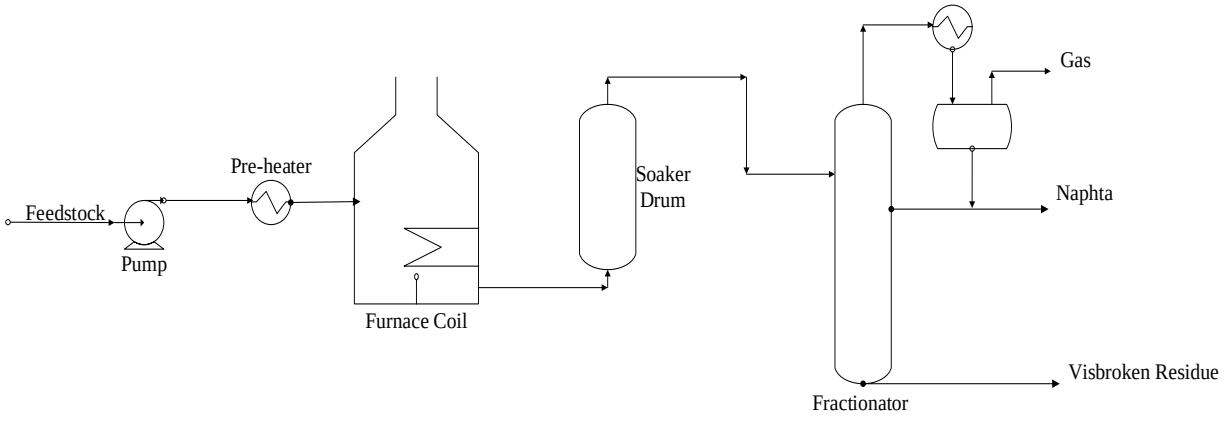

Figure 2.4 Soaker visbreaking process schematic.

Delayed Coking

Delayed coking is a higher severity thermal cracking process commonly used in refineries to upgrade the bottom-of-the-barrel into lighter products. This process uses long residence times to increase the yield of gas and distillates, while leaving coke as residue. The common configuration is several semi-batch reactors operating in parallel. The coke drum in operation is loaded with the vacuum residue at a temperature approximately 500°C. As the reactions proceed, the vapour product is removed from the top of the drum and quenched. During this time, the reactor in stand-by is being decoked typically by hydraulic drilling. Delayed coking is usually applied when the produced coke can be sold to an anode or graphitic carbon manufacturer, or no market for fuel oils exist (Gray, 2015; Speight, 2007).

Fluid Coking

This continuous coking process was developed to facilitate coke removal and increase distillate yield. The liquid feed is sprayed into a fluidized bed consisting of coke particles. These particles carry the feed through the reactor where thermal cracking reactions take place in a temperature range of 510-550°C. The vapour products are collected on top of the reactor, separated from coke particles on a cyclone, and quenched. The heat required is obtained by burning part of the coke in another vessel. The main disadvantages of this technology are long shutdown times to remove accumulated coke and high sulfur dioxide emissions from burning coke (Gray, 2015).

Flexicoking

This process was developed, as a variation of fluid coking, to gasify the solid coke without producing sulfur dioxide emissions. Instead of a burner, the coke is taken to a gasifier operating at temperatures from 830 to 1000°C. Inside the gasifier, the sulfur in the coke is reacted to hydrogen sulfide which is scrubbed from the downstream product. An additional vessel is placed to provide heat transfer between the reactor and the gasifier. The product yields are the same as in fluid coking since the coking reactor remains identical. However, this operation requires a large gasification unit and can be unattractive under current low natural gas prices (Gray, 2015).

2.5.2 Hydrogen Addition Processes

These processes add hydrogen and catalyst to alter the pathway of cracking reactions leading to more valuable products with higher H/C ratios. Hydrogen terminates many coke-producing polymerization reactions and increases selectivity towards low boiling point products. Catalytic hydrogenation can also remove up to about 90% of heteroatom contaminants such as nitrogen, oxygen, sulfur, and metals from liquid crude oils (Speight, 2007). The three main hydrogen addition technologies are hydroconversion, hydrotreating, and hydrocacking.

Hydroconversion

This operation is used mainly for heavy feeds with significant nitrogen content. These heteroatom groups significantly deactive acid cracking-type catalysts. Therefore, the catalyst for this process is designed mainly to promote hydrogenation reactions. Temperatures above 410°C are used to thermally crack the feed in the presence of hydrogen which inhibits coke formation. High operating pressures (7 to 10 MPa) are required for effective use of hydrogen (Gray, 2015).

Hydrotreating

Hydrotreating is performed at temperatures below 410°C to promote hydrogenation and heteroatom removal instead of thermal cracking. Operating conditions vary depending on the application with temperatures ranging from 350 to 410°C and pressures from 2 to 7 MPa. Light feeds are treated with less severe conditions to focus on product quality, while heavy feeds require higher severity to achieve significant nitrogen and sulfur removal (Gray, 2015).

Hydrocracking

Hydrocracking uses an acid-cracking catalyst and is applied to feeds with low nitrogen and sulfur content, such as gas oil or deasphalted oil, to avoid catalyst deactivation. Heavy aromatic and high molecular weight compounds are cracked and hydrogenated in the presence of a catalyst to obtain lower molecular weight products. Severe conditions are required for this operation, generally with temperatures ranging from 410 to 815°C and pressures from 7 to 14 MPa (Gray, 2015; Speight, 2007).

2.6 Effect of Visbreaking on Crude Oils

The changes in a visbroken crude oil depend on the nature of the feedstock and on conversion (the extent of reaction). Conversion is defined below and then the changes in oil composition and viscosity from visbreaking are discussed.

Conversion

Visbreaking involves free radical reactions including initiation, propagation, and termination steps (Raseev, 2003). The main reactions include side chain dealkylation, cracking of paraffinic chains, dehydrogenation, cyclization, aromatization, and condensation (Joshi *et al.,* 2008; Singh *et al.,* 1993). The extent of reaction depends on the process temperature, residence time, and chemical nature of the feedstock. Since there are multiple reactions, the extent of reaction is represented by the conversion which is commonly defined as the change in the mass fraction of a boiling point fraction from the feedstock to the reacted product (Henderson and Weber, 1965; Kataria *et al.,* 2004; Krishna *et al.,* 1988). In this thesis, conversion is based on the change in the vacuum residue fraction (+524°C), consistent with current industry trends (Powers *et al.,* 2016; Rueda-Velásquez and Gray, 2017), and is given by:

$$Conversion = \frac{(+524℃\ Feed) - (+524℃\ Product)}{+524℃\ Feed} 100 \qquad (2.5)$$

where $+524℃$ is the weight percentage of the SimDist (ASTM 7169) boiling fraction above that temperature.

Conversion increases as the severity of the reaction conditions increases; that is, with increasing temperature and residence time. Visbreaking severity is generally limited by three factors. First, conversion increases the density, aromaticity, and solubility parameter of the asphaltenes (Powers *et al.,* 2016; Zhao *et al.,* 2001), making them less soluble in the oil. Second, the distillate content of the oil increases making the oil less capable of solubilizing the asphaltenes. Both of these factors decrease the product stability eventually leading to asphaltene precipitation. Third, as conversion increases even further, dehydrogenation and condensation reactions in the asphaltene fraction

trigger solid coke formation (Raseev, 2003; Wiehe, 1993). Both precipitated asphaltenes and coke tend to plug equipment and alter the reactor temperature profile (Joshi *et al.*, 2008).

Visbreaking also depends on the pressure because pressure affects the degree of vapourization. Pressure can be a significant variable controlling the composition of the liquid feedstock and the residence time. Generally, pressure for industrial applications ranges between 0.3 to 5 MPa (Gray, 2015; Speight, 2012).

Effect of Visbreaking on Oil Composition

Thermal cracking involves a network of multiple parallel reactions particularly for a mixture as complex as crude oils. Hence, predicting product distribution becomes a challenging task. Earlier visbreaking studies focused on lumped kinetics of boiling point fractions and considered only first order cracking with negligible condensation/coking reactions. These studies include Athabasca bitumen (Henderson and Weber, 1965), Cold Lake bitumen (Shu and Venkatesan, 1984), Iraqi vacuum residue (Al-Soufi *et al.*, 1988) and Aghajari residue (Krishna *et al.*, 1988). In general, the light distillate yield was found to increase with increasing conversion. Di Carlo and Janis (1992) applied a first order kinetic approach to predict light distillate yield of three atmospheric residues from Egypt, Italy, and Libya. They reported a tendency of crude oils with a high asphaltene and resin content to react at lower temperatures with a higher selectivity towards gas (below 30°C). This behaviour was attributed to the higher reactivity of side chains linked to poly-condensed cores rather than more paraffinic or naphthenic structures. In oils rich with saturates, splitting reactions generated a higher selectivity towards gasoil (175-370 °C).

Kataria *et al.* (2004) studied the effect of visbreaking on vacuum residues at severities below coke formation. The minimum temperature where cracking takes place and product yields were found to vary between feeds. They developed a lumped kinetic model that took into account feedstock properties such as SARA composition and CCR. Wiehe (1992) studied the effect of visbreaking in residues by tracking pseudo-components based on SARA assays. The SARA fractions were reacted independently, obtaining the scheme represented in Figure 2.5. Reaction products are assigned to SARA classes, but may be chemically different than the native material in the same

classes. Carbognani *et al.,* (2007) reported the changes in SARA composition during visbreaking for an Athabasca vacuum residue. The resin content decreased and asphaltene content increased with increased conversion, particularly at the higher conversion range (above 15%). The change in resins/asphaltenes ratio was found to correlate with product stability.

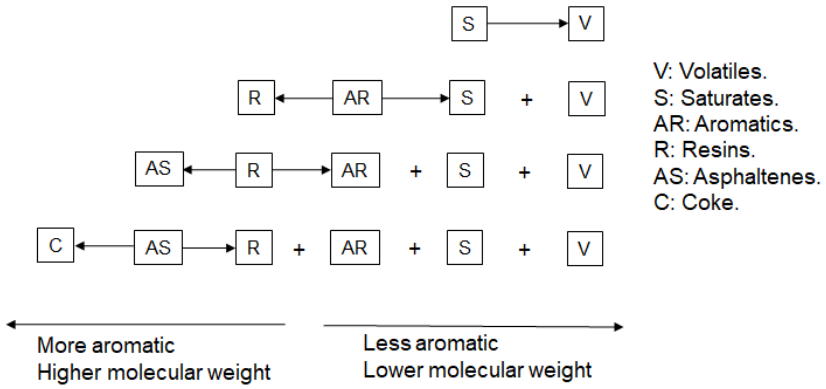

Figure 2.5 Thermal conversion reaction paths of SARA fractions (Adapted from Wiehe, 1992).

Yan (1990) performed a kinetic study at high severity visbreaking conditions and examined the effect of feedstock properties on coke formation for a mixed residue, an Arabian residue, and a Boscan crude oil. Coke propensity was found to correlate to asphaltene content, but not to API gravity or Conradson carbon residue (CCR). Del Bianco *et al.* (1993) studied coke formation during visbreaking of an Egyptian vacuum residue. An induction period was observed in the coke formation trend and as much as 60 minutes were required for coke to form at 410°C. This induction period was reduced as temperature increased. The activation energy of condensation reactions was found to be larger than that of cracking reactions, agreeing with industrial observation that lowering temperature and increasing residence time instead could reduce coke formation. Wiehe (1993) also studied this phenomena for a Cold Lake vacuum residue, postulating that during the induction period asphaltenes react to form only lower molecular weight compounds. As long as asphaltenes remain in solution, maltenes are capable of terminating asphaltene free-radicals, making the formation of coke precursors infrequent. At high conversions a second phase rich in asphaltenes forms where asphaltene radical recombination is frequent and coke forms quickly.

Effect of Visbreaking on Physical Properties

Early contributions reported the change of a fixed temperature-pressure viscosity point against conversion or another severity function (Henderson and Weber, 1965; Shu and Venkatesan, 1984; Al-Soufi *et al.,* 1988). These low severity studies reported viscosity reduction with increasing reaction severity (higher temperature and/or residence time). Krishna *et al.* (1988) reported a viscosity increase at higher conversions, which was attributed to condensation and polymerization reactions coming to dominate side chain cracking reactions.

Later studies tracked chemical changes in oil fractions. Wiehe (1992) measured the molecular weight and elemental composition of native and reacted SARA fractions. With the exception of the generated coke, the average molecular weight of each fraction decreased with increased conversion. The H/C ratio of the resins and asphaltenes decreased significantly with increased conversion while the H/C ratio for the saturates and aromatics varied little. Powers *et al.* (2016) studied solubility of native and visbroken asphaltenes with conversions up to 51%. Thermal cracking was found to reduce the asphaltenes molecular weight, increase their density, reduce their H/C ratio, and increase their solubility parameter. The reacted asphaltenes had a narrower molecular weight distribution than the feed asphaltenes, suggesting a slight reduction in self-association. Yarranton *et al.* (2018) reported the changes in the properties of saturate, aromatic and resin fractions after the volatiles were removed. The molecular weight of aromatics and resins decreased with increased conversion, while saturate molecular weights did not vary significantly. The density of the aromatics and resins increased with conversion but saturates density did not change considerably.

Viscosity Modeling

There are a number of kinetic studies on visbreaking which are not reviewed here but can be found elsewhere (Singh *et al.,* 2012). However, there have been few attempts to quantify the changes in physical properties such as density and viscosity. Dente and co-workers (Dente *et al.,* 1995; Dente *et al.,* 1997) developed a visbreaking model based on approximately 150 grouped components and 100 equivalent global reactions. The components included paraffins, aromatics, olefins and diolefins, among others, with different molecular characteristics such as degree of methylation and

number of rings. Bozzano *et al.* (2005) later added the effect of naphthenic compounds to this model. Specific gravity was calculated from the sum of the molecular volumes of components and group distributions. Viscosity was calculated with a modified Eyring approach, including the effects of carbon number and asphaltene content. Even though this approach was validated with industrial data, the physical properties were determined from correlations designed for small molecules, making them difficult to generalize for heavy oil applications (Rueda-Velásquez, 2013).

Rueda-Velásquez *et al.* (2017) divided two heavy oils and their visbroken products into four pseudo-components based on boiling point fractions. A viscosity model was developed assuming that the viscosity of each fraction would not vary with reaction, only their composition in the visbroken product. However, conversion dependent tuning parameters were added to the viscosity equation for the heaviest fraction to match the data. Hence, they established that visbroken oils viscosity could not be predicted by re-mixing the feedstock fractions in different proportions. It was concluded that to develop a predictive model, viscosity data for each fraction must be measured, requiring large scale experiments.

Chapter 3: Experimental Methods

This chapter presents the experimental methods used to react, fractionate, and measure the physical properties of each feedstock or visbroken product sample. The lab-scale plant used to visbreak the feedstocks is explained in detail. The methods used to fractionate the feed and product samples and to measure the viscosity, density, and molecular weight of the samples and their fractions are discussed.

3.1 Materials

Two bitumens and a vacuum residue were used as feedstock oils and are labelled as WC-B-A3, WC-B-A4 and ME-VR-A1, respectively.

- WC-B-A3 is a Western Canadian Athabasca bitumen from a SAGD well site provided by Japan Canada Oil Sands Ltd. Two different batches from this source were used, denoted as WC-B-A3(1) and WC-B-A3(2). The only notable difference between the two batches is their viscosity: 4400 mPa·s for A3(1) and 5370 mPa·s for A3(2) at 50 °C and atmospheric pressure. These samples were thermally cracked using an in-house visbreaking lab-scale plant at the University of Calgary at five different severity conditions.
- WC-B-A4 is another Western Canadian Athabasca bitumen produced by Suncor Energy and visbroken by Dr. de Klerk's research group at the University of Alberta. A single reacted sample was produced in a batch reactor under a nitrogen blanket at 340 °C for 1 hour.
- ME-VR-A1 is an Arabian vacuum residue supplied by SINOPEC Research Institute of Petroleum Processing (RIPP). Two thermally cracked oils from this sample were also provided by RIPP. The cracked samples were prepared using a batch reactor filled with nitrogen at near atmospheric pressure. For both reacted samples, the feedstock was ramped up to 420°C during an 80 minute period. The residence times inside the reactor after the preheat stage were 0 and 20 minutes, respectively. At the end of the specified residence time, the reactor was immediately quenched to a temperature below 350°C.

All of the feedstock and reacted products are listed in Table 3.1. Conversion was calculated from the change in +524°C content based on SimDist data, applying the following equation:

$$Conversion = \frac{(+524℃)\text{Feed} - (\mp 524℃)\text{Product}}{(+524℃)\ \text{Feed}} * 100\% \qquad (3.1)$$

where $+524℃$ is the weight percent of the +524ºC boiling cut from a SimDist assay.

Table 3.1 Samples used in this project.

Sample	Reaction Conditions	Conversion (%)
WC-B-A3	Feed	-
WC-B-A3-VIS5.1	6.5 MPa, 420ºC, 10 min	5.1
WC-B-A3-VIS4.9	6.5 MPa, 430ºC, 10 min	4.9
WC-B-A3-VIS8.1	6.5 MPa, 440ºC, 10 min	8.1
WC-B-A3-VIS19.3	6.5 MPa, 430ºC, 20 min	19.3
WC-B-A3-VIS38.1	6.5 MPa, 440ºC, 20 min	38.1
WC-B-A4	Feed	-
WC-B-A4-VIS1	0.1 MP	1
ME-VR-A1	Feed	-
ME-VR-A1-VIS12.5	0.1 MPa, 420ºC, 0 min*	12.5
ME-VR-A1-VIS18.8	0.1 MPa, 420ºC, 20 min*	18.8

* Sample heated to reaction temperature during 80 minutes previous the specified residence time.

ACS grade *n*-pentane, toluene and acetone from Fisher Scientific were used for asphaltene precipitation, SAR fractionation and toluene insolubles removal. OmniSolve high purity toluene (99.99%) obtained from VWR International LLC was used for molecular weight measurements. Sucrose octaacetate (98%) and octacosane (99%) were used for vapour pressure osmometer calibrations and were obtained from Sigma-Aldrich Chemical Company.

3.2 Visbreaking Lab-Scale Plant

3.2.1 Apparatus

The apparatus is a visbreaking unit consisting of three sections: feed, reaction, and product separation and recovery. The unit is a coil visbreaker but the experiments were performed at higher residence times and lower temperatures than is typical for a coil visbreaker in order to avoid coke formation. Hence the operating conditions were similar to those used in a soaker visbreaker. A schematic of the apparatus is provided in Figure 3.1. Each section is described below. The

apparatus operates continuously and can process 11 L of sample in one run. Temperatures, pressures, flow rates, valves and pumps operation are controlled from a LabVIEW program. The operating conditions are as follows: reaction temperatures from 300 to 500°C, pressures up to 1300 psig, and flow rates from 1 μL/min to 204 mL/min. Unless otherwise specified, all lines are insulated 1/4 inch i.d. stainless steel pipes with Briskheat heating cables.

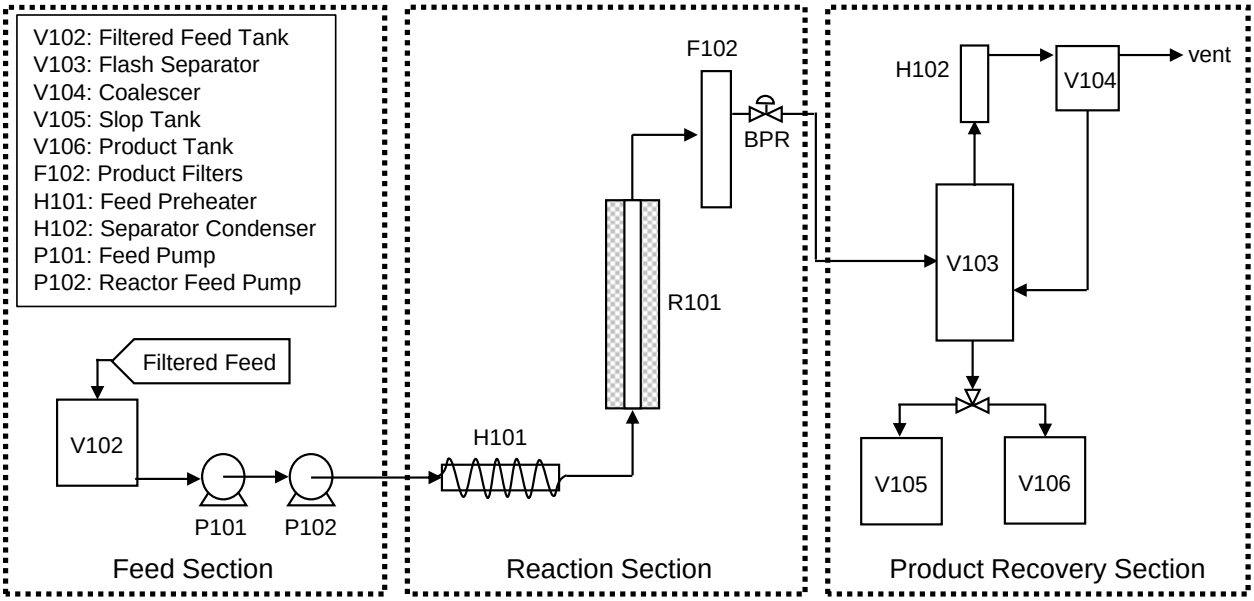

Figure 3.1 Schematic of the in-house visbreaking lab scale plant.

Feed Section

The lab-scale plant includes a batch filtering system to reduce the amount of solids in the sample below a 2% weight recommended by the manufacturer. Since both Athabasca WC-B-A3 samples have a low solids content (0.3% in weight) this section was not used and is not discussed further. The feed section consists of a filtered feed tank and two pumps with the following specifications:

- The Filtered Feed Tank (V102) is an 11 L stainless steel vessel equipped with a heating mantle (electrically heated from an external power source). The tank is also equipped with a port through which nitrogen can be injected. An internal thermocouple is placed inside the tank to monitor the temperature of the feedstock and two wall thermocouples are used to control the heating mantle. .

- The Filtered Feed Pump (P101) is a Liquiflo Model H3FL3333500000US 3-Series Magnetic Drive positive displacement pump. A pressure relief valve sets a maximum pressure of 1 MPag.
- The Reactor Feed Pump (P102) is a Teledyne Isco 500HV high pressure syringe pump which operates in continuous flow mode with flow rates ranging from < 1 μL/min to 204 mL/min with a maximum operating pressure of 26 MPag. The accuracy of the flow rate is ± 0.5% of the set point.

Reactor Section

This section includes a pre-heater, tubular reactor, product filters, and pressure control valve with the following specifications:

- The Preheater (H101) consists of a Watlow electric heater residing inside an aluminium casing. The tube length is 40 cm and the maximum voltage is 500 V. Temperature is controlled using two thermocouples, one inside the apparatus to monitor its temperature and one at the outlet to measure the temperature of the fluid exiting the preheater.
- The Reactor (R101) is a Hastelloy C276 reactor tube surrounded by an electrically heated furnace (ATS Series 3210). The reactor tube is 68.5 cm long and has an internal diameter of 1.27 cm. The furnace consists of three electrically heated zones each using a nichrome wire fixed inside a ceramic shell with a maximum temperature limit of 550°C. The reactor has three equidistantly located side ports, one for each zone, where thermocouples are attached to measure the reactor wall temperature. Pressure transducers are located at the inlet and at the outlet of the reactor.
- The Product Filter (F102) consists of two high pressure mini tee-type Series 4100 filters operating in parallel. The cartridge is a 304 stainless steel woven wire mesh (10 micron absolute).
- Pressure is controlled with a back pressure regulator at the exit of the Product Filter. Nitrogen pressure is used to control the set point.
- The first 37 inches of tubing downstream of the reactor are bare (no heating tape or insulation) to promote quenching.

Product Recovery Section

This section is used to separate and recover the visbroken products and consists of a flash separator, a slop tank, and a sample chamber.

- The Flash Separator (V103) is a 316 stainless steel vertical vessel with a capacity of 0.9 L (0.052 m I.D. and 0.4 m length). The maximum allowable operating conditions are 1.2 MPag and 100°C. Pressure is controlled by a pressure control valve placed on the vapour outlet line.
- The Slop Tank (V105) and Product Tank (V106) are cylindrical stainless steel vessels with capacities of 11.4 L and 1.25 L, respectively, and are rated for a maximum temperature of 100°C. They are each equipped with a nitrogen port and vent port at the top of the vessel.

3.2.2 Experimental Procedure

The Filtered Feed Tank (V102) was loaded with WC-B-A3 bitumen at ambient conditions. The tank was purged of oxygen by injecting nitrogen with the lid slightly open for over ten minutes. The tank was then sealed and nitrogen injection proceeded until the pressure reached 70 kPag. The tank and all lines in the feed section were later set to 60°C to reduce feedstock viscosity and facilitate flow.

The feedstock was pumped through the Filtered Feed Pump (P101) to the Reactor Feed Pump (P102) at a pressure approximately 420 kPag. This pump was set to operate on continuous flow mode at a flow rate specified to obtain the desired residence time inside the reactor. Residence times of 10 and 20 minutes were achieved by using flow rates of 8.7 and 4.3 mL/min, respectively. A pressure relief valve downstream of the Reactor Feed Pump ensured a maximum system pressure of 7.6 MPag.

The fluid was pumped through the pre-heater (H101), set at a temperature of 250°C, and then to the reactor (R101) where visbreaking took place at the set reaction temperature (from 420 to 440 °C). The pressure was monitored using the pressure transducers located at the inlet and at the outlet of the reactor. The temperature was monitored using three thermocouples located along the length

of the reactor tube. The visbreaker was considered to have reached a steady state when the temperature variations were within ± 0.5% of the set point for 10 minutes. Once stabilized, the product lines were purged with at least three line volumes of stabilized visbroken fluid to ensure representative sample collection.

The fluid exiting the reactor was rapidly quenched in a non-insulated line and then passed through the product filters (F102) to remove any residual coke generated during reaction. The back pressure regulator, located downstream, was set to 6.5 MPag, ensuring that the fluid remained in the liquid phase throughout the reactor.

The reacted product then entered the Flash Separator (V103) where the pressure was reduced to 0.1 MPag. The gas stream from this separator was vented since gas sample collection was beyond the scope of this study. The liquid product was sent to the Slop Tank (V105) until the visbreaking process stabilized and product lines were purged with stable reacted fluid. Then, the liquid product was redirected to the Liquid Product Tank (V106) and purged with nitrogen at a pressure of 0.07 MPag prior to product collection and analysis.

3.3 Fractionation Methods

All of the Athabasca whole oils were initially distilled using a Spinning Band Distillation apparatus as described in Section 3.3.1. This step was not performed on the Middle East samples where the amount of volatiles was too low to separate by distillation. Simulated distillation was performed on all samples, as described in Section 3.3.2. The distillation residue (+375°C) was further separated into saturate, aromatic, resin and asphaltene (SARA) fractions using the methodology described in Section 3.3.3.

3.3.1 Spinning Band Distillation (SBD)

A spinning band distillation (SBD) apparatus was used to distill all of the Athabasca feedstock and visbroken whole oils. The SBD apparatus (B/R Instrument Corporation, BR 36-100 mini distillation system) is shown in Figure 3.2. It includes a 200 mL round bottomed boiling flask, a spinning band column, a heating mantle, an automatic reflux valve, two thermocouples, a vacuum

pump, a condenser, and four 40 mL distillate receivers. The spinning band column is a Monel type with an internal diameter of 8 mm and a length of 45 cm. The first thermocouple is set inside an adapter connected to the bottom flask to measure the fluid temperature. The second thermocouple is set at the top of the column to measure the vapour temperature. The apparatus inputs such as heating rate, pressure and reflux ratio are controlled by the B/R Instrument distillation software.

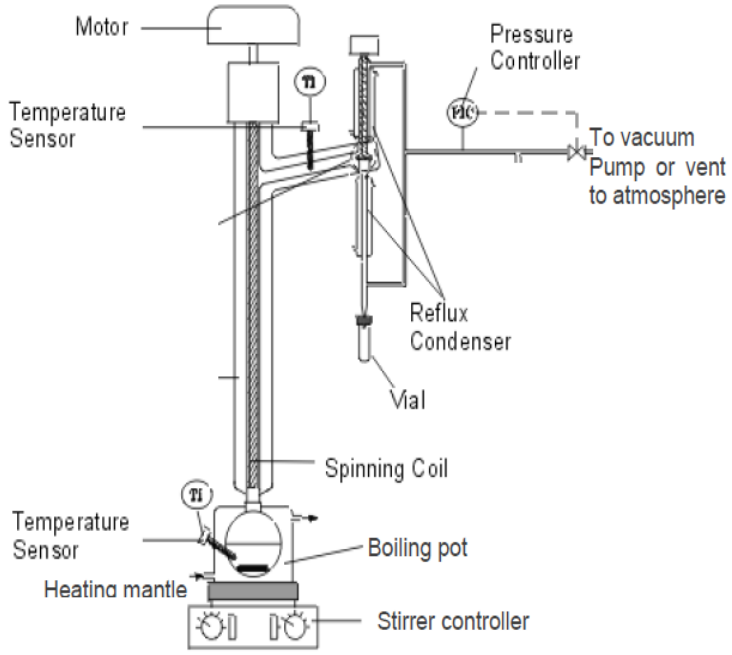

Figure 3.2 Schematic of spinning band distillation apparatus (Powers, 2014).

To start the procedure, the condenser temperature and the operating pressure were set at 5°C and 3 mmHg, respectively, and a known mass of bitumen (approximately 120 g) was added to the bottom flask. The sample was heated with constant stirring at an initial heating rate of 15%. When the first liquid drop was visible exiting the condenser, the spinning band was rotated, and the heating rate was increased such that a drop rate of 1 per second could be maintained. Equilibration between vapor and liquid was monitored in the software until the liquid and vapor temperatures curves reached a plateau. Once, 10 minutes of equilibrium time was complete, the reflux valve was opened, and the distillates were collected in the assigned receiver. Each cut was collected until the collection rate slowed and the color of the collected material started to change. Then, the temperature was raised, and the next cut collected. Throughout the distillation, the heating rate was

manually increased such that the liquid and vapor temperature curves were parallel to each other. This procedure was terminated when the sample flask reached 300°C to avoid cracking the sample.

Before applying this procedure to visbroken samples, an initial topping was performed at 100 mmHg following the same methodology. This topping was done to avoid light distillates drowning the column when the pressure was reduced to 3 mmHg. An average 2% weight loss was obtained during all distillation assays, which was assigned to the distillate fraction.

The vapor temperature was converted to atmospheric equivalent temperature using the Maxwell-Bonnell inter-conversion method for reduced distillations (Riazi, 2015). The normal boiling point is calculated as follows:

$$T_b = \frac{748.1\ QT}{1 + T * (0.3861\ Q - 0.00051606)} \tag{3.2}$$

$$Q = \frac{5.994296 - 0.972546 \log_{10} P}{2663.129 - 95.76 \log_{10} P} \tag{3.3}$$

where T_b is the atmospheric equivalent temperature in K, T is the vacuum vapour temperature in K, and P is the vacuum pressure in mmHg.

3.3.2 Simulated Distillation (SimDist)

Simulated distillation (SimDist) is a gas chromatographic method where boiling points are determined from correlations to the measured retention times. The output is a boiling point curve against weight percentage distilled. Extended SimDist (ASTM D7169) was carried out by Core Laboratories Canada Ltd. (Calgary) on the entire development dataset (WC-B-A3 feed and five reacted samples). The SINOPEC Research Institute and the University of Alberta provided SimDist assays for the samples they each supplied (ME-VR-A1, WC-B-A4 and their reacted products). The repeatability of this assay is ±7 °C (ASTM Standard D7169, 2018).

3.3.3 SARA Fractionation

Further fractionation of the distillation residue into saturates, aromatics, resins and asphaltenes was performed using a modified ASTM D4124 method (Alboudwarej *et al.,* 2002). First, the

asphaltene and solids were precipitated from the whole residue. Then, the solids were removed from the asphaltenes by toluene dilution and centrifugation. Finally, the de-asphalted residue (maltenes) was fractionated using liquid chromatography into saturates, aromatics and resins. Each of these steps is described in detail below.

Asphaltene Precipitation:

To precipitate asphaltenes from a vacuum residue, *n*-pentane was added to approximately 40 g of the residue at a 40:1 volume/weight (mL/g) ratio. The solution was sonicated for 60 minutes or until completely dissolved. After a total contact time of 24 hours, approximately three quarters of the mixture was filtered through a VWR GR413 filter of diameter of 25 cm. This procedure removed solvent and dissolved bitumen but not the precipitated asphaltenes. Then an amount of *n*-pentane equal to 10% of the initial volume of *n*-pentane was added to the mixture remaining in the beaker. This solution was sonicated for 90 minutes, left to settle for 16 hours, and all of the solution including the asphaltenes was filtered using the same filter paper. The filter cake was then washed three times a day over 6 days with approximately 25 mL of *n*-pentane for each wash until the effluent was colourless.

The filter cake was left to dry in the fume hood for four days and then placed inside a vacuum oven at 60°C until constant weight was obtained. The dried residue was termed "C5-Asphaltenes+Solids." The asphaltene+solids content is the mass of residue divided by the original mass of the oil sample and the repeatability of the asphaltene content was +/- 0.15 wt%.

The filtrate consisted of *n*-pentane and de-asphalted residue (maltenes). The maltenes were separated from the *n*-pentane using a rotary evaporator. The maltenes were left to dry in a fumehood for three days and then in a 60 °C vacuum oven until their mass was constant. The material recovered from the filtrate is termed "C5-Maltenes". The light end losses from the maltenes from the residues were negligible; the material balance of the asphaltenes and maltenes products versus the whole residue feed closed to within the error of the measurements in all cases.

Toluene Insoluble Solids Removal:

Solids were removed from the asphaltenes by initially adding 200 mL of toluene to 2 g of "Asphaltene+Solids". The solution was sonicated for 20 minutes, and left to settle for 60 minutes. This solution was then divided into plastic tubes and each was centrifuged at 4000 RPM for 6 minutes. The supernatant was filtered through a Grade #42 Whatman paper at vacuum and decanted into a 200 mL beaker. The toluene-insoluble solids collected at the bottom of the tubes and in the filter cake. All tubes and filter cakes were left in a fume hood to dry for five days. In addition, the filtercakes were later placed to a vacuum oven at 60°C until constant weight was obtained. The dried weights of each were recorded and the solids content was calculated gravimetrically. The solids were termed "Toluene Insolubles" (TI). The TI content is the mass of TI over the mass of C5-Asphalenes+Solids. The solids free asphaltene "C5-Asphaltenes" content was calculated as the difference between the C5-Asphaltene+Solids and TI contents.

Chromatographic Separation of Maltenes into Saturates, Aromatics and Resins:

The SARA fractionation apparatus consists of three liquid chromatography glass columns. Two upper columns were each packed with approximately 150 g of activated Attapulgus clay. The lower column was packed with approximately 250 g of activated silica gel. Separation was performed by means of adsorption: saturates passed through both columns, aromatics adsorb on silica gel, and resins adsorb on Attapulgus clay.

The experiment is started by preparing two flasks each with 5 g of maltenes diluted in 25 mL of *n*-pentane and sonicated for 20 minutes. One of the upper columns was connected to the lower column and the upper column was wet with 25 mL of *n*-pentane. Then, one of the maltenes+n-pentane solutions was poured into the upper column followed by 480 mL of *n*-pentane. The procedure was then repeated on the second upper column. The saturates and *n*-pentane that passed through both columns were collected in a flask. Next, mixtures of *n*-pentane and toluene (50 vol% of each) were prepared and used to elute the aromatics. The elutions were performed with the upper and lower columns connected and a total of 800 mL of each solvent mixture was used for each upper column. The elutions were collected in a flask. The lower column was then connected to a Soxhlet apparatus and refluxed with 250 mL of toluene for two hours to remove any residual

aromatics. The two upper columns were then connected and eluted twice with a mixture of acetone and toluene (200 mL:200 mL) to remove the resins. The elutions were collected in another flask. The solvents were removed from each diluted fraction in a rotary evaporator and then in a vacuum oven at 60°C until their mass was constant. Each recovered saturate, aromatics, and resin fraction was weighed, and the SARA composition of the sample determined.

3.4 Property Measurements

Whole oil density and viscosity were measured using a capillary viscometer method as described in Section 3.4.1. This method required at least 300 mL of sample and is therefore impractical for the small volumes of the fractions. Instead, the density of these fractions was measured using an atmospheric density meter as shown in Section 3.4.2. Their viscosity was measured using a Cone and Plate Rheometer as discussed in Section 3.4.3. Finally, molecular weight measurements for the whole oils were performed with a Vapour Pressure Osmometer as described in Section 3.4.4.

3.4.1 Viscosity and Density from a Capillary Viscometer Apparatus

When at least 300 mL of sample were available (whole oils), the viscosity and density were measured over a range of temperatures and pressures using a capillary viscometer equipped with an Anton Paar DMA HPM density meter, Figure 3.3. The viscometer includes two capillary tubes, two 350 mL transfer vessels, a Quizix SP-5200 pump, two pressure transducers, a back pressure regulator, and an air bath. The first capillary tube has an internal diameter of 6.35 mm and a length of 1 m. The second tube has an internal diameter of 1.4 mm and a length of 12 m. The pump capacity ranges from 0.01 to 15 mL/min with a precision of ±0.005 mL/min. The low pressure transducer is a Rosemount 1151 rated for 39.3 kPa with a precision of ±0.07 kPa. The high pressure transducer is a Rosemount 3051S rated for 2298 kPa with a precision of ±0.7 kPa. The absolute pressure was set using a back pressure regulator, monitored with a Bourbon gauge with a precision of ±0.05 MPa. The temperature was controlled by the air bath to within ±0.25 °C. The apparatus can operate from ambient conditions up to 180 ºC and 10 MPa.

To perform the measurements, the sample was loaded into one of the cylinders and the temperature and pressure were set to the target conditions. The sample was flowed back and forth through the

capillary tubes to ensure homogeneity, as indicated by consistent pressure drop readings. Once all lines were filled and homogeneous, the sample was pumped at five different flow rates through one of the capillary tubes. The differential pressure was measured at each flow rate with the pressure transducer. After the final flow rate, the flow was stopped and the density was measured. Then the temperature and/or pressure were set to the next condition and the procedure was repeated.

The viscosity at each condition was determined based on the Hagen-Poiseuille equation for laminar Newtonian fluid flow rate through a circular pipe, which for fixed pipe dimensions is given by:

$$Q = \frac{K}{\mu}\Delta P \tag{3.4}$$

where Q is the flow rate, K is a calibration constant, μ is the viscosity, and ΔP is the pressure drop. The flow rate is plotted versus the pressure drop and the viscosity is determined from the slope. The linearity is checked to confirm the laminar Newtonian flow assumption. The capillary viscometer was calibrated with *n*-heptane, toluene, and Canon Instruments calibration standards S20, S30000 and N450000. The repeatability of the viscosity was ±3% (Motahhari, 2013).

Density was measured directly with the Anton Paar density meter. The density meter was calibrated over the full range of temperatures and pressures with water and nitrogen. The repeatability of the density was ±0.5 kg/m³ (Motahhari, 2013).

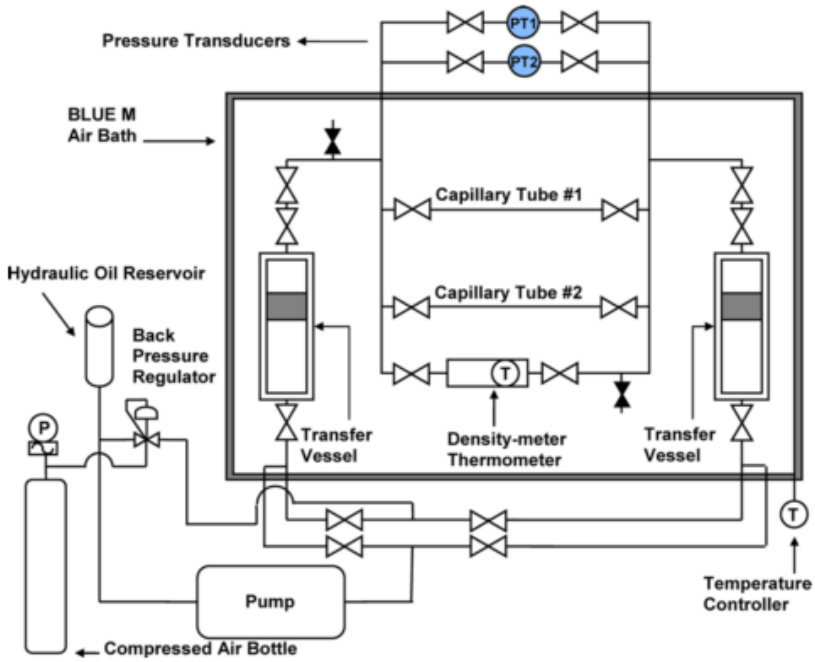

Figure 3.3 Capillary viscometer apparatus schematic (Ramos-Pallares *et al.*, 2015).

3.4.2. Viscosity from Cone and Plate Rheometer

The viscosity of the fractions was measured with an Anton Paar MCR-52 Cone and Plate Rheometer, Figure 3.4. This apparatus is a controlled shear rate rheometer with a Searle type sensor system. The torque (proportional to the shear stress) was measured at a value of angular velocity (proportional to shear rate) by a spring attached to the rotor while the lower plate remained stationary. The operating limits are atmospheric pressure, temperatures from 10 to 200°C, shear rates from 1 to 750 s^{-1}, and a maximum torque of 200,000 μN·m. The rheometer was calibrated to Canon Instrument standards S020, S600, S30000 and N450000, with an AARD of 4% and an MARD of 8%.

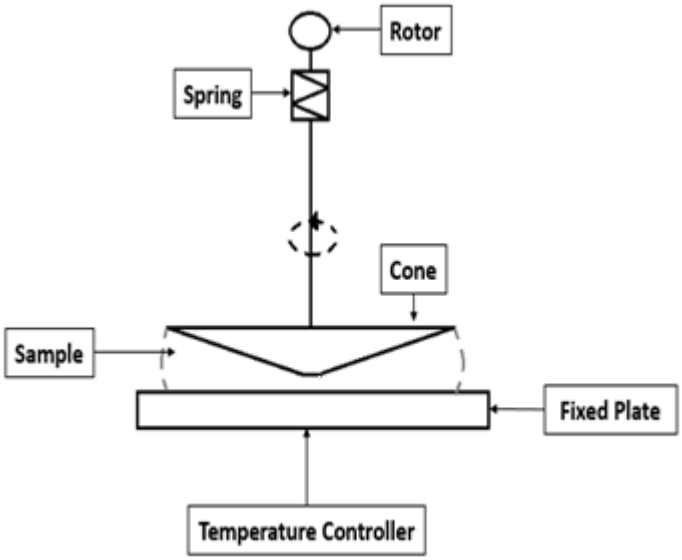

Figure 3.4 Cone and Plate Rheometer schematic.

3.4.3. Density

The density of fractions was measured using an Anton Paar DMA 4500M density meter at atmospheric pressure and temperatures up to 90°C. The instrument was calibrated using air, toluene and reverse osmosis water. The distillates, saturate and aromatic densities were measured directly. The precision and repeatability of this apparatus are ± 0.01 kg/m³ and ± 0.05 kg/m³ respectively.

3.4.4. Molecular Weight

The molecular weights of the SARA fractions were reported elsewhere (Rodriguez, 2018). The molecular weights of the whole crude oils were measured with a Jupiter Model 833 Vapour Pressure Osmometer. All measurements were performed at 50°C with toluene as the solvent. Solutions of 65, 30, 15, 5 and 2 mg oil /mL toluene were prepared for each measurement.

To perform a measurement, a droplet of pure solvent and a droplet of solution are injected onto the two respective thermistors. The vapour pressure difference between pure solvent and solution causes a change in temperature, generating a voltage differential between the thermistors which is

then measured and recorded. The voltage is related to the molecular weight of the solute by the following equation (Powers *et al*., 2016):

$$\frac{\Delta V}{C_2} = K\left(\frac{1}{M_2} + A_1 C_2 + A_2 C_2^{\,2} + \ldots\right) \tag{3.6}$$

where ΔV is the voltage difference between the thermistors, C_2 the solute concentration, K is a proportionality constant from calibration, and A_1 and A_2 are coefficients taking into account solution non-ideal behaviour. In most cases, at low concentrations, most of the higher order terms become negligible, and Eq. 3.6 reduces to:

$$\frac{\Delta V}{C_2} = K\left(\frac{1}{M_2} + A_1 C_2\right) \tag{3.7}$$

For an ideal system, the second term in Eq. 3.7 is zero and $\Delta V/C_2$ is constant. In this case, the molecular weight is given by:

$$M_2 = \frac{K}{\left(\Delta V \diagup C_2\right)} \tag{3.8}$$

For the calibration, the molecular weight of the solute is known, and the proportionality constant, *K*, is calculated by extrapolation of a plot of $\Delta V/C_2$ versus C_2 to zero concentration as per Eq. 3.7. For a non-ideal solution with an unknown solute, the molecular weight is calculated from the intercept of a plot of $\Delta V/C_2$ versus C_2 this time solving for M_2. For an ideal solution with an unknown solute, the molecular weight is calculated at each concentration from Eq. 3.8 and then averaged.

The instrument was calibrated with sucrose octaacetate (679 g/mol) and validated using octacosane (395 g/mol). The measured molecular weight during calibration was within 3% of the actual value. The molecular weight of the whole oil was calculated at each concentration and averaged; that is, an ideal solution was assumed (Eq. 3.8).

3.4.5. Micro Carbon Residue

The micro carbon residue (MCR) analysis (ASTM D4530) was carried out by Core Laboratories Canada Ltd. (Calgary) on the entire development dataset (WC-B-A3 feed and five reacted samples). The SINOPEC Research Institute provided micro carbon residue data for the samples they supplied (ME-VR-A1 and their reacted products). In the ASTM D4530 procedure, the sample is heated at a rate of 10-15 °C/min to 500°C under continuous nitrogen purging. Once a residence time of 15 minutes at 500°C is achieved, the residue is rapidly quenched and weighed. The MCR is the mass of residue divided by the mass of original sample.

Chapter 4: Methodology

This chapter presents the methodology used to adapt the Expanded Fluid (EF) viscosity model to visbroken bitumen. The methodology to characterize the oils into pseudo-components is outlined. The EF model is presented and the handling of its key input, density, is discussed. Finally, the processing of the measured data into the inputs required to develop and test correlations for the viscosity model parameters is described.

4.1. Oil Characterization

The oil characterization methodology was developed to be consistent with the methodology used in the Symmetry commercial process simulator (Hay, 2018). This software divides the oil into pseudo-components as a series of boiling point cuts each subdivided into saturates, aromatics, resins, and asphaltenes (SARA) fractions. In this way, both volatility and chemical family distributions are represented. Each pseudo-component is assigned a group of representative molecules matching both bulk and fraction physical properties. A reaction model is used to obtain the representative molecules of the visbroken product. Each molecule in the product is assigned to the boiling cut and SARA fraction that matches its properties and a new distribution of pseudo-components is generated.

There are simply too many pseudo-components in this methodology to experimentally determine their properties in a reasonable time. Instead, the oil was characterized into boiling point cuts for the distillable fraction of the oil (-370°C) and into SARA fractions for the distillation residue, as shown in Figure 4.1. Since the focus is on viscosity prediction, the required model inputs are the boiling point curve, mass fraction of the distillates, the mass fraction of the SARA fractions, and the density and viscosity model parameters of the distillates and each SARA fraction.

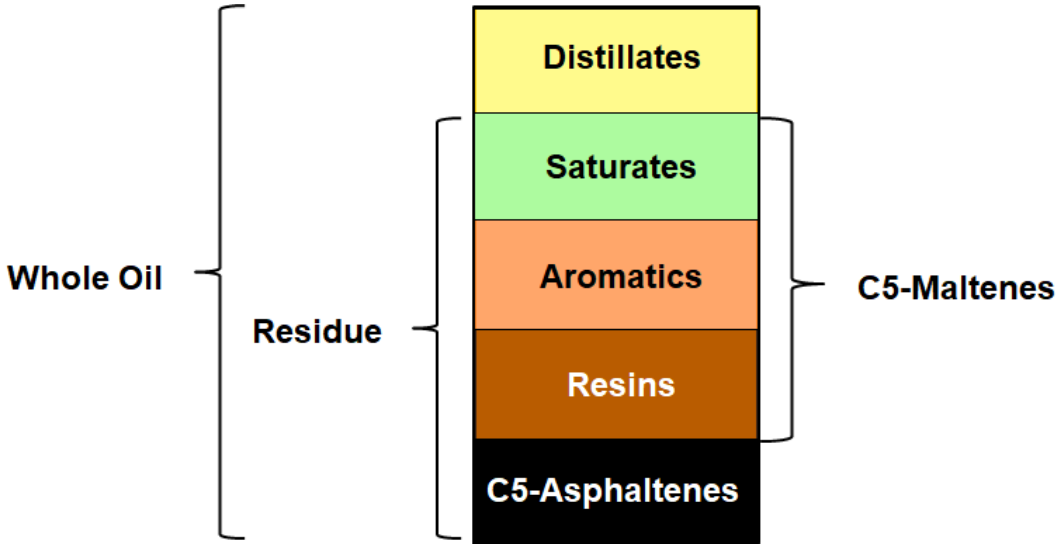

Figure 4.1 Oil fractions used in characterization methodology.

4.2. Viscosity and Density Prediction

4.2.1. Expanded Fluid (EF) Viscosity Model

The complete model for unreacted oils is described below and then the simplifications and updates to the model required for visbroken oils are discussed. The EF model is based on the observation that the viscosity of a fluid decreases as it expands from a compressed state of infinite viscosity until it reaches the gas state. Therefore, the viscosity of the fluid can be expressed as a departure from the dilute gas viscosity with the following equations (Yarranton and Satyro, 2009):

$$\mu - \mu_G = 0.165\{exp(c_2\beta - 1)\} \tag{4.1}$$

$$\beta = \frac{1}{exp\left\{\left(\frac{\rho^*}{\rho}\right)^{0.65} - 1\right\} - 1} \tag{4.2}$$

$$\rho^* = \frac{\rho_s^0}{[exp(-c_3\,|P - P_0|)]} \tag{4.3}$$

where μ is the viscosity, μ_G is the dilute gas viscosity, ρ is the density, P is the pressure and P_0 is the atmospheric pressure. The model has three fluid specific parameters: ρ_s^o is the compressed state density of the fluid in a vacuum; c_2 dictates the magnitude of the viscosity response to

expansion, and; c_3 dictates the magnitude of the viscosity response to pressure. This model is valid only for Newtonian single phase fluids and is applicable throughout the entire phase diagram.

The dilute gas viscosity can be calculated using Yaws (2008) equation:

$$\mu_G = A_0 + B_0 T + C_0 T^2 + D_0 T^3 \tag{4.4}$$

where T is the temperature in K and A_0, B_0, C_0 and D_0 are pure component specific parameters from Yaws's Handbook (Yaws, 2008).

Mixing Rules

For multicomponent systems, the following mass-based mixing rules were developed (Motahhari *et al.*, 2011):

$$\rho^o_{s,mix} = \left(\sum_{i=1}^{nc} \sum_{j=1}^{nc} \frac{w_i w_j}{2} \left(\frac{1}{\rho^o_{s,i}} + \frac{1}{\rho^o_{s,j}} \right) (1 - \propto_{ij}) \right)^{-1} \tag{4.5}$$

$$\frac{c_{2mix}}{\rho^o_{s,mix}} = \sum_{i=1}^{nc} \sum_{j=1}^{nc} \frac{w_i w_j}{2} \left(\frac{c_{2,i}}{\rho^o_{s,i}} + \frac{c_{2,j}}{\rho^o_{s,j}} \right) (1 - \propto_{ij}) \tag{4.6}$$

$$c_{3mix} = \left(\sum_{i=1}^{nc} \frac{w_i}{c_{3,i}} \right)^{-1} \tag{4.7}$$

where w_i and w_j are the mass fractions of the components and $\propto_{ij}$ is the binary interaction parameter. Ramos-Pallares *et al.* (2015) related the interaction parameter with the specific gravity (SG) and hydrogen to carbon ratio (H/C) using the following correlation:

$$\propto_{ij} = \propto_{ij}{}^{\circ} - \Delta \propto_{ij} \tag{4.8}$$

where $\propto_{ij}{}^{\circ}$ is the reference function given by:

$$\propto_{ij}{}^{\circ} = 0.021 \qquad \text{when } \Delta SG_{norm} \leq 0.165 \tag{4.9}$$

$$\propto_{ij}{}^{\circ} = 0.038304 - 0.10478 \Delta SG_{norm} \quad \text{when } \Delta SG_{norm} > 0.165 \tag{4.10}$$

$$\Delta SG_{norm} = \frac{2(SG_i - SG_j)}{SG_i + SG_j} \tag{4.11}$$

$\Delta \propto_{ij}$ is the departure function and is given by:

$$\Delta \propto_{ij} = 0.02756 - 0.1103 \Delta (H/C)_{norm} \quad \text{when } \Delta (H/C)_{norm} \leq 0.25 \tag{4.12}$$

$$\Delta\propto_{ij} = 0 \qquad \text{when } \Delta(H/C)_{norm} > 0.25 \tag{4.13}$$

$$\Delta(H/C)_{norm} = \frac{2((H/C)_i - (H/C)_j)}{(H/C)_i + (H/C)_j} \tag{4.14}$$

The dilute gas viscosity of the mixture is calculated using Wilke's equation (Wilke, 1950):

$$\mu_{G,mix} = \sum_i^{nc} \frac{x_i \mu_{G,i}}{\sum_j^{nc} x_i \emptyset_{ij}} \tag{4.15}$$

$$\emptyset_{ij} = \frac{\left[1 + \left(\mu_{G,i}/\mu_{G,j}\right)^{0.5}\left(M_j/M_i\right)^{0.25}\right]^2}{\left\{8\left[1 + \left(M_i/M_j\right)\right]\right\}^{0.5}} \tag{4.16}$$

where x_i is the molar fraction and M_i is the molecular weight. For crude oils systems where the dilute gas viscosity parameters are not available, these parameters are taken as the *n*-alkane with the closest molecular weight (Motahhari *et al.*, 2013).

Fluid Specific Parameters

Yarranton and Satyro (2009) provided a list of fluid specific parameters for commonly encountered pure components. However, crude oils are typically characterized into a set of pseudo-components that represent the property distributions within the oil. Correlations are used for the fluid specific parameters of these pseudo-components. The parameter c_3 for each pseudo-component is calculated as follows (Motahhari *et al.*, 2013):

$$c_3 = \frac{2.8 \cdot 10^{-7}}{1 + 3.23exp(-1.54 \cdot 10^{-2}M)} \tag{4.17}$$

where M is the molecular weight of the pseudo-component.

Ramos-Pallares *et al.* (2016) developed a methodology to estimate the c_2 and ρ_s^o parameters of unreacted crude oils based on a distillation assay. The pentane insoluble asphaltenes and the maltenes are characterized separately. The asphaltenes are treated as a single pseudo-component with the following fluid specific parameters:

$$c_2 = 0.9057$$

$$\rho_s^{\circ} = 1113.7\ kg/m^3$$

The maltene fraction is first divided into pseudo-components of known TBP and their properties, such as specific gravity and molecular weight, are determined from correlations (Riazi, 2005). The EF parameters (c_2 and ρ_s^o) are then calculated as follows:

$$c_2 = A\left(1 - \frac{T_b}{1435.73}\right)^{-1} exp\left(\frac{T_b}{410.21}\right) + B \tag{4.18}$$

$$\rho_s^0 = \rho_T \left[1 + ln\left(1 + \frac{C_2}{ln\left(1 + \frac{\mu_{37.7} - \mu_G}{0.165}\right)}\right)\right]^{1/0.65} \tag{4.19}$$

where $\mu_{37.7,}$ A and B are defined as:

$$ln\left(\frac{\mu_{37.7}}{\rho_{37.7}} + \frac{250}{T_b}\right) = ln\left({v_{37.7}}^0 + \frac{250}{T_b}\right)\left(\frac{1+2f}{1-2f}\right)^2 \tag{4.20}$$

$$f = 1.8152|x|\delta - 17.449\frac{\delta^2}{{T_b}^{0.5}} \;\; , \; x = 2.3625 - \frac{51.588}{T_b^{0.5}} \tag{4.21}$$

$$\delta = (1.5819 - 2.0124 * \Delta SG)\exp\left(10651.1T_b^{-1.335}\right) * \Delta SG^2 \tag{4.22}$$

$$A = 0.02135 - 0.0554\Delta SG \tag{4.23}$$

$$B = 0.1417 - 0.0521\Delta SG \tag{4.24}$$

$$\Delta SG = SG - SG_{alkane} \tag{4.25}$$

$$log[log({v_{37.7}}^0 + 1)] = (0.0036T_b - 2.0942)0.95^{T_b/200} \tag{4.26}$$

The density of the pseudocomponents at 37.7°C is calculated using the Rackett correlation (Rackett, 1970). The dilute gas viscosity of the pseudo-component, μ_G, is calculated as the dilute gas viscosity of the *n*-alkane with the closest molecular weight.

This approach predicted the viscosities of 14 sets of unreacted heavy oils with an AARD of 41%. The deviation was reduced to 21% when one parameter (c_2 or ρ_s^o) was tuned to a single viscosity data point, and to 7% when both parameters were tuned to 2 viscosity data points (Ramos-Pallares *et al.*, 2017). The model is sensitive to the value of ρ_s^o; a 1% variation in ρ_s^o increases the AARD by approximately 800%. The same variation in c_2 increases the AARD by 10%.

Adapting the EF Model for Visbroken Material

To adapt the model for visbroken fluids, the effect of visbreaking on the input parameters must be considered. The input parameters are the pressure, density, dilute gas viscosity, and the fluid specific parameters for each pseudo-component. The pressure is measured and the density of the fluid is measured or determined from the measured and fitted densities of the pseudo-components. The dilute gas viscosity can be neglected because bitumen and the visbroken products have high viscosities compared to dilute gases. The effect of visbreaking on the fluid specific parameters are discussed in Chapter 5. Once the component properties are determined, the existing mixing rules are used to obtain the density and viscosity of the visbroken oils. The effect of visbreaking on the binary interaction parameters in the viscosity parameter mixing rules is discussed in Chapter 5.

4.2.2. Density

The key input for the viscosity model is the density of the fluid or of each component in the fluid. In this thesis, only atmospheric pressure is considered but the effect of temperature on density was required because in some cases viscosities were measured at different temperatures for different oil components. Many of the mixture viscosities (maltenes, residues, whole oils) were measured at different temperatures than the component densities. In this case, the component densities had to be interpolated or extrapolated to the mixture temperature. Density varies linearly with temperature for small ranges and the data were fit with the following linear relationship:

$$\rho = \rho_{REF} + b(T - T_{REF}) \tag{4.27}$$

where ρ is the density, b is the temperature dependence, T the temperature, and subscript *REF* indicates the reference condition.

The density of mixtures was calculated from the component densities using a regular solution approach, given by:

$$\frac{1}{\rho} = \sum \frac{w_i}{\rho_i} \tag{4.28}$$

This mixing rule assumes that there is zero excess volume of mixing. Ramos-Pallares *et al.*, (2016) evaluated the performance of predicted densities with regular solution as EF inputs for heavy oils.

Similar accuracy was obtained in comparison to using measured densities, suggesting this approach is suitable for density recombination applied to EF viscosity prediction.

4.3. Data Processing

The methodology required to obtain the density and viscosity parameters of each fraction is illustrated in Figure 4.2. Each step is described in detail below.

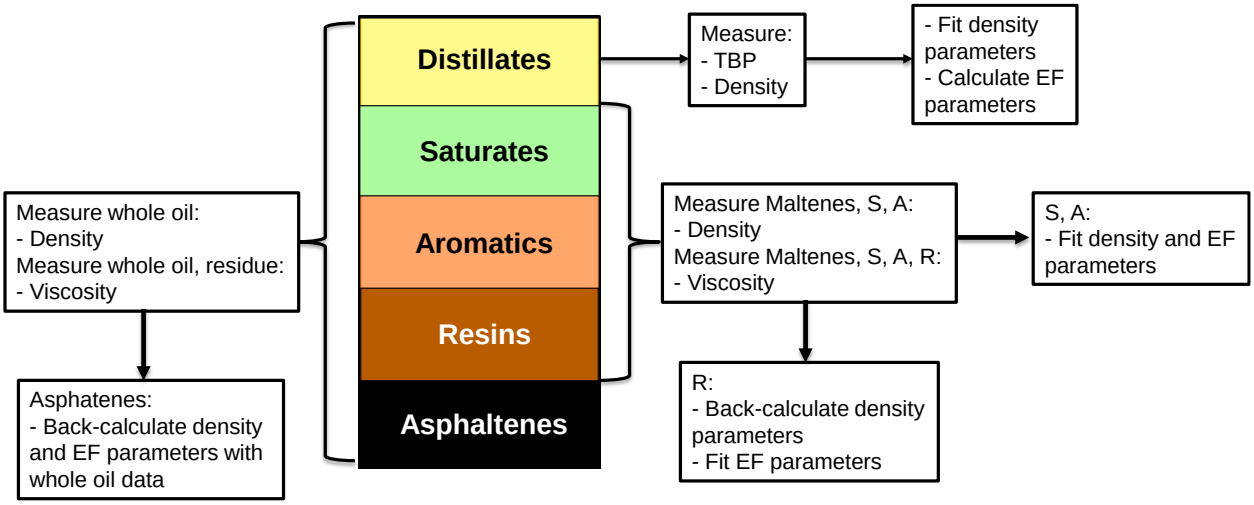

Figure 4.2 Methodology to obtain density and EF parameters for each fraction.

Distillate Properties

The densities of the distillates were measured directly from 10 to 50°C. The boiling point distribution was taken from the SBD distillation assay. Recall that this assay provides true boiling point against cumulative volume distilled. The following iterative procedure was applied to convert from cumulative volume to cumulative mass:

- Set the specific gravity of the whole distillates (initialize outer loop).
- Guess initial molecular weight values for each 2 mL cut (initialize inner loop).
- Use the Sanchez-Lemus correlation (Sánchez-Lemus *et al.*, 2016) to determine the specific gravity of each cut as a function of boiling point and molecular weight.
- Use the modified Soreide correlation (Sánchez-Lemus *et al.*, 2016) to calculate boiling point based on specific gravity and molecular weight.

- Calculate the total sum of square errors between the experimental and calculated boiling points.
- Modify the molecular weight guess to minimize the boiling point sum of square errors (end of inner loop).
- Calculate the sum of square errors between the experimental and calculated specific gravity.
- Modify the specific gravity of the distillates with a single multiplier to the specific gravity sum of square errors (end of outer loop).

The cumulative mass fraction is finally calculated using the distilled volume and calculated density of each cut.

The viscosities of all of the reacted distillates were below the range of the cone and plate rheometer and could not be measured. Instead Equations 4.18 to 4.26 were used to determine the Expanded Fluid parameters based on their density and boiling point distributions. These correlations were developed for unreacted material. It was assumed that the changes in the distillate properties after visbreaking that influence viscosity were sufficiently captured by the changes in boiling point and specific gravity. The correlations were develop based on a wide range of pure components, distillation cuts, and native crude oils. The reacted components within any fraction will differ from the original components but are still species with the range of the materials considered in the original correlation. Therefore, it is expected that the correlations will still apply to the visbroken distillates.

Whole Oils, Residues, Maltenes, and SAR Fractions

The density and viscosity of the whole oils were measured over a range of temperatures and pressures in the capillary viscometer. The density of the C5-maltenes, saturates, and aromatics were measured directly. The viscosities of the resins and residues were too high to allow direct density measurements. Hence their density was obtained using the regular solution approach as follows:

$$\frac{w_{Resins}}{\rho_{Resins}} = \frac{1}{\rho_{Maltenes}} - \frac{w_{Saturates}}{\rho_{Saturates}} - \frac{w_{Aromatics}}{\rho_{Aromatics}} \tag{4.29}$$

$$\frac{1}{\rho_{Residue}} = \frac{w_{Saturates}}{\rho_{Saturates}} + \frac{w_{Aromatics}}{\rho_{Aromatics}} + \frac{w_{Resins}}{\rho_{Resins}} + \frac{w_{Asphaltenes}}{\rho_{Asphaltenes}} \quad (4.30)$$

where *w* and b are the pseudo-component weight fraction and density, respectively.

The viscosity of the distillation residue, C5-maltenes, saturate, aromatic, and resin fractions were measured in the cone and plate rheometer at atmospheric pressure over a limited range of temperatures. The lower temperature was set according to the viscosity of the sample: 10°C for low viscosity samples and at a high enough temperature to obtain a measurable viscosity for high viscosity samples. The upper temperature was set to avoid the evaporation of volatile components in the cone and plate rheometer. The Expanded Fluid parameters were calculated from the density and viscosity data by minimizing the following objective function:

$$OF = \sum \left[ln(\frac{\mu_{pr}}{\mu_{me}})^2 \right] \quad (4.31)$$

where μ_{pr} is the predicted viscosity and μ_{me} is the measured viscosity.

C5-Asphaltenes Properties

Neither the C5-asphaltenes viscosity nor their density could be measured directly due to the high melting point of these samples (above 200°C). Instead, the density was determined indirectly using the following regular solution approach:

$$\frac{w_{Asphaltenes}}{\rho_{Asphaltenes}} = \frac{1}{\rho_{Whole\ Oil}} - \frac{w_{Distillates}}{\rho_{Distillates}} - \frac{w_{Saturates}}{\rho_{Saturates}} - \frac{w_{Aromatics}}{\rho_{Aromatics}} - \frac{w_{Resins}}{\rho_{Resins}} \quad (4.32)$$

The C5-asphaltene Expanded Fluid parameters were fitted to match residue data when recombined with saturates, aromatics and resins. The fitting of the asphaltenes EF parameters is discussed in more detail in Chapter 5.

Summary of Available Data

The data for WC-B-A3 were used to develop the correlations for the visbroken products and are defined as the Development Dataset. The data for WC-B-A4 and MW-VR-A1 were used to test the proposed model and are defined as the Test Dateset.

Table 4.1 summarizes what data are available for the Development Dataset. The data are tabulated in Appendix A and C. As noted above, the density parameters for distillates, saturates, aromatics, resins and asphaltenes were determined from the measured component properties and from the residue and whole oil densities. The viscosity parameters were determined from the measured component properties and the residue viscosity. The parameter fitting is discussed in Chapter 5 along with the development of the parameter correlations. The maltenes and whole oil viscosity data were not used in any step of the EF parameter estimation and were instead used to test the model mixing rules. The model testing is presented in Chapter 5.

Table 4.1 Summary of what data are available for each fraction.

Property	**Whole**	**Dist**	**Residue**	**Malt**	**S**	**A**	**R**	**Asph**
Density	Yes	Yes	No	Yes	Yes	Yes	No	No
Viscosity	Yes	No	Yes	Yes	Yes	Yes	Yes	No

* Note: Whole = whole oil, Dist = distillates, Malt = maltenes, S = saturates, A = aromatics, R = resins, Asph = asphaltenes.

The same measurements were performed for the Test Dataset except that there were no distillates and no whole oil for the ME-VR-A1 samples because the feedstock was a residue. The data are provided in Appendix A and C and discussed in Chapter 5.

Chapter 5: Results and Discussion

In this chapter, the effect of visbreaking on the composition and physical properties of the whole oil and SARA fractions from the development dataset are presented. Correlations for density and the Expanded Fluid viscosity parameters of each fraction are developed as a function of conversion. A recombination methodology is developed to model the density and viscosity of the maltenes, the distillation residue, and the whole oil. Finally the correlations are tested on an oil from a similar geographical location and another oil from a different region.

5.1. Effect of Visbreaking on Oil Composition and Properties

5.1.1. Conversion and Oil Composition

Two feedstock samples were used for the Development Dataset, both from the same source. Figure 5.1 shows that the Spinning Band distillation assays for both feeds are the same within the error of the measurement (±2°C). Since there was not enough sample to perform the complete characterization of WC-B-A3(1), the amount, composition, and properties of the SARA fractions were assumed to be identical to the those measured for WC-B-A3(2).

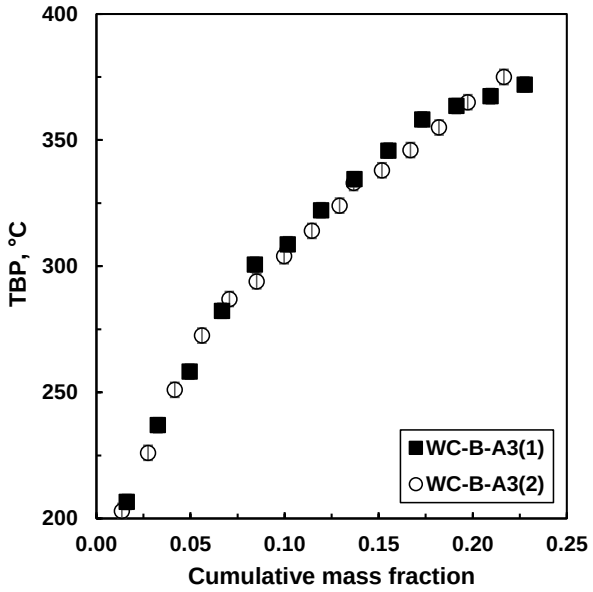

Figure 5.1 Comparison between distillation assays of both Development Dataset feeds.

Recall that spinning band distillation was used to separate the samples into distillate and residue fractions while Extended SimDist was used to calculate conversion. Figures 5.2a and 5.2b compare the two assays for the Athabasca feed and the 19.3% conversion visbroken product, respectively. The assays matched to within the error of the measurement for all samples. The conversion was determined as the relative change of the +524°C SimDist fraction between feed and visbroken product. The reactions conditions and conversions for the Development Dataset are provided in Table 5.1.

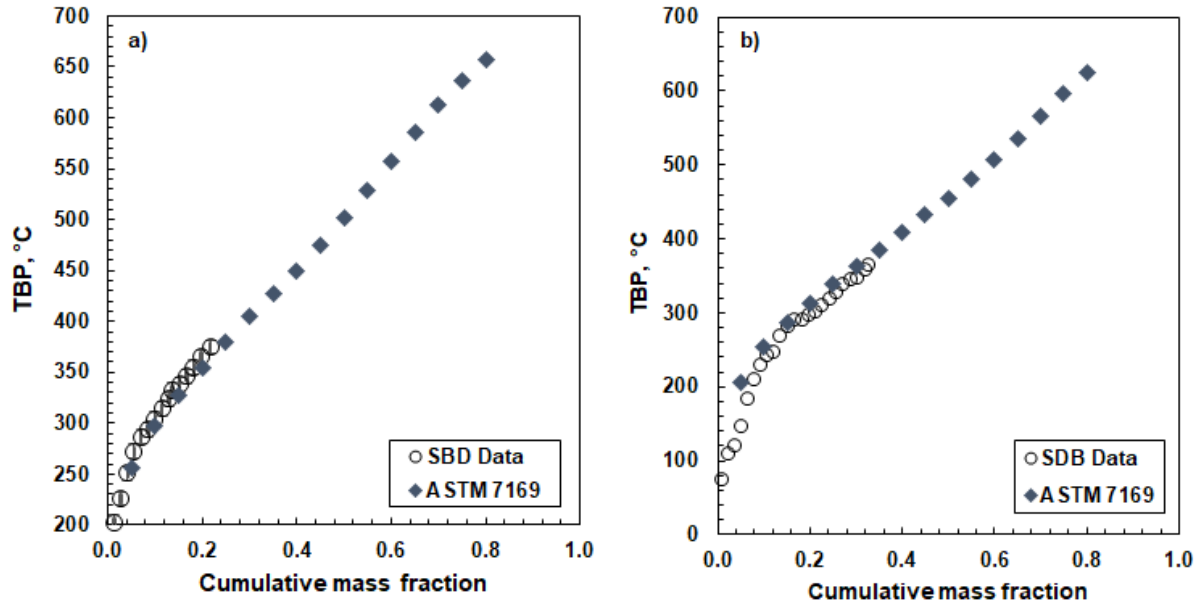

Figure 5.2 Comparison between SBD and ASTM 7169 for: a) WC-B-A3 feedstock; b) WC-B-A3(2)-VIS19.3 visbroken sample.

Table 5.1 Reaction conditions and conversions of the Development Dataset.

Sample	Reaction Conditions	Conversion, %
WC-B-A3	-	-
WC-B-A3(1)-VIS5.1	420 °C, 10 min	5.1
WC-B-A3(2)-VIS4.9	430 °C, 10 min	4.9
WC-B-A3(2)-VIS8.1	440 °C, 10 min	8.1
WC-B-A3(2)-VIS19.3	430 °C, 20 min	19.3
WC-B-A3(2)-VIS38.1	440 °C, 20 min	38.1

Figure 5.3 shows the effect of visbreaking on the boiling point distribution. As expected the curves shifted downwards as reaction severity increased because light products were generated. However, the 10 min products at 420°C and 430°C had almost identical boiling point distributions and conversion. As will be shown later, despite having an almost identical conversion, their physical properties were different. All distillation data collected is provided in Appendix B.

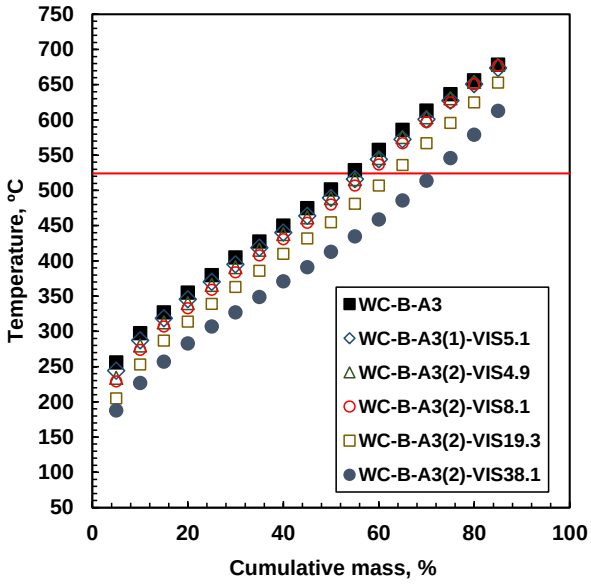

Figure 5.3 Extended SimDist (ASTM D7169) of the feedstock and visbroken products in the Development Dataset. The part of the curve above the horizontal line is the +524°C fraction.

The composition of the feeds and visbroken products are listed in Table 5.2 and shown in Figure 5.4. As expected the distillate yield increased with conversion (Figure 5.4a), suggesting that side-chain fragments from the heavier fractions tend to concentrate in the -370°C range. The toluene insoluble (TI) yield remained nearly constant until the 19.3% conversion point (Table 5.2) and then increased, suggesting that coke was generated at high conversions.

The SARA composition in the distillation residues of the feed and visbroken products are shown in Figure 5.4(b). The proportion of saturates and aromatics did not vary significantly with conversion. The proportion of resins decreased with conversion, particularly at higher conversions.

The proportion of asphaltenes decreased slightly at lower conversions but increased significantly above 8% conversion. The trends are consistent with the removal of alkyl side chains from the heavier aromatic fractions with the fragments becoming part of the distillates. At higher conversion range (above 8%), condensation reactions appear to occur increasing asphaltene yield and eventually forming coke. Similar results were obtained by Carbognani *et al.,* (2007) for an Athabasca vacuum residue. Due to losses during nitrogen purging, the gas yield could not be quantified for the reacted products.

Table 5.2 Composition of the feedstock and visbroken products in the Development Dataset. Compositions were repeatable to ± 0.2, 0.2, 0.7, 0.6 and 0.2 wt% for distillates, saturates, aromatics, resins, asphaltenes and toluene insolubles (TI), respectively.

Sample	**Distillate**	**Saturates**	**Aromatics**	**Resins**	**Asphaltenes**	**TI**
	wt%	**wt%**	**wt%**	**wt%**	**wt%**	**wt%**
WC-B-A3	22.1	9.1	32.5	16.4	19.6	0.3
WC-B-A3(1)-VIS5.1	22.8	9.5	33.1	16.2	18.1	0.3
WC-B-A3(2)-VIS4.9	26.7	8.2	31.5	15.7	17.7	0.2
WC-B-A3(2)-VIS8.1	28.6	8.1	29.8	14.9	18.4	0.2
WC-B-A3(2)-VIS19.3	33.3	8.4	27.8	12.7	17.4	0.4
WC-B-A3(2)-VIS38.1	37.6	6.9	25.1	10	19.1	1.3

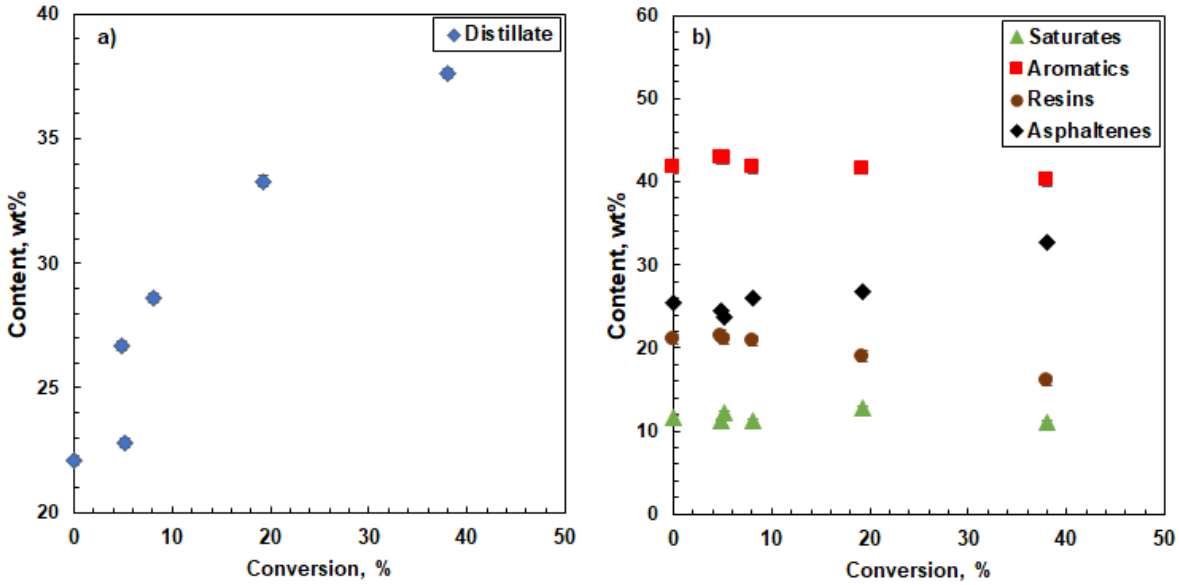

Figure 5.4 Effect of conversion on the Development Dataset feedstock and visbroken product composition: a) distillate content in whole oil; b) saturate, aromatic, resin, and asphaltene contents in the residue.

5.1.2. Physical Properties

Whole Oil

Figure 5.5a shows the change in the relative viscosity of the whole oil feedstock and visbroken products with conversion. Relative viscosity is defined as the visbroken product viscosity divided by the feedstock viscosity. As expected, visbreaking significantly reduced the whole oil viscosity, even at the lower conversion range. Overall, the viscosity decreased from 5370 mPa·s in the feed to 123 mPa·s at the highest conversion.

Figure 5.5b shows the change in specific gravity of the whole oils with conversion. Initially, the specific gravity decreased with increased conversion consistent with increased distillate yield giving a more paraffinic, lower molecular weight crude oil. Above 19% conversion, the trend reversed and specific gravity increased with increased conversion, suggesting increasing aromaticity resulting from condensation reactions in the heavier fractions.

Figure 5.5c shows that the molecular weight of the whole oils decreased monotonically with increased conversion, even at the higher conversions where condensation reactions are expected. It appears that side chain removal has the predominant effect on the average molecular weight.

Figure 5.5d shows that the micro carbon residue (MCR) of the whole oils increased monotonically with conversion. This change is consistent with aromatics shifting to coke precursors as reactions take place. There was a significant increase in MCR above 19% conversion where the condensation reactions are believed to occur.

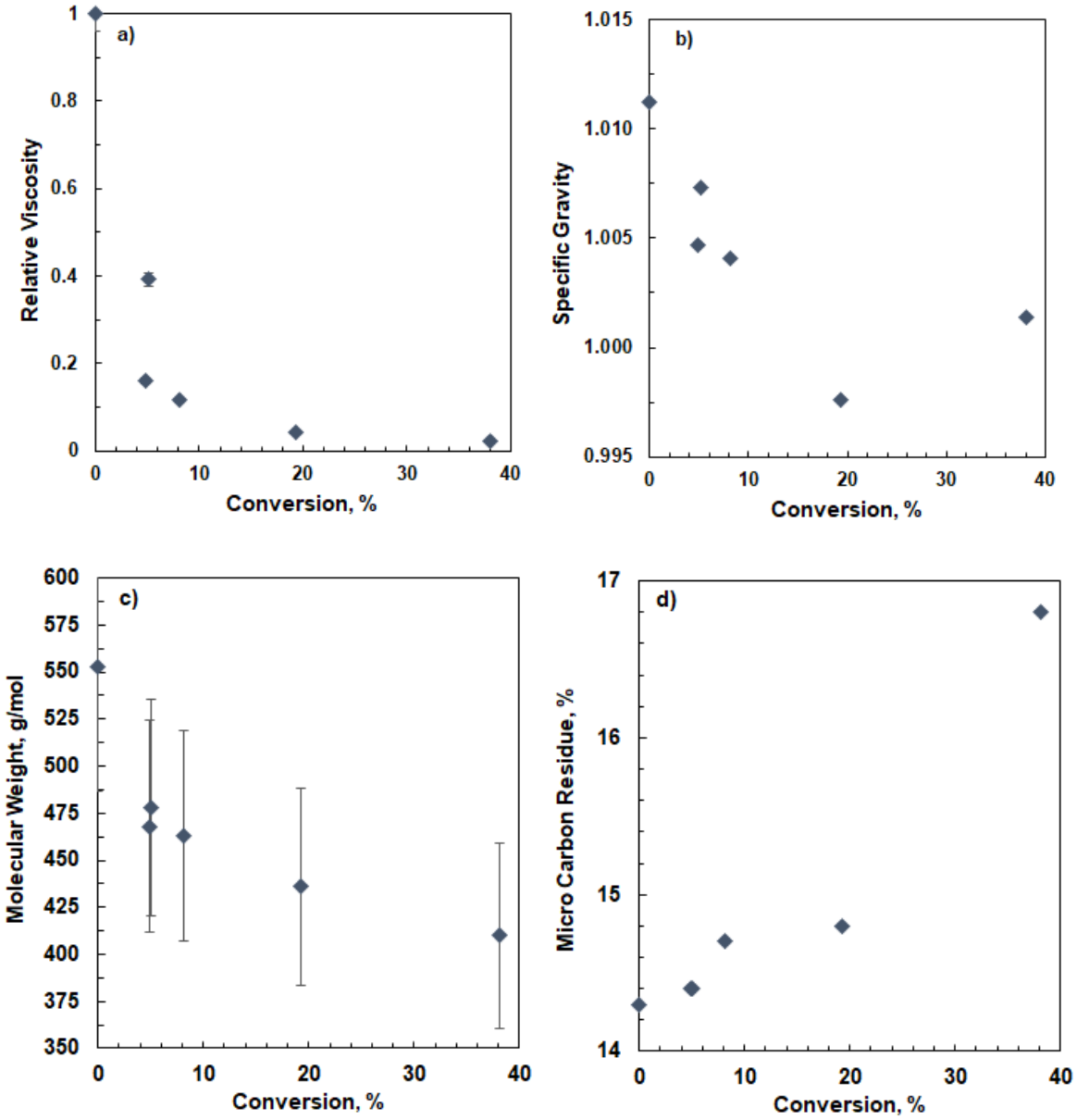

Figure 5.5 Effect of conversion on the properties of feedstock and visbroken products from the Development Dataset: a) relative viscosity; b) specific gravity; c) molecular weight; d) microcarbon residue. All viscosities measured at 50°C and atmospheric pressure. The molecular weights are from Rodriguez (2018).

Density and Viscosity of Oil Fractions

The amount of components and reactions involved in heavy oil visbreaking makes interpreting and modeling whole oil data a challenging task. Here, the goal is to develop correlations based on the density and viscosity of the distillate and SARA fractions. The density and viscosity measurements are presented below. The repeatability of fractions measurements was ±0.0002 for specific gravity and ±10% for viscosity.

Figure 5.6 shows that the specific gravity of the distillates decreased with increased conversion, as expected with the accumulation of relatively small, paraffinic or naphthenic fragments. The viscosities of the distillates are not discussed because they could not be measured; they were below the range of the cone and plate rheometer.

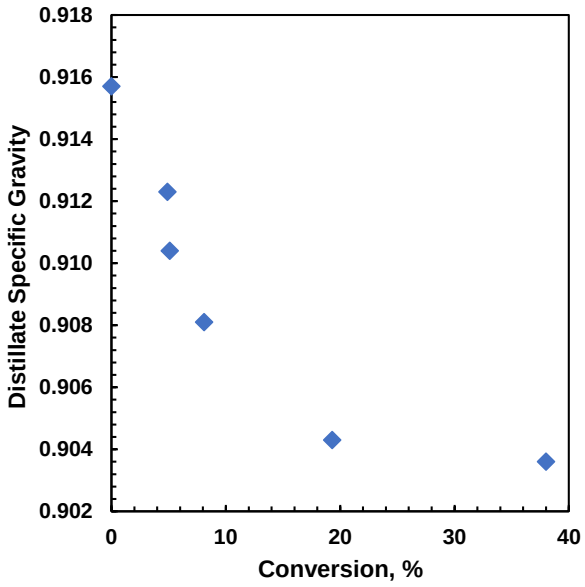

Figure 5.6 Effect of conversion on the specific gravity of distillates from the Development Dataset. The error in specific gravity measurement is ± 0.0002 and the error bars are too small to see.

Figure 5.7a shows that specific gravity of the saturates decreased with conversion, suggesting that this fraction became more paraffinic. Figure 5.7b shows that the viscosity of the saturates also decreased with increased conversion. These changes could be caused by thermal cracking of the

original saturates or the addition of alkyl and naphthenic side chains coming from heavier fractions.

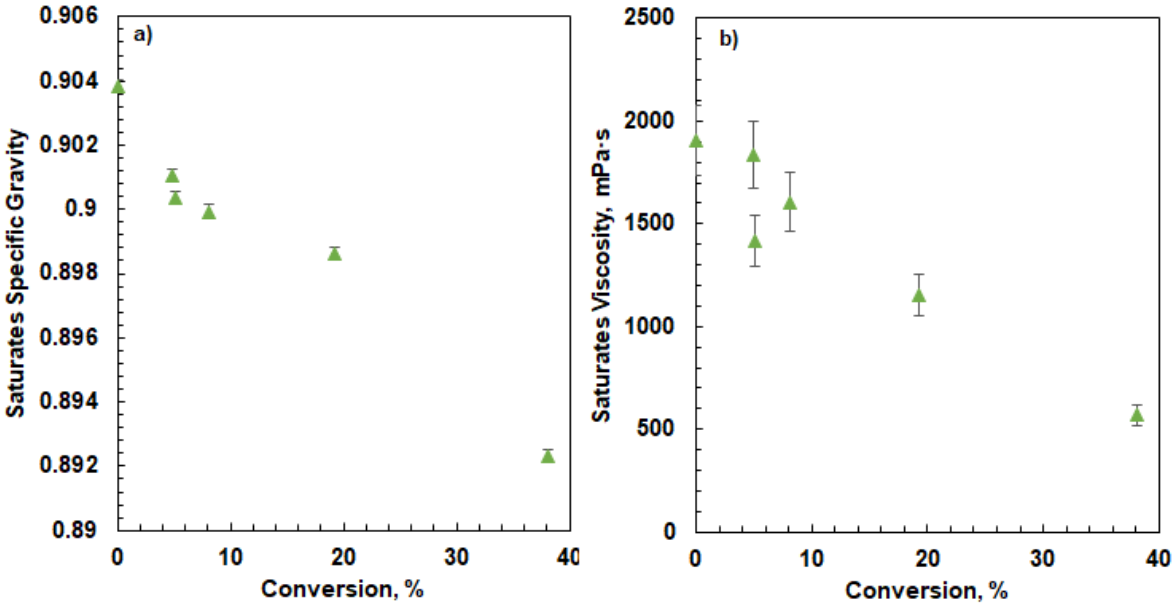

Figure 5.7 Effect of conversion on the properties of the saturates from the Development Dataset: a) specific gravity; b) viscosity. All viscosity measurements were performed at 15°C and atmospheric pressure.

Figure 5.8a shows that the specific gravity of the aromatics (hence their aromaticity) increased as conversion increased. Figure 5.8b shows that their viscosity decreased with increased conversion. These changes could be caused by dilution with smaller aromatic cores coming from cracking resins and asphaltenes or by the removal of paraffinic side chains from the original aromatics.

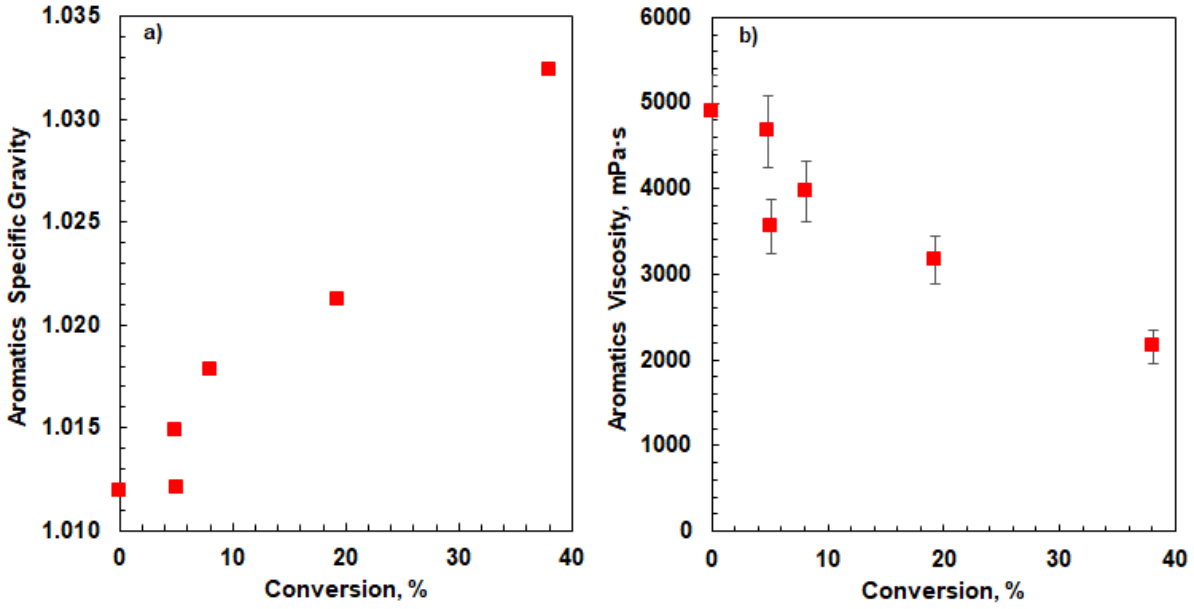

Figure 5.8 Effect of conversion on the properties of the aromatics from the Development Dataset: a) specific gravity; b) viscosity. Note: All viscosity measurements performed at 50°C and atmospheric pressure. The error in specific gravity measurement is ± 0.0002 and the error bars are too small to see.

Figures 5.9a and 5.9b show the changes in resins specific gravity (a) and viscosity (b) with conversion. Recall that the specific gravity of the resins was calculated indirectly from the specific gravities of the maltenes, saturates, and aromatics assuming a regular solution. The specific gravity of the resins increased with increased conversion; however their viscosity first decreased and then at 8.1% conversion reversed trend and gradually increased. The change in trend is consistent with two different types of reaction: 1) removal of paraffinic or naphthenic side chains and/or dilution with aromatic cores, making the overall fraction more aromatic but lower molecular weight (Rodriguez, 2018) and less viscous, 2) condensation reactions, making the overall fraction more aromatic, but with relatively little change in the residual molecular weight (Rodriguez, 2018), and therefore more viscous. It appears that side chain removal dominates at low conversion while condensation reactions begin dominate above 8.1% conversion.

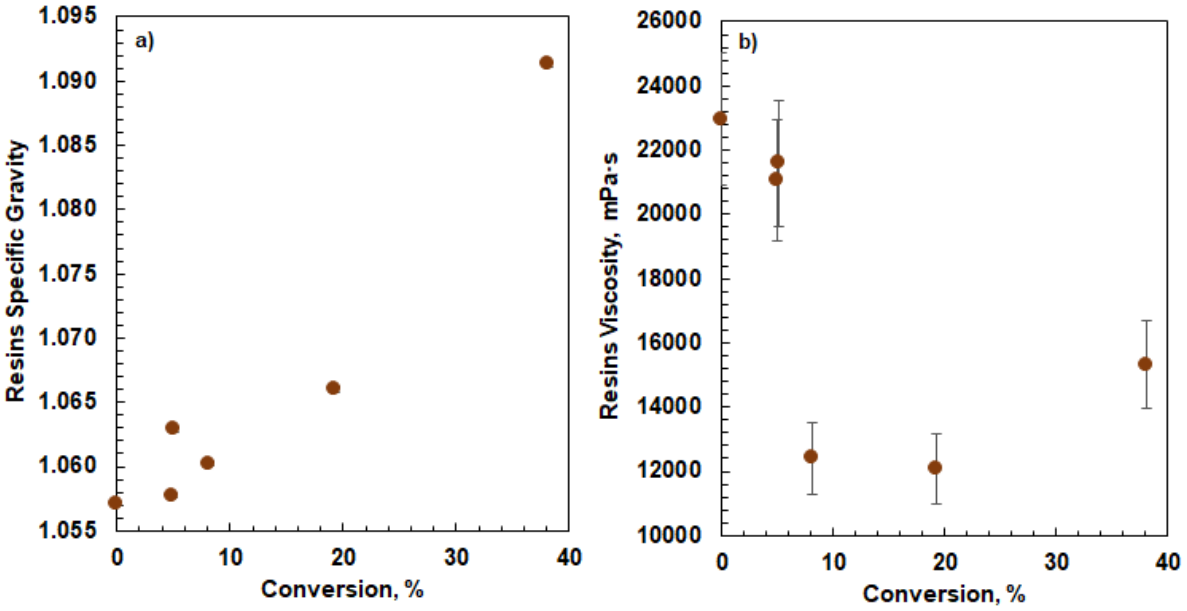

Figure 5.9 Effect of conversion on the properties of the resins from the Development Dataset: a) specific gravity; b) viscosity. The specific gravity was calculated indirectly from the specific gravities of the maltenes, saturates, and aromatics assuming a regular solution. All viscosity measurements performed at 100 °C and atmospheric pressure. The error in specific gravity measurement is ± 0.0002 and the error bars are too small to see.

Figure 5.10 shows that the specific gravity of the asphaltenes increased with increased conversion. As with the resins, their specific gravity was calculated indirectly from the specific gravities of the whole oil and the maltenes assuming a regular solution. It was not possible to measure the viscosity of the asphaltenes because they were a solid at the temperatures attainable in the cone and plate viscometer. The increase in specific gravity is consistent with asphaltenes becoming more aromatic from paraffinic side chains removal and eventually from condensation reactions leading to coke precursors.

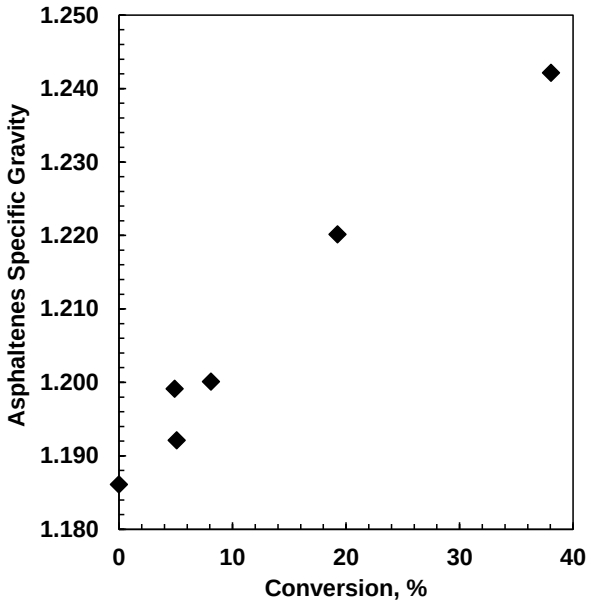

Figure 5.10 Effect of conversion on the specific gravity of the asphaltenes from the Development Dataset. The specific gravity was calculated indirectly from the specific gravities of the whole oil and the maltenes assuming a regular solution.

5.2. Density and Viscosity Correlations for Oil Fractions

The correlations developed in this section are normalized to the corresponding feedstock parameters so that they can be applied to other oils. Linear or first order differential equations were fitted to the experimental data based on the observed trends in the data. The correlations were formulated to ensure that all parameters are equal to the feed at 0% conversion.

5.2.1. Density

The viscosity model requires the density at the temperature and pressure at which the viscosity is to be determined. In this thesis, the viscosities were determined at atmospheric pressure over a range of temperatures. Therefore, the densities of the oil fractions were measured (or determined indirectly form other density measurements) over a range of temperatures and correlated in order to predict the input density at the required conditions. The densities all were linearly related to temperature and were fit with Eq. 4.27, reproduced here for the reader's convenience:

$$\rho = \rho_{REF} + b(T - T_{REF}) \tag{5.1}$$

where ρ_{REF} is the extrapolated density at 0°C and b is the temperature dependence. The density data and the fitted parameters for the feedstock and visbroken products are tabulated in Appendices A, C and D.

The parameters for each fraction were in turn correlated to conversion as discussed below. For comparison with data from other sources, the reference density was normalized to the feedstock reference density and the temperature dependence was normalized to the feedstock value.

Distillates:

Figures 5.11a and 5.11b show the measured and fitted normalized reference density and temperature dependence, respectively, of the distillates from the feedstock and visbroken samples. The data were fit with the following empirical equations:

$$\frac{\rho_{REF}}{\rho_{REF\,0}} = 1 - 0.01313\,[1 - exp(-0.1005\,X)] \tag{5.2}$$

$$\frac{b}{b_0} = 1 + 0.05676\,[1 - exp(-0.03981\,X)] \tag{5.3}$$

The proposed correlations fit the distillate reference density and temperature dependence, with an average absolute relative deviation (AARD) of 0.08% and 0.45%, respectively.

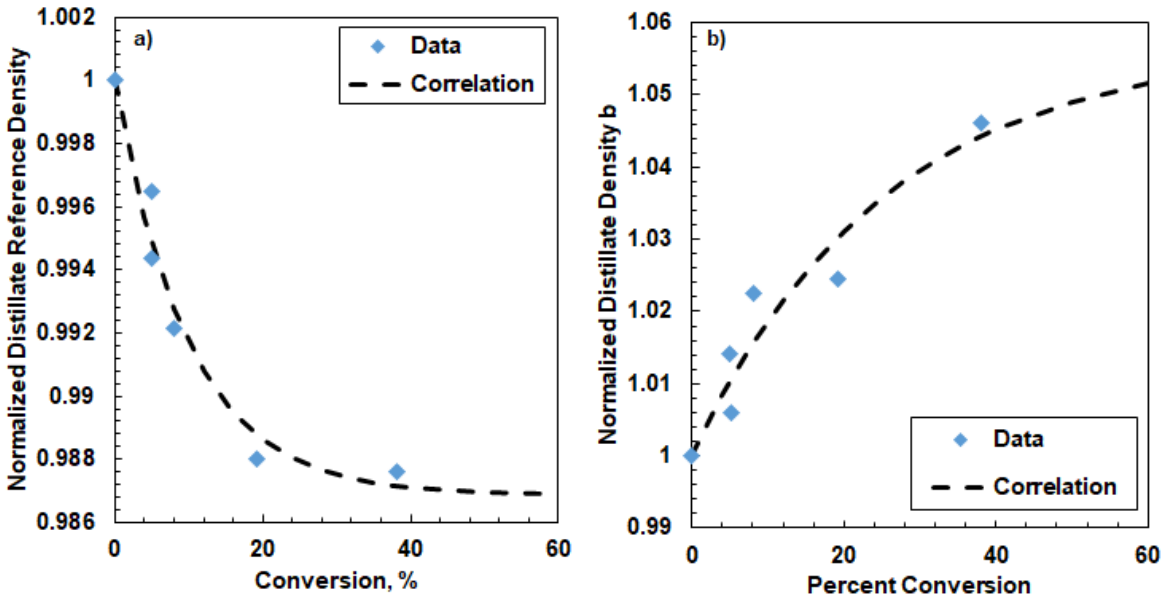

Figure 5.11 Effect of conversion on normalized distillate density parameters from the Development Dataset: a) reference density; b) slope.

Saturates:

Figures 5.12a and 5.12b show the measured and fitted normalized reference density and temperature dependence, respectively, of the saturates from the feedstock and visbroken samples. The data were fit with the following empirical equations:

$$\frac{\rho_{REF}}{\rho_{REF\ 0}} = 1 - 0.01914\ [1 - exp(-0.02418\ X)] \tag{5.4}$$

$$\frac{b}{b_0} = 1 \tag{5.5}$$

The proposed correlations fit the saturate reference density and temperature dependence, with an AARD of 0.12% and 0.18%, respectively.

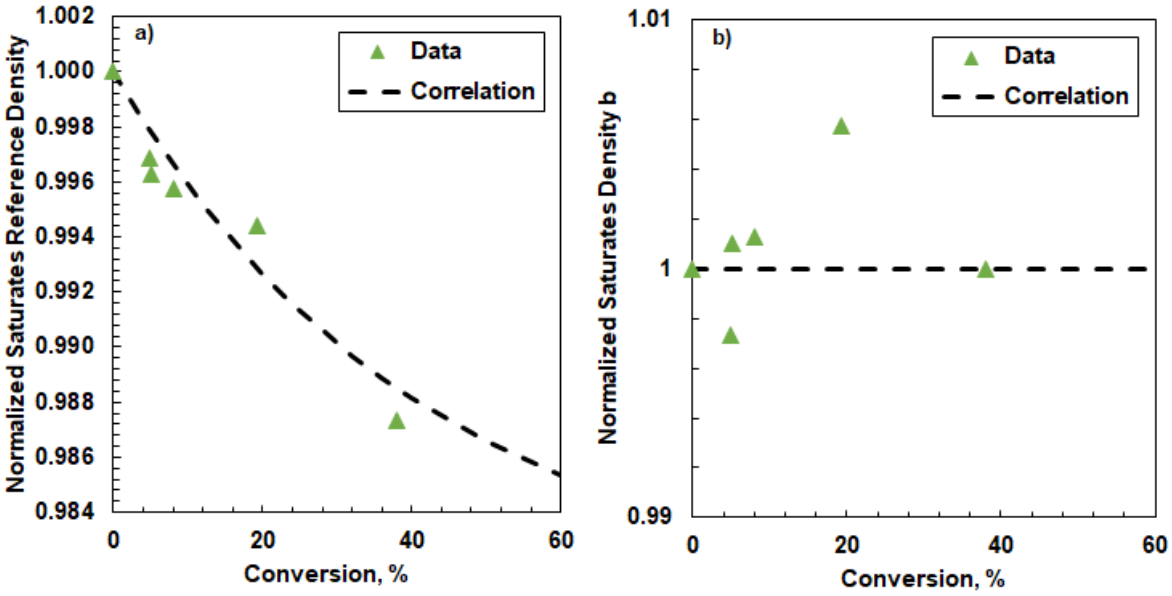

Figure 5.12 Effect of conversion on normalized saturate density parameters from the Development Dataset: a) reference density; b) slope.

Aromatics and Resins:

Figures 5.13a and 5.13b show the measured (aromatics), measurement derived (resins), and fitted normalized reference density and temperature dependence, respectively, of the aromatics and resins from the feedstock and visbroken samples. As observed by Yarranton *et al.*, (2018), both aromatics and resins follow the same linear relationship with conversion. Therefore, the aromatic and resin data were fit together with the following empirical equations:

$$\frac{\rho_{REF}}{\rho_{REF\,0}} = 1 + 0.00064\,X \tag{5.6}$$

$$\frac{b}{b_0} = 1 + 0.00105\,X \tag{5.7}$$

The proposed correlations fit the aromatic reference density and temperature dependence, with an AARD of 0.30% and 1.7%, respectively.

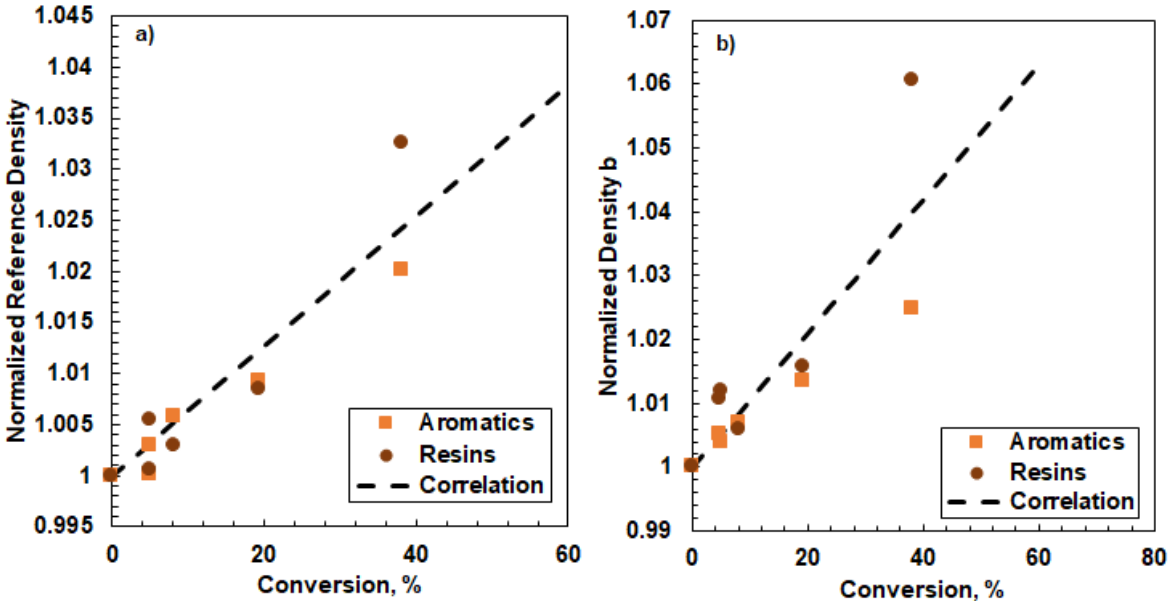

Figure 5.13 Effect of conversion on normalized aromatic and resin density parameters from the Development Dataset: a) reference density; b) slope. The densities of the resins were calculated indirectly from the densities of the maltenes, saturates, and aromatics assuming a regular solution.

Asphaltenes:

Recall that the asphaltene densities were calculated indirectly from the whole oil and other component densities, assuming a regular solution. Hence, all of the errors in the density measurements or from non-zero excess volumes of mixing will be accumulated in this fraction. Figures 5.14a and 5.14b show the measurement derived and fitted normalized reference density and temperature dependence, respectively, of the asphaltenes from the feedstock and visbroken samples. Not surprisingly, the measurement-derived values are scattered. One of the normalized temperature dependence was eliminated as an outlier as shown on Figure 5.14b. The remaining data were fit with the following empirical equations:

$$\frac{\rho_{REF}}{\rho_{REF\ 0}} = 1 + 0.00061\ X \tag{5.8}$$

$$\frac{b}{b_0} = 1 + 0.08768\ [1 - \exp(-0.1842\ X)] \tag{5.9}$$

The AARD for the normalized reference density was 0.16%. The AARD for the temperature dependence parameter was 1.6% excluding the outlier.

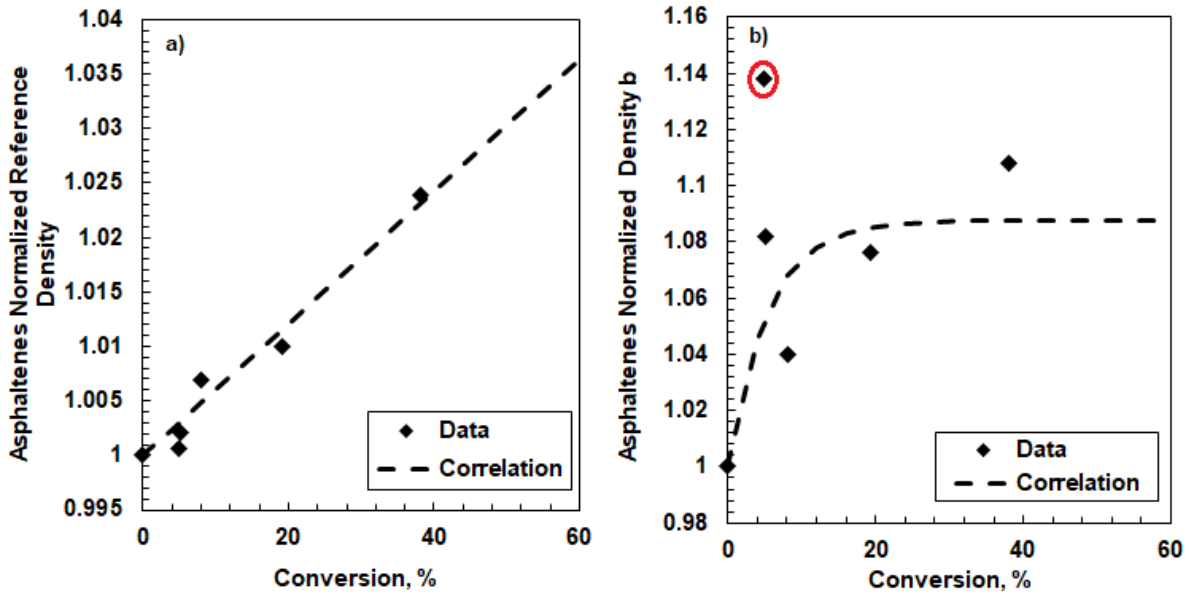

Figure 5.14 Effect of conversion on normalized asphaltene density parameters from the Development Dataset: a) reference density; b) slope. The asphaltene densities were calculated indirectly from the whole oil and other component densities, assuming a regular solution.

5.2.2. Viscosity

The Expanded Fluid viscosity model used in this thesis requires three parameters for each fluid or fluid component (C_2, $\rho_s°$, and C_3). Except for distillates and asphaltenes, these parameters were determined by fitting the viscosity data provided in Appendix C. Distillates parameters were calculated based on boiling point and density using Equations 4.18 to 4.26. The asphaltene parameters were determined indirectly from matching residue viscosities. The parameters for the whole oils and their fractions are discussed below.

Whole Oils

Figure 5.15a to 5.15c show C_2, $\rho_s°$, and C_3, respectively, for the feedstock and visbroken oils. The value of the C_3 parameter did not vary considerable with conversion. Therefore, this parameter was fixed at the feed value as follows:

$$C_3 = C_{3_0} \tag{5.10}$$

where subscript *0* denotes the feed condition. Since high pressure density and viscosity data were only collected for WC-B-A3(1), C_3 was assumed to be the same for both feeds. The C_2 and $\rho_s°$ parameters did vary with conversion and therefore correlations for these parameters were required. The correlations were developed for the distillates and fractions rather than the whole oils to better capture the chemical changes within the oil.

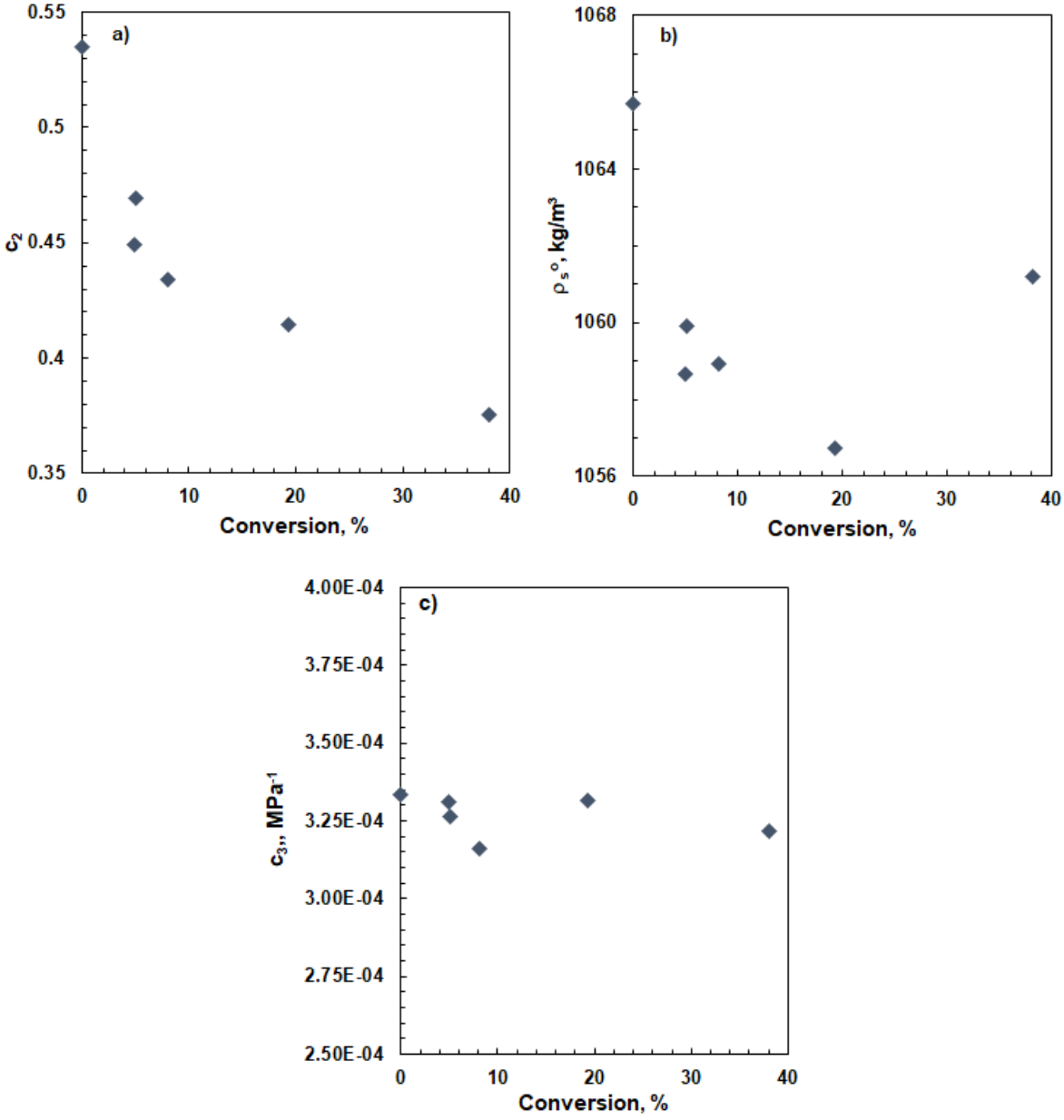

Figure 5.15 Effect of conversion on the viscosity parameters of the feedstock and visbroken products from the Development Dataset: a) C_2, b) $\rho_s°$; c) C_3.

Distillates:

As previously stated, EF parameters for the distillates were calculated from their boiling point curve and specific gravity using Eqs. 4.18 to 4.26. Table 5.3 lists the calculated EF parameters for the distillates from the feedstock and visbroken products. Viscosity data were only available for the feedstock and the model with the predicted parameters predicted the measured viscosities with an AARD of 6%.

Table 5.3 EF model parameters for distillates from the Development Dataset.

Parameter	WC-B-A3	VIS5.1	VIS4.9	VIS8.1	VIS19.3	VIS38.1
C_2	0.2324	0.2318	0.2342	0.2289	0.2277	0.2265
$\rho_s°$	983.97	980.18	981.56	981.51	980.77	982.95

Saturates:

Figure 5.16a shows that the C_2 parameter for the saturates remained constant up to a conversion of 18.3% and then decreased at higher conversion. The following expression was found to capture this trend:

$$If\ X \leq 18.3\%, \qquad C_2 = C_{2_0} \tag{5.11}$$

$$Else, \qquad C_2 = C_{2_0}(1.05968 - 0.00298\,X)$$

Figure 5.16b shows that the $\rho_s°$ parameter decreased monotonically with conversion. It was fit with the following expression:

$$\frac{{\rho_s}^0}{{\rho_s}^0{}_0} = 1 - 0.00915[1 - exp(-0.03556\,X)] \tag{5.12}$$

The average relative deviations were 0.59% for C_2 and 0.12% for $\rho_s°$. The EF model with the correlated parameters matched the measured saturates viscosities with an AARD of 11%.

Aromatics and Resins:

Figure 5.17 show that the C_2 and $\rho_s°$ parameters were both linearly related to conversion and that the aromatics and resins both followed the same trends. The data were fit with the following equations:

$$\frac{C_2}{C_{2\ 0}} = 1 - 0.00246\ X \tag{5.13}$$

$$\frac{\rho_s{}^0}{\rho_s{}^0{}_0} = 1 + 0.00056\ X \tag{5.14}$$

The average relative deviations were 1.33% for C_2 and 0.28% for $\rho_s°$. The EF model with the correlated parameters matched the measured aromatics and resins viscosity with AARD of 21% and 48%, respectively.

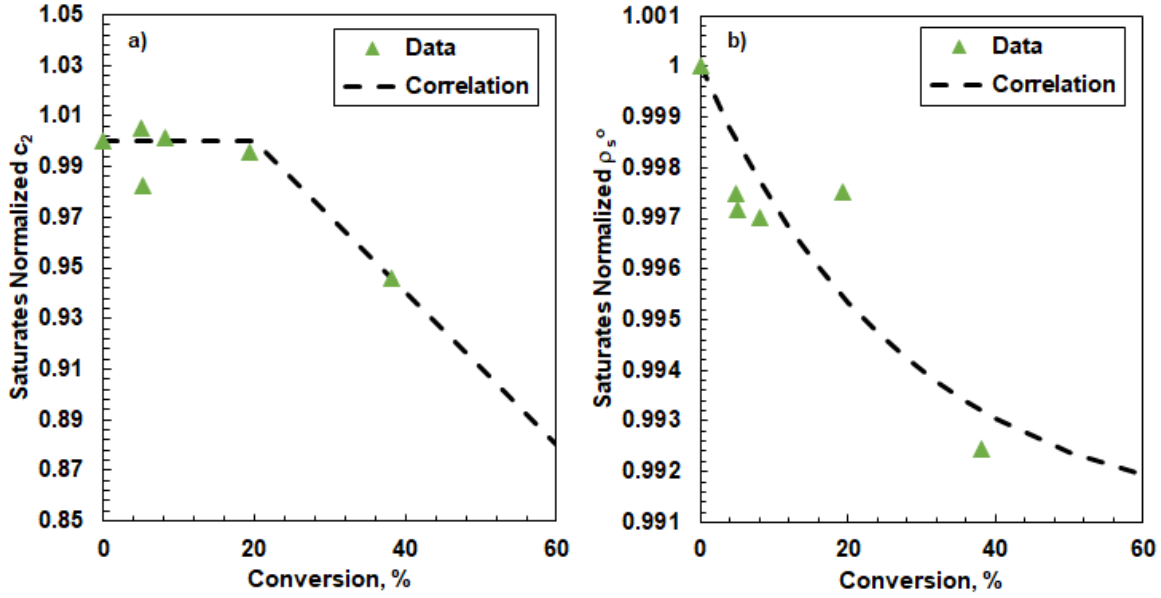

Figure 5.16 Effect of conversion on the EF model parameters for saturates from the Development Dataset: a) C_2; b) $\rho_s°$.

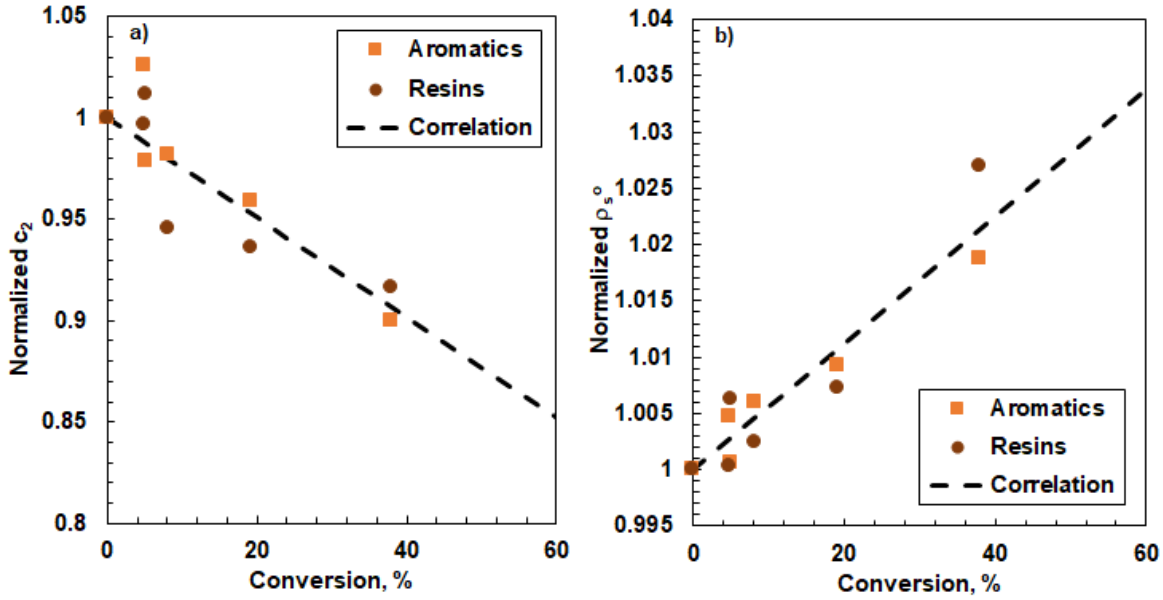

Figure 5.17 Effect of conversion on the EF model parameters for aromatics and resins from the Development Dataset: a) C_2; b) $\rho_s°$.

Asphaltenes:

Since there were no asphaltene viscosity data available, the asphaltene parameters were calculated indirectly by modeling a fluid that contained asphaltenes and other constituents with known parameters. Both the whole oil and the residue met this requirement and the residue data was chosen to eliminate the error from uncertainties in the distillate parameters or incorrectly captured distillate-asphaltenes interactions. The asphaltenes and distillates are the two most dissimilar fractions in terms of molecular size, boiling point, chemical family, and polarity, and thus the most likely to have non-ideal interactions.

The asphaltene viscosity parameters were adjusted to match the measured residue viscosity as shown in Figure 5.18. The input density of the residue could not be directly measured and was determined by recombining all of the SARA fractions assuming a regular solution. The back-calculated viscosity parameters are shown in Figure 5.19 and were fitted with the following equations:

$$\frac{C_2}{C_{2\,0}} = 1 - 0.219\,[1 - \exp(-0.073\,X)] \tag{5.15}$$

$$\frac{\rho_s{}^0}{\rho_s{}^0{}_0} = 1 + 0.00024\,X \tag{5.16}$$

As with their density data, the back-calculated asphaltenes viscosity parameters show some scatter because all of the measurement deviations of all of the SAR fractions are accumulated in the asphaltene parameters. Nonetheless, the proposed correlations match the data with average relative deviations of 5.0% for C_2 and 0.18% for $\rho_s°$.

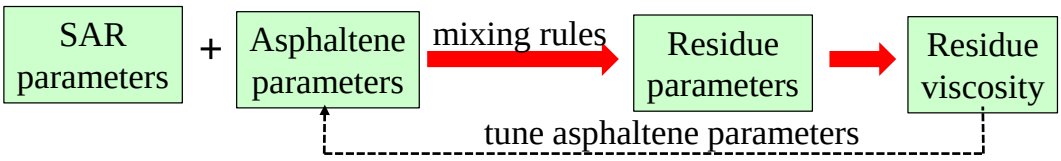

Figure 5.18 Asphaltenes EF parameters estimation approach.

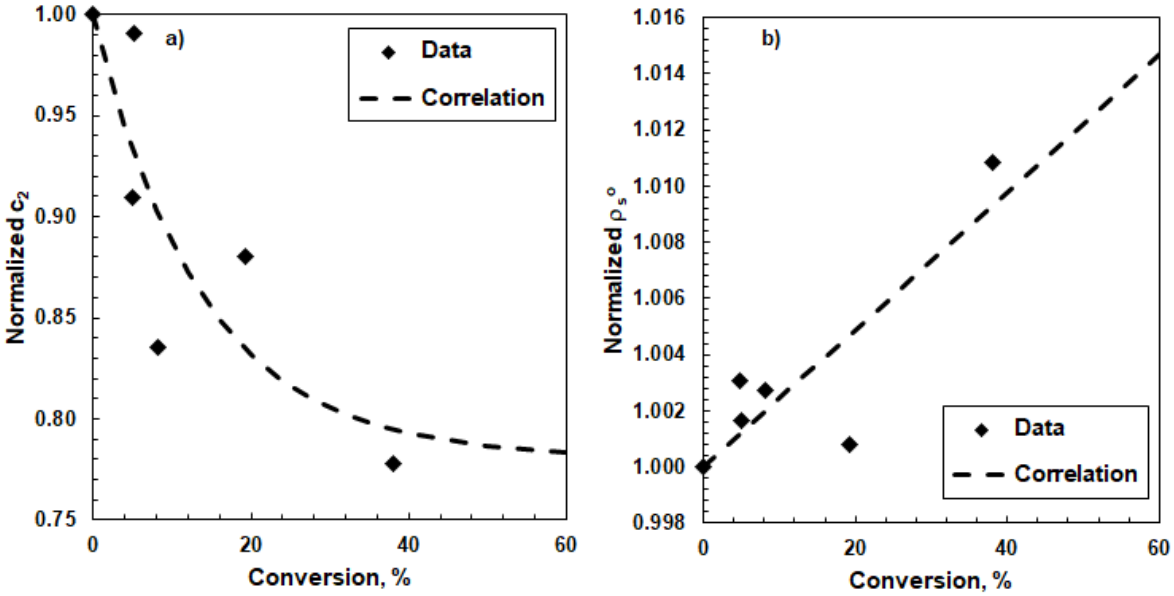

Figure 5.19 Asphaltenes EF parameters against conversion.

Since the asphaltene parameters could not be compared to asphaltene viscosities, the predicted residue viscosities were examined instead. Two cases were considered for the SARA fractions: 1) using fitted density parameters and correlated EF parameters; 2) using correlated density and EF parameters. The deviations in the predicted residue viscosities for the feedstock and visbroken samples from the Development Dataset are provided in Table 5.4. The average absolute relative deviations were 28 and 31% for Case 1 and 2, respectively. The use of correlated densities does not significantly change the overall deviations. Hence, the main source of error is in the correlated viscosity parameters and/or the viscosity parameter mixing rules.

Table 5.4 Average absolute relative deviations in the model for the residue viscosities from the Development Dataset. Case 1 is based on fitted density parameters and correlated viscosity parameters. Case 2 is based on correlated density and viscosity parameters.

Case	AARD, %					
	VIS5.1	**VIS4.9**	**VIS8.1**	**VIS19.3**	**VIS38.1**	**Average**
1	24	12	34	39	31	28
2	8	38	44	8	58	31

5.2.3. Model Evaluation with Development Dataset

The EF viscosity model requires the fluid density as an input. The density is determined from the component densities and a regular solution mixing rule. The model uses another set of mixing rules (Eqs. 4.5 to 4.14) to determine the EF fluid parameters for the oil from the component parameters. The binary interaction parameters in the mixing rules were obtained from Ramos-Pallares *et al*. (2016). Therefore, the accuracy of the model depends on both set of mixing rules as well as the accuracy of the component property correlations. Since the properties of the maltene and whole fractions were measured directly, it was possible to test the mixing rules and property correlations on these data.

Recombined Maltenes:

In this case, the density of the resins was calculated by matching maltenes data. Hence, the maltenes density data could not be used as a test of the density mixing rules. However, the data

were used to assess the error introduced by the density correlations. Figure 5.20 compares the measured and recombined correlated densities of the maltenes for two visbroken samples. The average absolute deviations (AAD) for all of the samples are provided in Table 5.5; the overall AAD was 1.7 kg/m³.

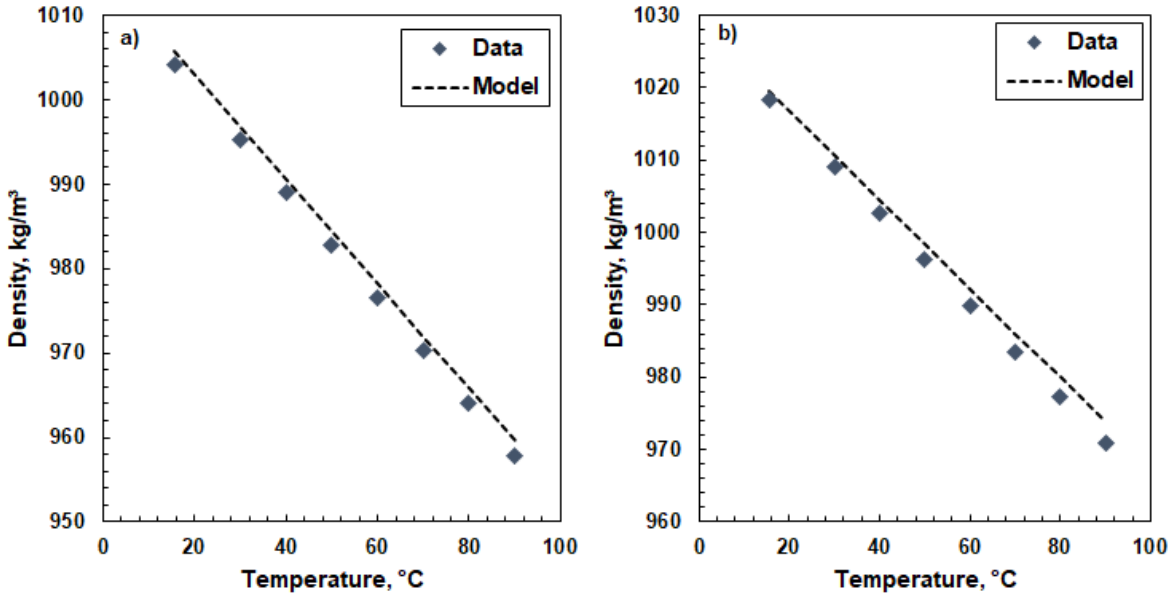

Figure 5.20 Measured and modeled density of maltenes versus temperature at atmospheric pressure: a) WC-B-A3(1)-VIS5.1; b) WC-B-A3(2)VIS38.1.

Table 5.5 Average absolute deviations (AAD) in SAR recombinations for maltene densities.

Sample	VIS5.1	VIS4.9	VIS8.1	VIS19.3	VIS38.1	Average
AAD, kg/m³	1.7	1.2	0.6	2.9	2	1.7

The viscosities of all of the maltene components were measured directly and therefore the viscosity mixing rules could be tested. Figure 5.21 compares the measured and predicted maltenes viscosity for Athabasca Feed #2 and two visbroken samples. Table 5.6 lists the average absolute relative deviations for all of the samples for three cases: 1) using measured maltenes densities and fitted SAR viscosity parameters; 2) using measured maltenes densities and correlated SAR viscosity parameters from Eqs. 5.9 to 5.12; 3) using correlated SAR densities and viscosity parameters from

Eqs. 5.3 to 5.6 and 5.9 to 5.12, respectively. The average absolute relative deviations were 13%, 15%, and 12% for Cases 1 to 3, respectively. The similar error in each case indicates that the density and viscosity parameters correlations do not significantly increase the deviation of the viscosity model. The main source of error appears to be the mixing rules.

Table 5.6 Average absolute relative deviations in the model for the maltenes viscosity. Three cases are presented: 1) measured densities and fitted EF parameters, 2) measured densities and correlated EF parameters and 3) correlated densities and EF parameters.

Case	AARD, %						
	Feedstock	**VIS5.1**	**VIS4.9**	**VIS8.1**	**VIS19.3**	**VIS38.1**	**Average**
1	17	10	16	3	13	19	13
2	-	15	9	10	28	15	15
3	-	11	11	21	9	10	12

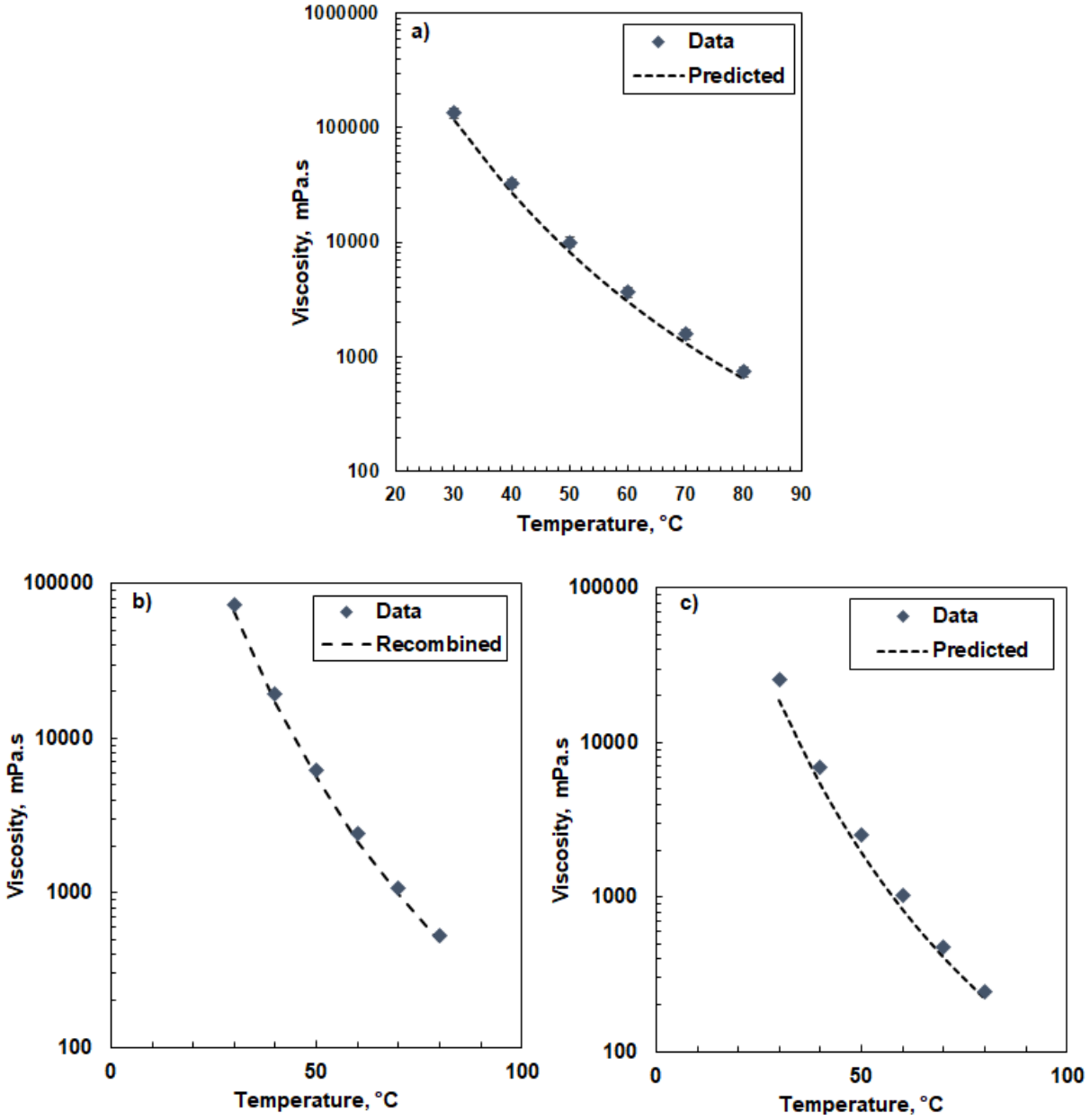

Figure 5.21 Measured and modeled viscosity of maltenes versus temperature at atmospheric pressure: a) WC-B-A3(2); b) WC-B-A3(1)-VIS5.1; c) WC-B-A3(2)VIS38.1.

Recombined Whole Oil:

Recall that the whole oil density data was used to back-calculate the asphaltene density parameters; hence, the recombination of the component densities will always match the whole oil. The whole oil data can only be used to evaluate the proposed density correlations. Figure 5.22 compares the

measured and recombined correlated densities of the whole oils for two visbroken samples. The average absolute deviations (AAD) for all of the visbroken samples are provided in Table 5.7; the overall AAD was 1.1 kg/m³.

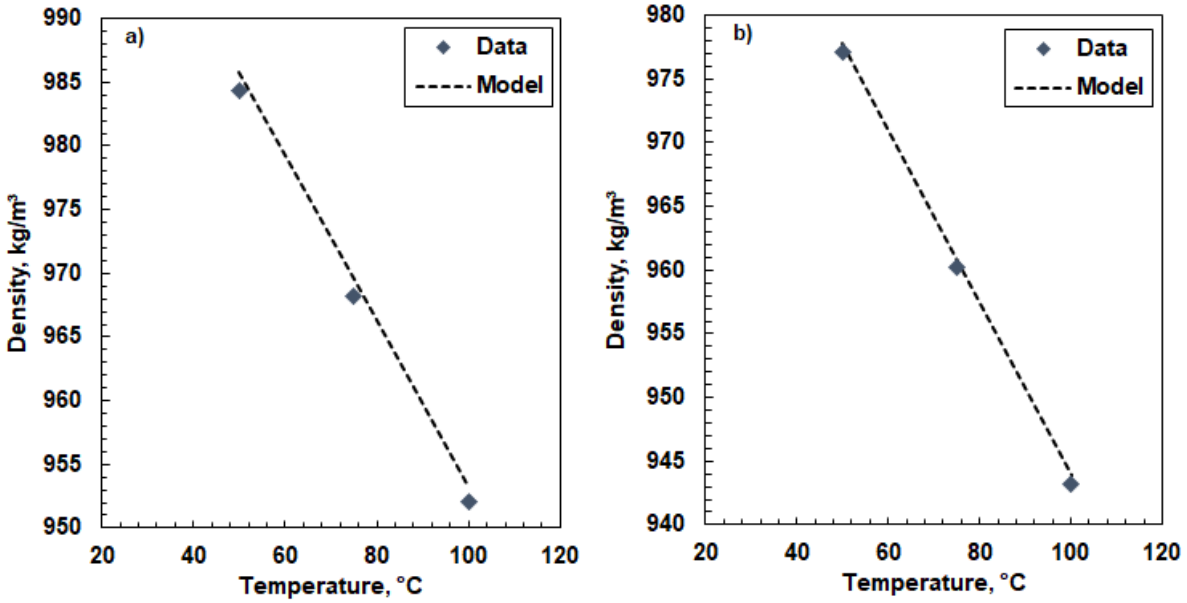

Figure 5.22 Measured and modeled density of whole oils versus temperature at atmospheric pressure: a) WC-B-A3(1)-VIS5.1; b) WC-B-A3(2)-VIS38.1.

Table 5.7 Average absolute deviations (AAD) in component recombination for whole oil density.

Sample	VIS5.1	VIS4.9	VIS8.1	VIS19.3	VIS38.1	Average
AAD, kg/m³	1.4	1.2	0.2	1.9	0.7	1.1

The viscosity data of the whole oils was not used to develop any of the property correlations and therefore could be used to test the viscosity correlations and the mixing rules. Figure 5.23 compares the measured and correlated whole oil viscosity for Athabasca Feed #2 and two visbroken samples. In this case, both the density and viscosity parameters of the components were fitted. The average absolute relative deviations for the feedstock was 25%, within the expected error of the mixing rules. However, the deviation for the reacted samples was much higher with an average absolute relative deviation for all of the visbroken samples of 71%. The high error indicates that either the

reacted asphaltene parameters are incorrect or the interactions between reacted asphaltenes and the other fractions were not correctly accounted for with Equations 4.8 to 4.14. The asphaltene parameters were obtained from the residue viscosity data and changing them would introduce an inconsistency between the residue and whole oil viscosity predictions. In addition, tuning the asphaltenes EF parameters to match the whole oil data was found to generate unrealistically low asphaltenes viscosity values. Therefore, the binary interaction parameters in the mixing rules were tuned instead.

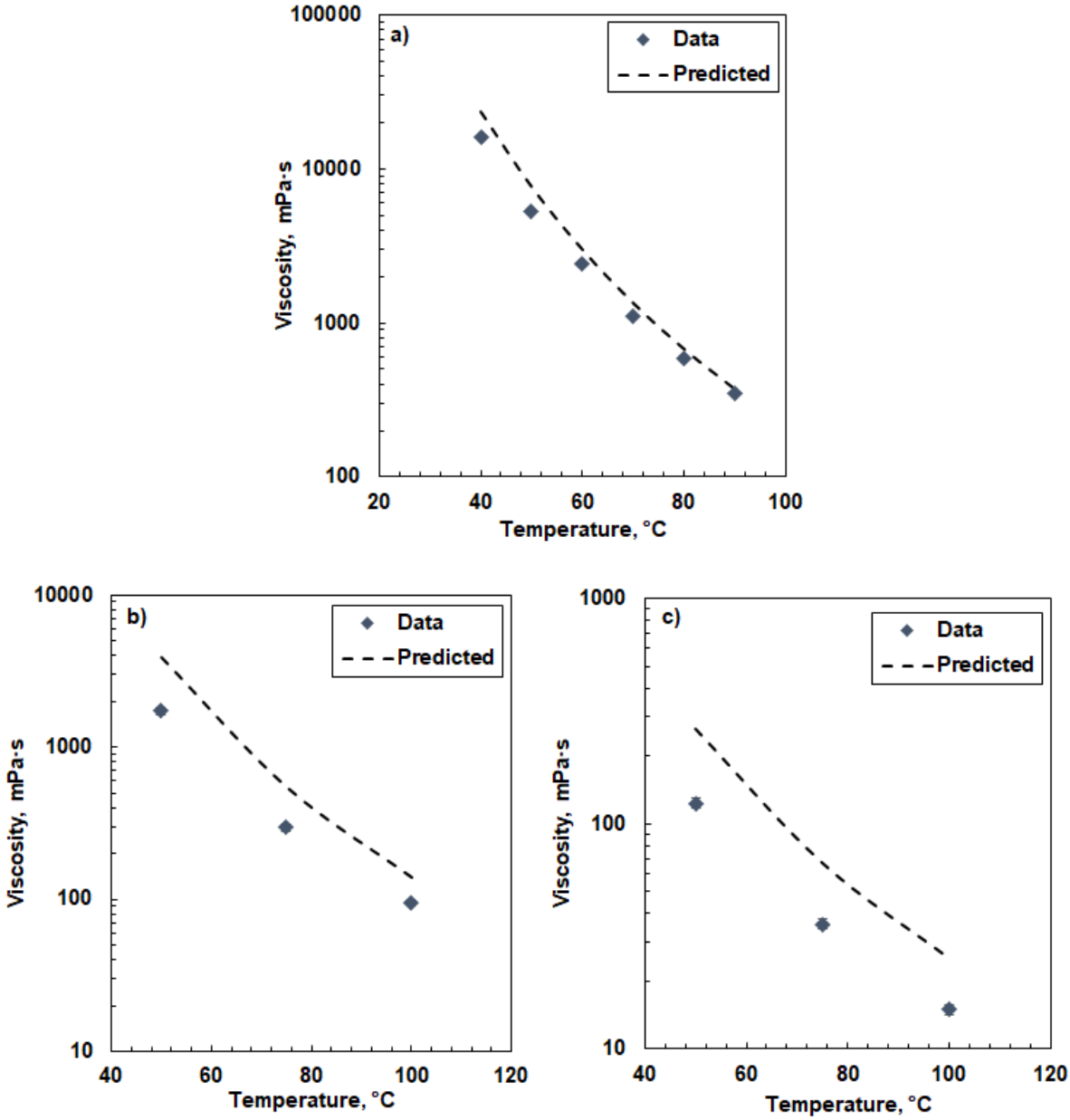

Figure 5.23 Measured and modeled viscosity of whole oils versus temperature at atmospheric pressure: a) WC-B-A3(1); b) WC-B-A3(1)-VIS5.1; c) WC-B-A3(2)VIS38.1. All viscosity data shown at atmospheric pressure; similar trends were observed up to 10 MPa.

Four binary interaction parameters are required for asphaltenes interactions: one each for the interactions with the distillates, saturates, aromatics, and resins. Only the distillates-asphaltenes parameter was chosen for tuning for the following reasons: 1) distillates and asphaltenes are the

two most dissimilar fractions and the difference increases with conversion; 2) the distillates are the fraction that distinguishes the whole oil from the residue; 3) tuning other parameters would add too many variables. The distillates-asphaltenes binary interaction parameter was tuned to match the whole oil viscosity data for each of visbroken samples. Figure 5.24 plots the difference between the tuned and original binary interaction parameters (BIP). The difference was fitted with the following expression:

$$\Delta a_{Dist-Asph} = 0.07651\,[1 - \exp(-4.065\,X)] \tag{5.17}$$

where $\Delta a_{Dist\text{-}Asph}$ is the BIP increment. The average absolute relative deviation between the correlated and tuned BIP increment is 13% for all visbroken samples.

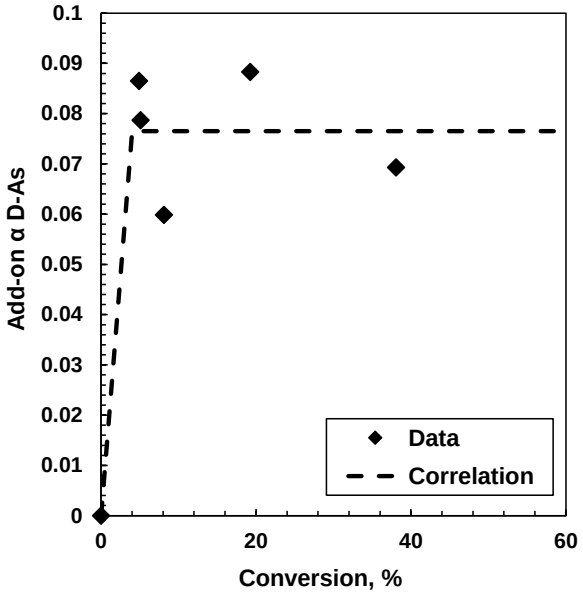

Figure 5.24 Distillates-asphaltenes BIP increments for the visbroken samples in the Development Dataset.

Figure 5.25 compares the measured and modeled whole oil viscosity for two visbroken samples where the model included the revised binary interaction parameters. Table 5.8 lists the average absolute relative deviations for all of the samples for two cases: 1) using fitted whole oil densities and correlated component viscosity parameters; 2) using correlated component densities and viscosities. The AARD was 8% for both cases. Hence, the use of correlated density parameters

does not increase the error. The mixing rules could not be tested because the binary interaction parameters were retuned to fit the data.

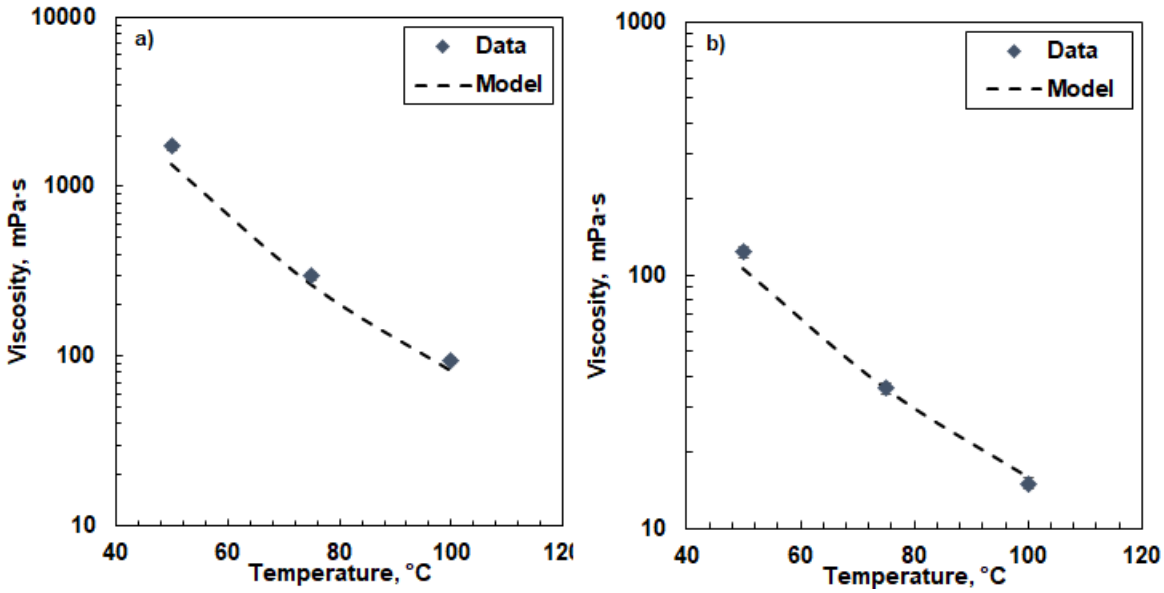

Figure 5.25 Correlated whole oil viscosity for WC-B-A3(1)-VIS5.1 (a) and WC-B-A3(2)-VIS38.1 (b) using fitted densities. Note: All viscosity data shown at atmospheric pressure, similar trends observed up to 10 MPa.

Table 5.8 Average absolute relative deviations in the model for the whole oil viscosity. Two cases are presented: 1) fitted densities and correlated EF parameters, 2) correlated densities and EF parameters.

Case	AARD, %					
	VIS5.1	VIS4.9	VIS8.1	VIS19.3	VIS38.1	Average
1	9	9	6	10	8	8
2	5	16	8	5	7	8

5.2.4. Model Sensitivity

The next step to evaluate the model is to determine how uncertainties in the inputs affect the predicted density and viscosity. Recall that the inputs for this methodology are: the feed density and viscosity parameters for each fraction, conversion, and the visbroken product composition.

The effect of changing these inputs within the error of the measurement is assessed in Tables 5.9, 5.10 and 5.11 for whole oil density, viscosity using fitted densities, and viscosity using predicted densities, respectively.

For all inputs except SARA composition, the repeatabilities reported in Section 5.1 were used for this analysis. As SARA composition is known to vary considerably among different laboratories (Kharrat *et al.*, 2007), the reproducibilities of saturates, aromatics and resins were taken from the ASTM standard (ASTM D2007, 2016), while for asphaltenes ±2.2% was selected based on our research laboratory experience (Yarranton, 2009). The model shows similar sensitivity towards all inputs, with an overall average AAD below 3.7 kg/m³ for density and an overall average ARD below 18% for viscosity.

Table 5.9 Sensitivity of the predicted whole oil density to model input errors.

Input	**Change**	**AAD, kg/m³**					
		VIS5.1	**VIS4.9**	**VIS8.1**	**VIS19.3**	**VIS38.1**	**Average**
Conversion	+2.7%	1.6	1.4	0.4	2.5	3.4	1.9
	-2.7%	1.3	1.4	0.1	1.4	0.2	0.9
Distillate	+0.2 wt%	1.1	1.0	0.2	1.6	0.4	0.9
Composition	-0.2 wt%	1.7	1.5	0.4	2.2	1.1	1.4
Saturate	+4 wt%	2.2	2.1	3.2	1.3	2.3	2.2
Composition	-4 wt%	0.9	4.6	3.4	5.1	3.8	3.6
Aromatic	+3.3 wt%	1.8	1.5	0.4	2.4	1.3	1.5
Composition	-3.3 wt%	1.0	1.0	0.2	1.4	0.2	0.8
Resin	+1.8 wt%	2.2	1.9	0.7	2.5	1.3	1.7
Composition	-1.8 wt%	0.7	0.6	0.6	1.3	0.2	0.7
Asphaltene	+2.2 wt%	3.8	3.5	2.3	4.0	2.7	3.3
Composition	-2.2 wt%	1.0	1.0	2.1	0.2	1.2	1.1

Table 5.10 Average absolute relative deviations in the model for the whole oil viscosity using fitted densities.

Input	Change	AARD, %					
		VIS5.1	VIS4.9	VIS8.1	VIS19.3	VIS38.1	Average
Conversion	+2.7%	20	7	8	12	37	17
	-2.7%	13	32	22	6	10	17
Feed	+10%	8	14	16	6	11	11
Viscosity	+10%	15	6	7	11	8	9
Distillate	+0.2 wt%	9	9	10	6	8	8
Composition	-0.2 wt%	9	9	10	6	9	9
Saturate	+4 wt%	7	23	24	6	13	15
Composition	-4 wt%	21	9	9	15	10	13
Aromatic	+3.3 wt%	13	7	9	9	8	9
Composition	-3.3 wt%	7	12	13	5	9	9
Resin	+1.8 wt%	10	9	10	6	9	9
Composition	-1.8 wt%	8	9	10	5	8	8
Asphaltene	+2.2 wt%	15	9	10	11	9	11
Composition	-2.2 wt%	4	15	16	4	9	10

Table 5.11 Average absolute relative deviations in the model for the whole oil viscosity using predicted densities.

Input	Change	AARD, %					
		VIS5.1	VIS4.9	VIS8.1	VIS19.3	VIS38.1	Average
Conversion	+2.7%	19	6	6	5	9	9
	-2.7%	3	33	22	8	8	15
Feed	+0.2 kg/m^3	4	18	9	5	7	9
Density	-0.2 kg/m^3	7	14	7	5	6	8
Distillate	+0.2 wt%	8	14	6	5	7	8
Composition	-0.2 wt%	4	18	10	6	8	9
Saturate	+4 wt%	15	7	5	6	6	8
Composition	-4 wt%	7	27	17	9	8	14
Aromatic	+3.3 wt%	8	13	6	6	8	8
Composition	-3.3 wt%	4	19	10	5	7	9
Resin	+1.8 wt%	4	21	12	6	8	10
Composition	-1.8 wt%	12	12	6	4	7	8
Asphaltene	+2.2 wt%	5	38	28	18	14	21
Composition	-2.2 wt%	15	7	9	10	10	10

5.3. Model Evaluation with Test Dataset

The proposed viscosity model was tested on two oils and their visbroken samples: another Western Canadian bitumen (WC-B-A4) and a Middle Eastern vacuum residue (ME-VR-A1). Selected properties of the two oils are compared with the WC-B-A3(2) feedstock from the Development Dataset in Table 5.12. WC-B-A4 is heavier than WC-B-A3(2) but is expected to be chemically similar. ME-VR-A1 is a vacuum residue and is expected to be chemically different. All measurements performed on both samples from the Test Dataset are presented in Appendices A and C.

Table 5.12 Comparison between the feedstocks for the Development Dataset (WC-B-A3(2) and Test Dataset (WC-B-A4 and ME-VR-A1). All viscosities shown at 50°C and atmospheric pressure. The ME-VR-A1 viscosity was determined indirectly from the EF model fitted to higher temperature and pressure viscosity data.

Property	WC-B-A3(2)	WC-B-A4	ME-VR-A1
Viscosity, mPa·s	5,370	12,200	29,300,000
Specific Gravity	1.011	1.014	1.054
Asphaltene content, wt%	19.1	18.8	30.6

5.3.1. Similar Oil (WC-B-A4)

Composition and Properties of Whole Oil and its Fractions

The samples available for the similar oil test were a feedstock and a single visbroken product. Figure 5.26 shows the SimDist boiling point distribution of the feedstock and visbroken sample. The conversion was determined to be 1%. Since the repeatability of SimDist was ± 7 °C, conversions calculated based on this assay have a deviation of ± 2.7%. Therefore, this conversion point could not be distinguished from zero within the error of the measurement. Table 5.13 provides the distillates content, specific gravity and viscosity for the feedstock and product. As was observed at low conversion in the Development Dataset, the distillate content increased and the specific gravity and viscosity decreases after visbreaking. Therefore, visbreaking reactions took place and the conversion must be above zero. Table 5.14 shows the SARA contents of the residue for the feedstock and the visbroken product. As expected, there was little change in

composition with the low conversion. There was a slight reduction in the aromatic content and small increase in the asphaltene content after visbreaking.

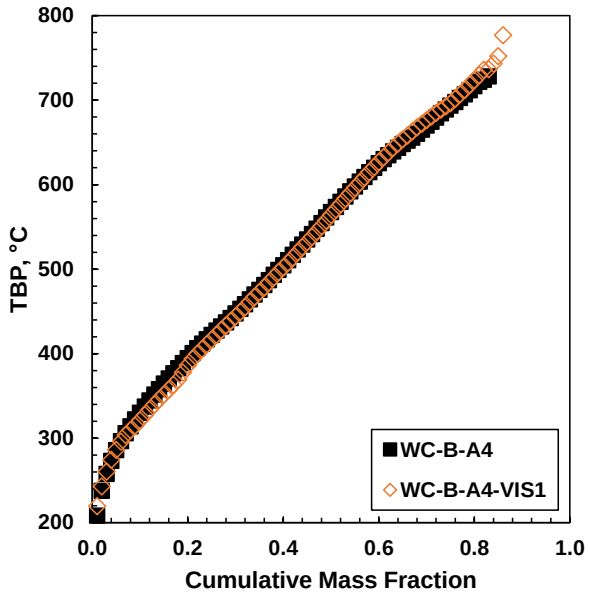

Figure 5.26 Extended SimDist (ASTM D7169) of the WC-B-A4 feedstock and visbroken product.

Table 5.13 Distillate content, specific gravity and viscosity of the WC-B-A4 feedstock and visbroken product. Note: All viscosities measured at 50 °C and atmospheric pressure.

Sample	Distillate wt%	Specific Gravity	Viscosity mPa·s
WC-B-A4	16.2	1.014	12,200
WC-B-A4-VIS1	16.8	1.013	8,270

Table 5.14 SARA content of the residues from the WC-B-A4 feedstock and visbroken product.

Sample	Saturates wt%	Aromatics wt%	Resins wt%	Asphaltenes wt%	TI wt%
WC-B-A4	9	45.6	22.6	22.4	0.3
WC-B-A4-VIS1	9.3	44.8	22.5	23.1	0.3

Table 5.15 presents the specific gravity of each fraction. As for the Development Dataset, the specific gravities of the distillates, saturates, and aromatics were measured directly while the specific gravities of the resins and asphaltenes were obtained by matching maltenes and whole oil density data, respectively. The density of the residue could not be directly measured, and was determined by recombining all of the SARA fractions assuming a regular solution. The complete set of density data is provided in Appendices A and C. Most of the changes after visbreaking at such a low conversion were within the error of the measurement (±0.0002). One surprising observation was a slight increase in distillates specific gravity from feed to visbroken oil. A possible explanation is that some volatile components evaporated when venting the batch reactor, effectively topping the oil. At such a low conversion, the paraffinic and naphthenic fragments added to this fraction may not be enough to compensate for the topping.

Table 5.15 Specific gravity of the distillates and saturate, aromatic, and resin fractions from the WC-B-A4 feedstock and visbroken product. The distillate, saturate, and aromatic densities were measured directly. The resin and asphaltene densities were back-calculated from maltene and whole oil density densities, respectively.

Sample	Specific Gravity				
	Distillates	**Saturates**	**Aromatics**	**Resins**	**Asphaltenes**
WC-B-A4	0.9120	0.9015	1.005	1.0440	1.1735
WC-B-A4-VIS1	0.9127	0.9017	1.006	1.0457	1.1737

Table 5.16 presents the viscosity of the saturates, aromatics, resins, and distillation residue. The complete set of viscosities over a range of temperatures is provided in Appendices A and C. As with the Development Dataset, the distillate and asphaltene viscosities could not be measured. The viscosities did not change within the error of the measurements (±10%). However, the viscosity of the whole oil did decrease significantly suggesting that the main viscosity reduction mechanism at very low conversion was the increase in the distillate content and/or a change in the viscosity interaction parameters.

Table 5.16 Measured viscosity of the saturate, aromatic, and resin fractions and distillation residue from the WC-B-A4 feedstock and visbroken product at atmospheric pressure and a temperature of 15, 50, 100, 80°C for the saturates, aromatics, resins, and residue, respectively.

Sample	Viscosity, mPa·s			
	Saturates	**Aromatics**	**Resins**	**Residue**
WC-B-A4	1,330	3,105	22,740	10,780
WC-B-A4-VIS1	1355	2,810	21,590	9,700

Model Parameters

Two sets of model parameters were determined for the visbroken sample: a fitted set and a correlated set. The fitted set was determined as described for the Development Dataset. The EF model parameters for saturates, aromatics and resins were determined by fitting the model to the measured viscosity data. The distillate parameters were obtained from Eqs. 4.18 to 4.26 and the asphaltenes parameters were back-calculated by matching the model to residue viscosity data. The density parameters for the distillates, saturates, and aromatics were determined by fitting their measured densities over a range of temperatures. The densities of the resins and asphaltenes were determined by fitting the maltene and whole oil densities. The fitted parameters are provided in Appendix D.

The correlated density parameters for the distillates, saturates, aromatics, resins, and asphaltenes were determined from the feedstock properties and the proposed density correlations (Eqs. 5.2 to 5.9). The feedstock densities were determined as described above. The correlated viscosity parameters for the saturates, aromatics, resins and asphaltenes were determined from the feedstock properties and the proposed viscosity correlations (Eqs. 5.11 to 5.16). Their feedstock properties were determined as described above. The distillate parameters were obtained from Eqs. 4.18 to 4.26.

The binary interaction parameters for the viscosity mixing rules were obtained in two ways: 1) from the original correlations (Eqs. 4.8 to 4.14); 2) from the modified correlations (Eqs. 4.8 to 4.14, Eq. 5.17). The following tests were performed on the proposed model: 1) fitted density and

viscosity parameters and original interaction parameters; 2) fitted density and viscosity parameters and modified interaction parameters; 3) correlated density and viscosity parameters and modified interaction parameters. The first two tests are intended to evaluate the viscosity model mixing rules. The latter test is intended to evaluate the density and viscosity prediction (using correlated density and viscosity properties) for a visbroken product. The inputs for the prediction are the boiling point curve and SARA composition of the visbroken product, the fitted feed fraction parameters, and conversion.

Test of Viscosity Model Mixing Rules

Figures 5.27 and 5.28 show the model results for the maltenes and whole oils, respectively, where the model uses the fitted density and viscosity parameters and either the original or modified mixing rules. With the original mixing rules, the AARD are 6% for the maltene viscosities, 25% for the feedstock whole oil, and 96% for the visbroken whole oil. The large deviation for the visbroken oil indicates that the original binary interaction parameters for the asphaltenes fail even at very low conversions. When the modified binary interaction parameters for the asphaltenes and distillates are used, the AARD for the visbroken whole oil is reduced to 5%. The deviations in the modeled viscosities are similar to the Development Dataset results (AARD of 8%).

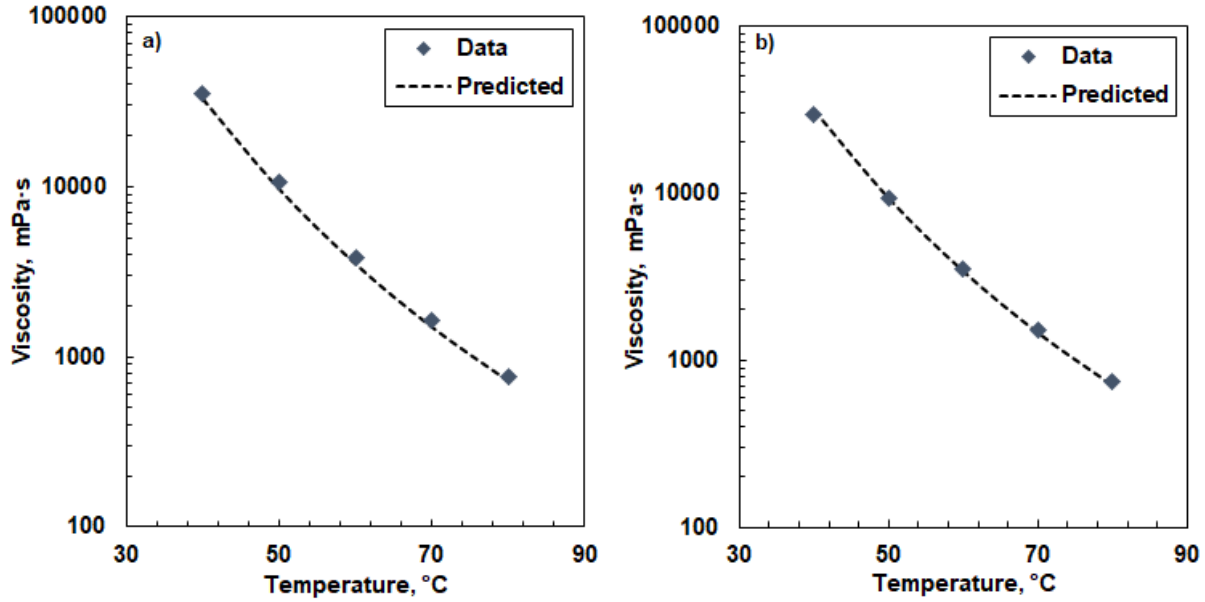

Figure 5.27 Measured and modeled atmospheric pressure viscosity of maltenes from: a) WC-B-A4; b) WC-B-A4-VIS1. The model used fitted density and viscosity parameters.

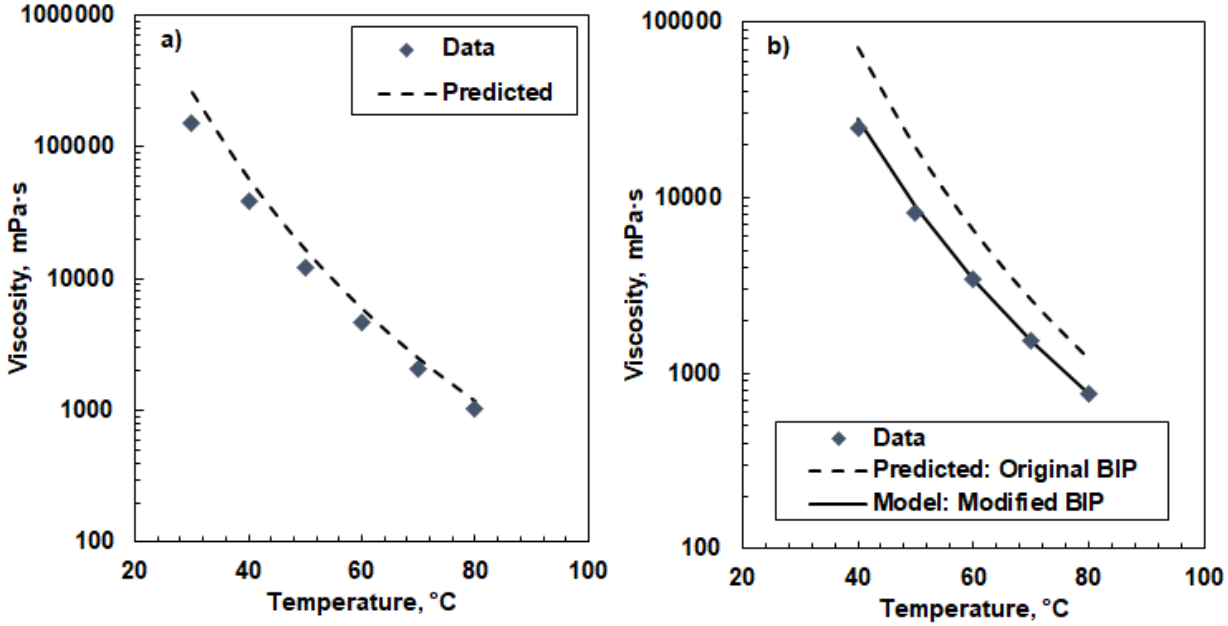

Figure 5.28 Measured and modeled atmospheric pressure viscosity of whole oils: a) WC-B-A4; b) WC-B-A4-VIS1. The model used fitted density and viscosity parameters.

Viscosity Prediction

Figures 5.29, 5.30 and 5.31 present predictions for maltenes, residue, and whole oil respectively. The AAD of the predicted densities were 0.4 kg/m³ for the maltenes and 1.0 kg/m^3 for the whole oil. The AARD of the predicted viscosities were 9, 10, and 20% for the maltenes, residue, and whole oil, respectively. The deviations in the modeled viscosities are higher than the Development Dataset results (AARD of 8%) but still within 20% of the measured values. In other words, the model can be applied to Western Canadian bitumens within expected errors of less than 20%.

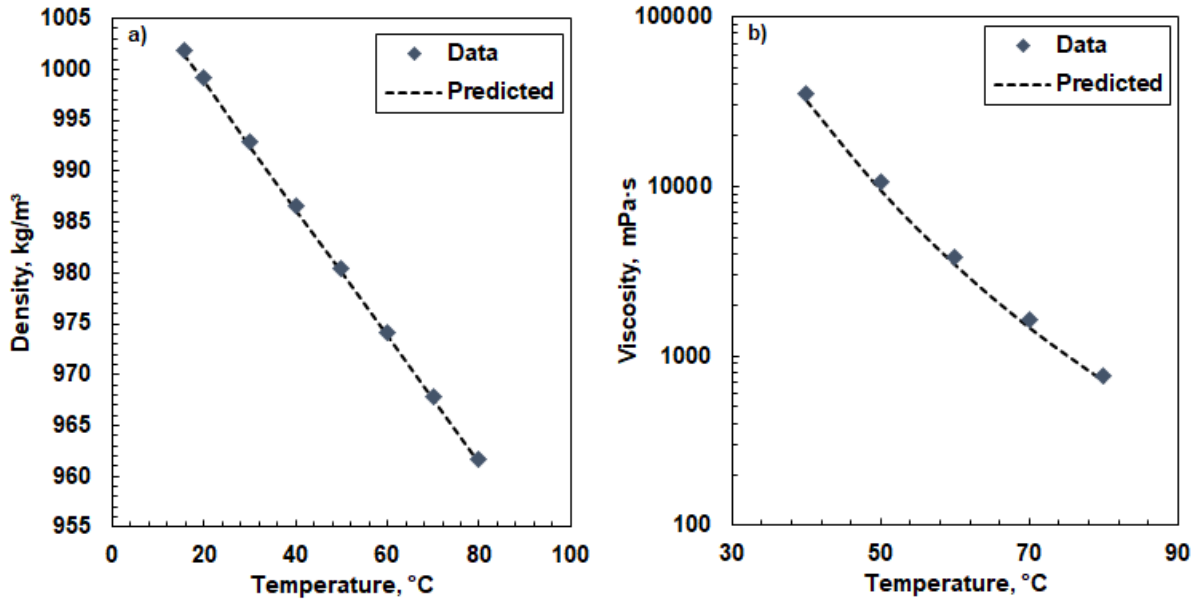

Figure 5.29 Measured and predicted atmospheric pressure properties of WC-B-B4-VIS1 maltenes: a) density; b) viscosity.

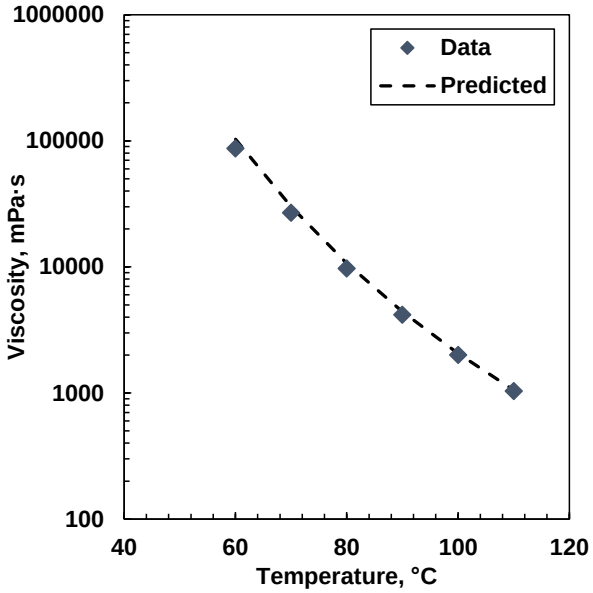

Figure 5.30 Measured and predicted atmospheric pressure viscosity of WC-B-B4-VIS1 residue.

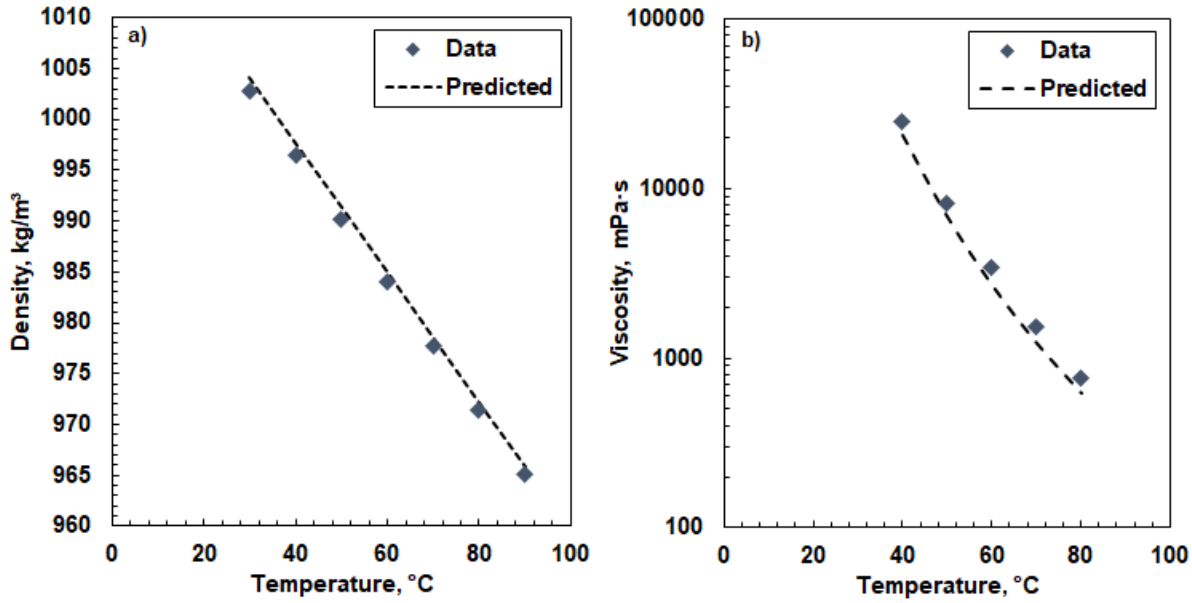

Figure 5.31 Measured and predicted atmospheric pressure properties of WC-B-B4-VIS1 whole oils: a) density; b) viscosity.

5.3.2. Dissimilar Oil (ME-VR-A1)

Composition and Properties of Whole Oil and its Fractions

The samples provided for the dissimilar oil test were a vacuum residue feedstock and two visbroken samples. Figure 5.32 shows the SimDist boiling point distribution of all three samples. The conversions of the products were 12.5 and 18.8%. The amount of distillates in both visbroken oils was insufficient to be physically separated and recovered by Spinning Band Distillation. Therefore, all three samples were only fractionated into saturates, aromatics, resins and asphaltenes.

Table 5.17 provides the specific gravity, viscosity, and micro carbon residue for all three samples. Since atmospheric density measurements were not possible for these samples, specific gravity was extrapolated from high temperature and pressure data with the following empirical equation (Saryazdi *et al.*, 2013):

$$\rho = (A + BT)exp[C(P - 0.1)exp(DT)] \quad (5.18)$$

As was observed in the Development Dataset, at low conversions, the specific gravity and viscosity decreased with increased conversion but the trend reversed at higher conversions. Unexpectedly, there was negligible change in the micro carbon residue content with reaction even though an increased high toluene insoluble content was observed in the products (as will be shown later). The reason for this discrepancy is not known and further investigation was constrained because these assays were provided by a third party and further details about the procedure were not available.

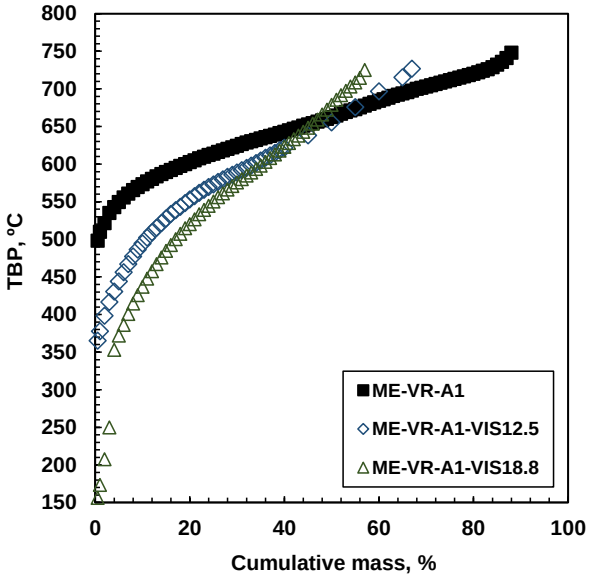

Figure 5.32 Extended SimDist (ASTM D7169) of dissimilar oil test dataset. Data provided by RIPP, 2017.

Table 5.17 Properties of ME-VR-A1 and its visbroken products. All viscosities reported at 50°C and atmospheric pressure. The ME-VR-A1 and ME-VR-A1-VIS18.8 viscosities were determined indirectly from the EF model fitted to high pressure viscosity data. Micro carbon residue data were provided by RIPP (2017).

Sample	Specific Gravity	Viscosity, mPa·s	Micro Carbon Residue, wt%
ME-VR-A1	1.0534	29,298,760	26.3
ME-VR-A1-VIS12.5	1.0425	126,740	26.1
ME-VR-A1-VIS18.8	1.0512	1,135,000	26.2

Table 5.18 shows the SARA contents of all three samples. The saturate and toluene insoluble contents increased with increased conversion, while the aromatic and resin contents decreased. The asphaltenes content initially increased and then decreased with increased conversion. These trends can be explained by: 1) removed paraffinic and naphthenic side chains from aromatics cores accumulating in saturates; 2) condensation of aromatics and resins to produce resins and asphaltenes; 3) further condensation and polymerization of asphaltenes yielding coke.

Table 5.18 SARA contents of ME-VR-A1 and its visbroken products.

Sample	Saturates wt%	Aromatics wt%	Resins wt%	Asphaltenes wt%	TI wt%
ME-VR-A1	6.8	39.3	22.9	30.8	0.2
ME-VR-A1-VIS12.5	11.7	38.5	15.8	32.9	1.1
ME-VR-A1-VIS18.8	13.4	32.8	14	31.2	8.6

Tables 5.19 and 5.20 present specific gravity and viscosity, respectively, for the saturate, aromatic, and resin (SAR) fractions. The complete set of density and viscosity data is provided in Appendices A and C. Recall that specific gravity is measured for saturates and aromatics, and back-calculated from the specific gravity of the maltenes for the resins and of the whole vacuum residue for the asphaltenes. The asphaltene specific gravity could be back-calculated for the feedstock, however both visbroken products had small amount of distillable material that could not be characterized (below 3%). Therefore, the visbroken asphaltenes densities could not be back-calculated accurately for the visbroken samples and are not reported. Viscosity was measured for all SAR fractions. The specific gravity of the saturates decreased significantly with conversion while the specific gravity of aromatics and resins increased significantly. The viscosity of the saturates and aromatics significantly decreased with increased conversion while the viscosity of the resins initially decreased and then increased at higher conversion.

Table 5.19 Specific gravity of ME-VR-A1 feedstock and its visbroken products.

Sample	Saturates	Aromatics	Resins	Asphaltenes
ME-VR-A1	0.8905	1.0070	1.0455	1.1787
ME-VR-A1-VIS12.5	0.8680	1.0084	1.0494	-
ME-VR-A1-VIS18.8	0.8564	1.0200	1.0532	-

Table 5.20 Viscosity of the saturates, aromatics, and resins from the ME-VR-A1 feedstock and its visbroken products. All measurements performed at atmospheric pressure and at 15, 50 and 100°C for saturates, aromatics and resins, respectively.

Sample	**Saturates**	**Aromatics**	**Resins**
	mPa·s	mPa·s	mPa·s
ME-VR-A1	2,340	13,570	44,030
ME-VR-A1-VIS12.5	92.6	862	8,190
ME-VR-A1-VIS18.8	65	613.1	10,283

The observed trends for specific gravity, viscosity, and content of resins, asphaltenes and TI for ME-VR-B1 are qualitatively similar to the trends for the Development Dataset (WC-B-A3). However, the properties change significantly more with conversion than with the WC-B-A3. In other words, the Middle East vacuum residue appears to be more "reactive" than Athabasca bitumen at a fixed conversion point. Condensation reactions and coke formation appear to take place at lower conversions. In addition, the saturates content increased more rapidly with conversion than for WC-B-A3 but far less distillates were produced (almost none). This observation suggests that heavier (higher boiling point) paraffinic and naphthenic fragments were removed from the aromatic cores of the Middle East vacuum residue in comparison to Athabasca bitumen.

Model Parameters

Two sets of model parameters were determined for the visbroken samples: a fitted set and a correlated set. The parameters were determined as described for the similar oil (WC-B-A4) samples. However, since the feed for this dataset is a vacuum residue and the visbroken products have insignificant amount of distillable material, the feed asphaltene density and viscosity parameters are calculated from whole oil instead of the residue data. Also, since there were no distillates, the original and modified viscosity mixing rules are the same.

The following tests were performed on the proposed model: 1) fitted density and viscosity parameters; 2) correlated density and viscosity parameters. The first test is intended to evaluate the viscosity model mixing rules. The latter test is intended to evaluate the density and viscosity

prediction (using correlated density and viscosity properties) for a visbroken product. As before, the inputs for the prediction are the boiling point curve and SARA composition of the visbroken product, the fitted feed fraction parameters, and conversion.

Test of Viscosity Model Mixing Rules

Figures 5.33a to 5.33c compared the measured and modeled viscosity of the maltenes from the ME-VR-A1 feedstock and its visbroken products where the model used fitted density and viscosity parameters. The AARD are 26, 24, and 7% for the maltenes from the ME-VR-A1, ME-VR-A1-VIS12.5, and ME-VR-A1-VIS18.8 maltenes, respectively. The deviations are higher than those observed for the Development Dataset (average of 13%). The errors a still less than 30% and is likely a combination of experimental error and a failure of the predicted binary interaction parameters.

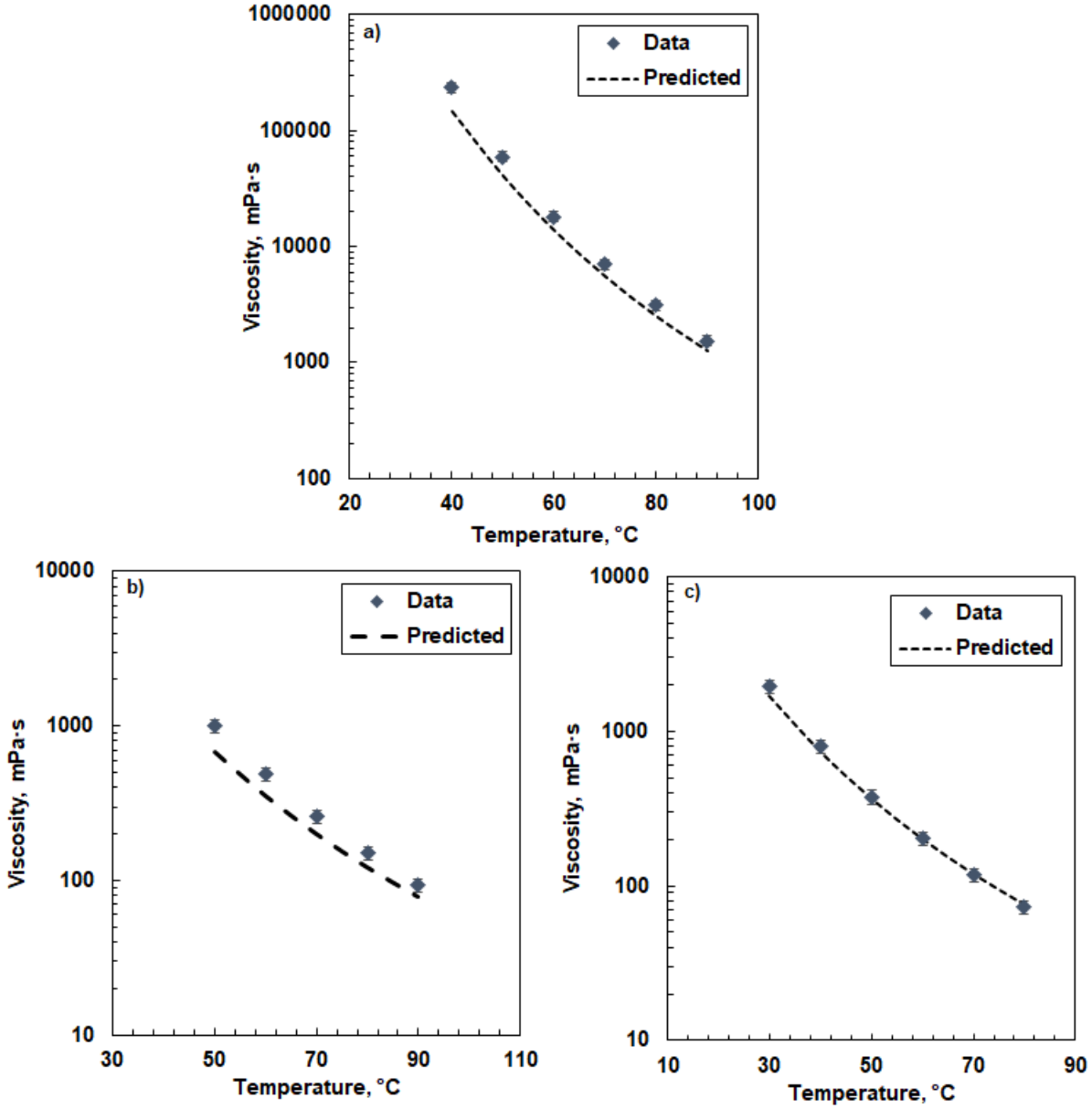

Figure 5.33 Measured and modeled atmospheric pressure viscosity of maltenes from: a) ME-VR-A1; b) ME-VR-A1-VIS12.5; c) ME-VR-A1-VIS18.8. The model used fitted density and viscosity.

Viscosity Prediction

Figures 5.34, 5.35 and 5.36 present predictions for ME-VR-A1-VIS12.5 maltenes, ME-VR-A1-VIS18.8 maltenes, and ME-VR-A1-VIS12.5 whole vacuum residue, respectively. The ME-VR-A1-VIS18.8 whole residue sample could not be modeled with the proposed framework for two reasons: 1) non-Newtonian behaviour was observed at relatively high temperatures (above 75 °C) and the model only applies to Newtonian fluids; 2) the toluene insolubles were lumped with the asphaltene fraction for modeling purposes; however, the large TI content in this sample (8.6%) could alter the properties of the lumped fraction significantly.

The AAD of the predicted densities were 10.8 kg/m^3 for the maltenes and 14.8 kg/m^3 for the whole vacuum residue. The AARD of the predicted viscosities using fitted densities were 97, 220, and 67% for the ME-VR-A1-12.5 maltenes, ME-VR-A1-VIS18.8 maltenes, and ME-VR-A1-12.5 whole vacuum residue, respectively. The deviations in the predicted density were too large to provide accurate viscosity predictions and these results are not reported. The deviations in the modeled viscosities with fitted densities are far larger than the Development Dataset results (AARD of 15%). The high deviation occurs because all of the proposed correlations are based on feedstock properties and conversion but the properties of the visbroken products in this dataset vary considerably in comparison to the others at the same conversion. Clearly, conversion alone is not adequate to capture the chemical and property changes in oils with different chemistry. Vacuum residues or oils from different sources with a different chemical make-up likely react differently than whole bitumens from Western Canada. Additional input properties would be required to generalize the correlations such as specific gravity, hydrogen to carbon ratio, or carbon residue. A much larger development dataset comprised of feed and visbroken oils and residues from different geographical locations would be required to develop a more robust correlation.

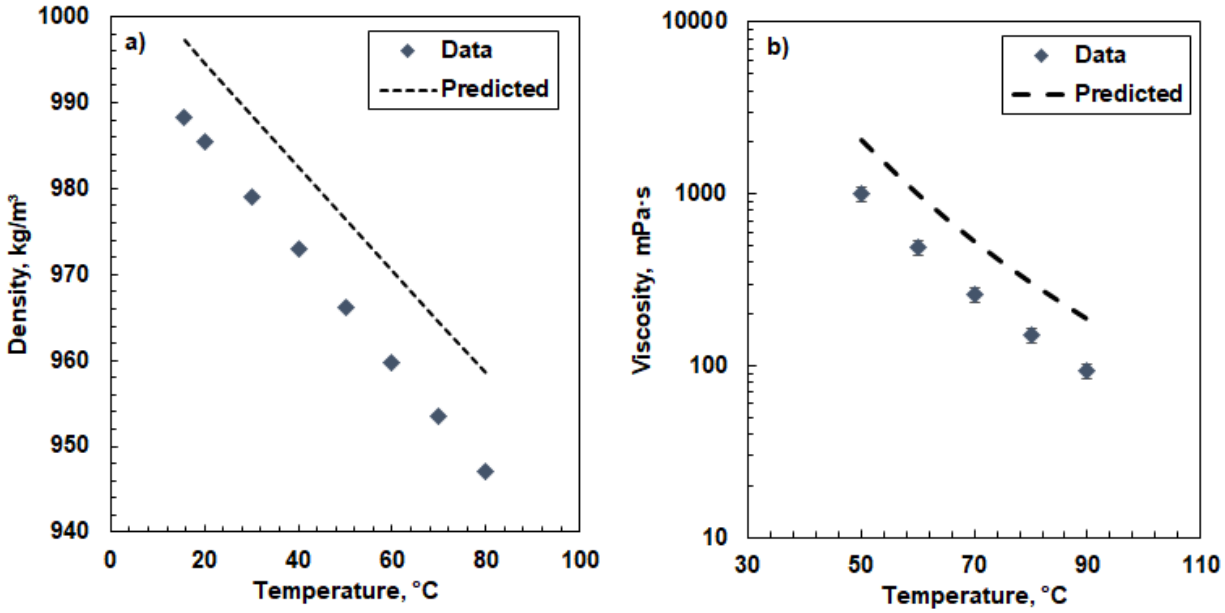

Figure 5.34 Measured and predicted atmospheric pressure properties of WC-VR-A1-VIS12.5 maltenes: a) density; b) viscosity.

.

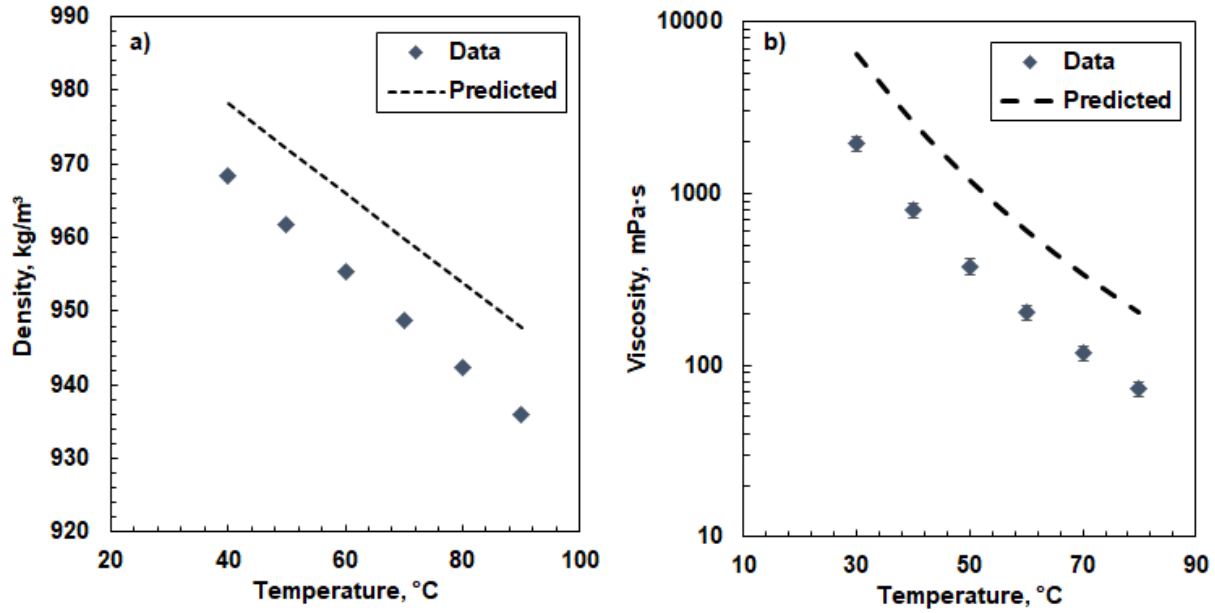

Figure 5.35 Measured and predicted atmospheric pressure properties of WC-VR-A1-VIS18.8 maltenes: a) density; b) viscosity.

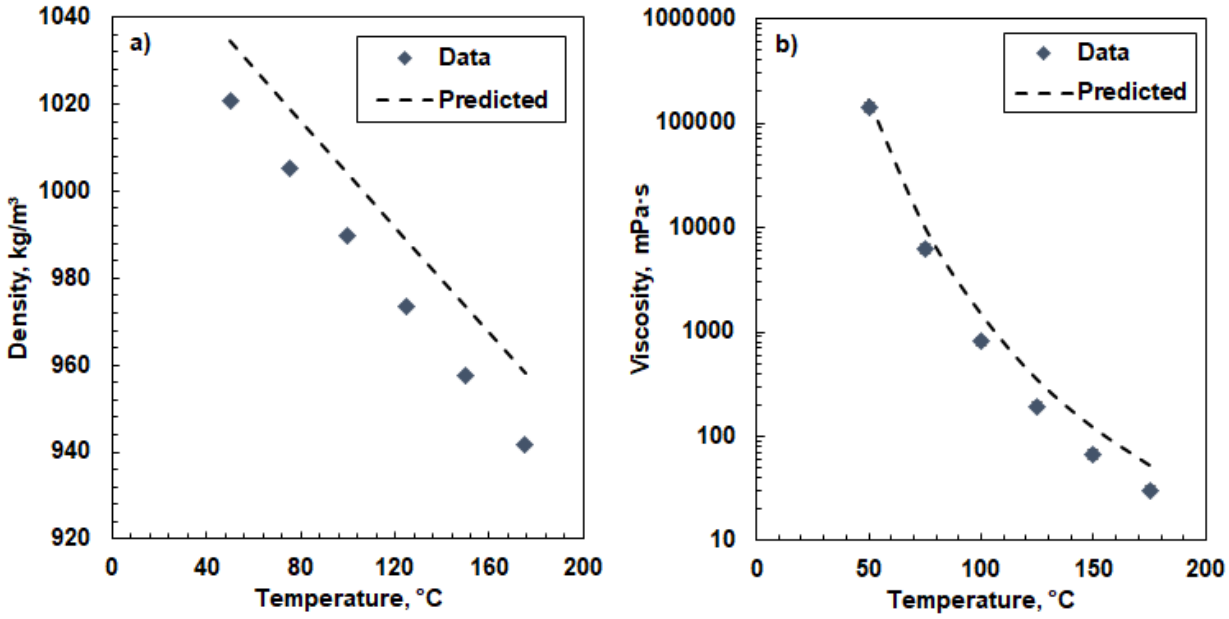

Figure 5.36 Measured and predicted properties of WC-B-B4-VIS12.5 whole oil at 2.5 MPa. Similar trends were observed at pressures up to 10 MPa.

Chapter 6: Conclusions and Recommendations

The main contribution of this thesis is extending the Expanded Fluid model to predict the viscosity of visbroken oils. A characterization methodology consistent with Symmetry process simulator was applied, dividing the oils into distillate, saturate, aromatic, resin and asphaltene fractions. Density and viscosity parameters for each fraction were correlated against conversion, and a recombination methodology was validated to predict whole oil properties. This model can be applied to optimize the visbreaking process for Western Canadian bitumens; for example, in predicting the conversion required to achieve density and viscosity transport specifications or desired cut properties. The main conclusions and recommendations for future research projects are presented below.

6.1. Conclusions

Within the investigated conversion range, visbreaking had the following effects on Western Canadian bitumens:

- Increased distillate content (shifting the true boiling point curve to lower values) with reduced specific gravity.
- Increased microcarbon residue content, decreased viscosity, and decreased molecular weight. Specific gravity initially decreased and then started to increase after approximately 19% conversion.
- Altered distillation residue properties: 1) resins content decreased, 2) asphaltenes content initially decreased and then increased after approximately 8% conversion, 3) coke formation started at approximately 38% conversion. The saturates and aromatics content did not change significantly.
- Altered maltene properties: 1) specific gravity and viscosity of saturates decreased, 2) specific gravity of aromatics increased and their viscosity decreased, 3) specific gravity of resins increased while their viscosity decreased until 8% conversion and then increased.

These observations are consistent with several viscosity reduction mechanisms including: 1) alkyl and naphthenic side chain removal from heavier fractions accumulating in distillates and saturates, 2) breakage of smaller aromatic cores from resins and asphaltenes becoming aromatics and resins,

3) condensation reactions taking place after 8% conversion, leading to increasing asphaltene content and eventual coke formation.

Correlations for the density and viscosity parameters of each fraction were developed as a function of conversion. A regular solution mixing rule and Expanded Fluid (EF) viscosity model mixing rules were used to recombine density and viscosity, respectively. The EF mixing rules require a binary interaction parameter as input. The correlations developed by Ramos-Pallares *et al.*, (2016) to predict this binary interaction parameter were validated for the maltenes of all native and visbroken samples. However, these equations did not accurately capture the interactions of reacted asphaltenes with the other fractions. These interactions were empirically accounted for with a modified correlation for the visbroken distillates-asphaltenes binary interaction parameter.

The inputs of this model are: the composition of each fraction in feed and visbroken oils, pressure, temperature, conversion, and the density and viscosity parameters of each fraction in the feedstock. This model correlates whole oil density and viscosity of the Development Dataset with average deviations of 1.1 kg/m³ and 8%, respectively. The use of correlations only increased the deviations slightly from using fitted parameters.

Two datasets were used to test these model. The first dataset was a Western Canadian bitumen and its visbroken product. This bitumen is expected to be chemically similar to the bitumen used n the Development Dataset. The model was able to predict whole oil density and viscosity of the single 1% conversion product with average deviations of 1 kg/m³ and 20%, respectively. The second dataset was a Middle East Vacuum residue and two of its visbroken products. This oil is expected to be chemically dissimilar to the Development Dataset bitumen. Qualitatively, the properties of the products and fractions from this oil changed with conversion is the same way as observed in the Development Dataset. However, the magnitude of the property changes at the same conversion was much larger. In other words, this oil “reacted” more at the same conversion value. Therefore, the viscosity of the visbroken products could not be accurately modeled using the correlations obtained from the Development Dataset.

The issue is that the correlations depend on conversion which is defined as the change in the mass fraction change of a fixed boiling point cut with reaction. Changes in boiling point do not capture all of the chemical changes within the oil and therefore are insufficient to correlation property changes with conversion where different reaction pathways are followed. Feeds of different chemistry likely follow different reaction pathways. Therefore, the model with the proposed conversion based correlations is expected to perform well for oils chemically similar to Western Canadian bitumen but is not recommended for chemically dissimilar oils. Nor do the correlations necessarily apply to feedstocks from bitumen fractions such as vacuum residues.

6.2. Recommendations

It is recommended to:

- Apply the proposed characterization and measurement methodology to oils from different geographical locations. The data obtained from these measurements could be used to find a second parameter in addition to conversion with which to capture chemical changes within each fraction after reaction. Possible candidates for this parameter are the bulk specific gravity, hydrogen to carbon ratio, or carbon residue.
- Compare the effects of using a vacuum residue and a whole oil as feedstock. These measurements would help to differentiate between possibly different reactions pathways in field upgrading and refinery applications. Again, a second parameter could be found to better correlation the property changes with conversion.
- Use a reaction model for the visbreaking process, such as the one in VMG Symmetry software, to predict visbroken product compositions in terms of the model compound distribution and distillate and SARA fraction contents in defined boiling ranges. Adapt the proposed property correlations to better predict viscosity based on the additional chemical information provided by the reaction model.
- Measure visbroken distillates viscosity using a highly torque sensitive rheometer, such as an Anton Paar MCR-92.
- Measure visbroken asphaltenes viscosity by dilution in different solvents. The data could be used to differentiate between pure asphaltenes viscosity parameters and interactions due to mixing rules. A capillary viscometer could be used for this application, allowing

measurements at different temperatures and pressures. The drawback with this method is that it requires a large amount of asphaltenes samples, making it significantly time consuming.

References

Abivin, P., Taylor, S. D., Freed, D. (2012). Thermal Behavior and Viscoelasticity of Heavy Oils. *Energy & Fuels, 26*(6), 3448-3461.

Al-Soufi, H., Savaya, Z., Mohammed, H., Al-Azawi, I. (1988). Thermal conversion (visbreaking) of heavy Iraqi residue. *Fuel, 67*(12), 1714-1715.

Alboudwarej, H., Beck, J., Svrcek, W. Y., Yarranton, H. W., & Akbarzadeh, K. (2002). Sensitivity of asphaltene properties to separation techniques. *Energy & Fuels*, *16*(2), 462-469.

Allal, A., Boned, C., Baylaucq, A. (2001). Free-volume viscosity model for fluids in the dense and gaseous states. *Physical Review E, 64*(1).

Altgelt, K. H., Boduszynski, M. M. (1994). *Composition and analysis of heavy petroleum fractions*. New York, NY: Dekker.

ASTM Standard D7169. 2018. "Standard Test Method for Boiling Point Distribution of Samples with Residues Such as Crude Oils and Atmospheric and Vacuum Residues by High Temperature Gas Chromatography".

ASTM Standard D2007. 2016. "Standard Test Method for Characteristic Groups in Rubber Extender and Processing Oils and Other Petroleum-Derived Oils by the Clay-Gel Absorption Chromatographic Method".

Badamchi-Zadeh, A., Yarranton, H., Svrcek, W., Maini, B. (2009). Phase Behaviour and Physical Property Measurements for VAPEX Solvents: Part I. Propane and Athabasca Bitumen. *J. Can. Petro. Tech., 48*(01), 54-61.

Badamchi-Zadeh, A., Yarranton, H., Maini, B., Satyro, M. (2009). Phase Behaviour and Physical Property Measurements for VAPEX Solvents: Part II. Propane, Carbon Dioxide and Athabasca Bitumen. *J. Can. Pet. Tech., 48*(03), 57-65.

Baltatu, M. E. (1982). Prediction of the liquid viscosity for petroleum fractions. *Ind. Eng. Chem. Proc. Des. Devlp., 21*(1), 192-195.

Bianco, A. D., Panariti, N., Anelli, M., Beltrame, P., Carniti, P. (1993). Thermal cracking of petroleum residues. *Fuel, 72*(1), 75-80.

Bird, R. B., Stewart, W. E., Lightfoot, E. N. (2002). *Transport phenomena*. New York: J. Wiley.
Bozzano, G., Dente, M., Carlucci, F. (2005). The effect of naphthenic components in the visbreaking modeling. *Computers & Chemical Engineering, 29*(6), 1439-1446.

BP Statistical Review of World Energy 2018. (n.d.). Retrieved from: https://www.bp.com/content/dam/bp/en/corporate/pdf/energy-economics/statistical-review/bp-stats-review-2018-full-report.pdf

Carbognani, L., Gonzalez, M. F., Pereira-Almao, P. (2007). Characterization of Athabasca Vacuum Residue and Its Visbroken Products. Stability and Fast Hydrocarbon Group-Type Distributions. *Energy & Fuels, 21*(3), 1631-1639.

Carbognani, L., Lubkowitz, J., Gonzalez, M. F., Pereira-Almao, P. (2007). High Temperature Simulated Distillation of Athabasca Vacuum Residue Fractions. Bimodal Distributions and Evidence for Secondary “On-Column” Cracking of Heavy Hydrocarbons. *Energy & Fuels, 21*(5), 2831-2839.

Carlo, S. D., Janis, B. (1992). Composition and visbreakability of petroleum residues. *Chem. Eng. Sci., 47*(9-11), 2695-2700.

Chung, T. H., Ajlan, M., Lee, L. L., Starling, K. E. (1988). Generalized multiparameter correlation for nonpolar and polar fluid transport properties. *Ind. Eng. Chem. Res.*, *27*(4), 671-679.

Cohen, M. H., Turnbull, D. (1959). Molecular Transport in Liquids and Glasses. *J. Chem. Phys.*, *31*(5), 1164-1169.

De Klerk, Arno, Murray R. Gray, and N Zerpa. 2014. "Unconventional Oil and Gas: Oilsands." In *Future Energy. Improved, Sustainable, and Clean Options for Our Planet.*, Amsterdam: Elsevier, 95–116.

Dente, M., Bozzano, G., Bussani, G. (1995). The visbreaking process simulation: Products amount and their properties prediction. *Comp. Chem. Eng.*, *19*, 205-210.

Dente, M., Bozzano, G., Bussani, G. (1997). A comprehensive program for visbreaking simulation: Product amounts and their properties prediction. *Comp. Chem. Eng.*, *21*(10), 1125-1134.

Eastick, R. R., Mehrotra, A. K. (1990). Viscosity data and correlation for mixtures of bitumen fractions. *Fuel Processing Technology*, *26*(1), 25-37.

Ely, J. F., Hanley, H. J. (1981). Prediction of transport properties. 1. Viscosity of fluids and mixtures. *Ind. Eng. Chem. Fund.*, *20*(4), 323-332.

Gray, M. R. (1994). *Upgrading Petroleum Residues and Heavy Oils*. New York: M. Dekker.

Gray, M. R. (2015). *Upgrading Oilsands Bitumen and Heavy Oil*. Edmonton, Alberta, Canada: Pica Pica Press, an imprint of The University of Alberta Press.

Hay, G. Personal Communication. Calgary, Canada, 2018.

Hanley, H., Mccarty, R., & Haynes, W. (1975). Equations for the viscosity and thermal conductivity coefficients of methane. *Cryogenics,15*(7), 413-417.

Hanley, H. (1976). Prediction of the viscosity and thermal conductivity coefficients of mixtures. *Cryogenics,16*(11), 643-651.

Henderson, J., Weber, L. (1965). Physical Upgrading of Heavy Crude Oils by the Application of Heat. *J. Can. Pet. Tech.,4*(04), 206-212.

Hildebrand, J. H. (1971). Motions of Molecules in Liquids: Viscosity and Diffusivity. *Science, 174*(4008), 490-493.

Joshi, J. B., Pandit, A. B., Kataria, K. L., Kulkarni, R. P., Sawarkar, A. N., Tandon, D., Kumar, M. M. (2008). Petroleum Residue Upgradation via Visbreaking: A Review. *Ind. Eng. Chem. Res., 47*(23), 8960-8988.

Kataria, K. L., Kulkarni, R. P., Pandit, A. B., Joshi, J. B., Kumar, M. (2004). Kinetic Studies of Low Severity Visbreaking. *Ind. Eng. Chem. Res., 43*(6), 1373-1387.

Krishna, R., Kuchhal, Y., Sarna, G., Singh, I. (1988). Visbreaking studies on Aghajari long residue. *Fuel, 67*(3), 379-383.

Kumar, A., Henni, A., Shirif, E. (2011). Heavy Oil Viscosity Modeling with Friction Theory. *Energy & Fuels, 25*(2), 493-498.

Li, H., Zheng, S., Yang, D. (. (2013). Enhanced Swelling Effect and Viscosity Reduction of Solvent(s)/CO2/Heavy-Oil Systems. *SPE Journal, 18*(04), 695-707.

Lindeloff, N., Pedersen, K., Ronningsen, H., Milter, J. (2004). The Corresponding States Viscosity Model Applied to Heavy Oil Systems. *J. Can. Pet. Tech., 43*(09).

Maxwell, J. B., Bonnell, L. S. (1957). Derivation and Precision of a New Vapor Pressure Correlation for Petroleum Hydrocarbons. *Ind. Eng. Chem., 49*(7), 1187-1196.

Mckenna, A. M., Donald, L. J., Fitzsimmons, J. E., Juyal, P., Spicer, V., Standing, K. G., Rodgers, R. P. (2013). Heavy Petroleum Composition. 3. Asphaltene Aggregation. *Energy & Fuels, 27*(3), 1246-1256.

Mehrotra, A. K., Svrcek, W. Y. (1986). Viscosity of compressed athabasca bitumen. *Can. J. Chem. Eng., 64*(5), 844-847.

Mehrotra, A. K. (1990). Development of mixing rules for predicting the viscosity of bitumen and its fractions blended with toluene. *Can. J. Chem. Eng., 68*(5), 839-848.

Mehrotra, A. K. (1990). Modeling the effects of temperature, pressure, and composition on the viscosity of crude oil mixtures. *Ind. Eng. Chem. Res., 29*(7), 1574-1578.

Motahhari, H., Satyro, M. A., Yarranton, H. W. (2011). Predicting the Viscosity of Asymmetric Hydrocarbon Mixtures with the Expanded Fluid Viscosity Correlation. *Ind. Eng. Chem. Res., 50*(22), 12831-12843.

Motahhari, H., Satyro, M. A., Taylor, S. D., Yarranton, H. W. (2013). Extension of the Expanded Fluid Viscosity Model to Characterized Oils. *Energy & Fuels, 27*(4), 1881-1898.

Motahhari, H., Schoeggl, F., Satyro, M., & Yarranton, H. (2013). Viscosity Prediction for Solvent-Diluted Live Bitumen and Heavy Oil at Temperatures Up to 175°C. *J. Can. Pet. Tech., 52*(05), 376-390.

Motahhari, H. “Development of Viscosity Model for Petroleum Industry Applications.” PhD Thesis, 2013, University of Calgary, Calgary, Canada.

Pedersen, K. S., Fredenslund, A., Christensen, P. L., Thomassen, P. (1984). Viscosity of crude oils. *Chem. Eng. Sci., 39*(6), 1011-1016.

Pedersen, K. S., Fredenslund, A. (1987). An improved corresponding states model for the prediction of oil and gas viscosities and thermal conductivities. *Chem. Eng. Sci., 42*(1), 182-186.

Porte, J. D., Kossack, C. (2014). A liquid phase viscosity–temperature model for long-chain n -alkanes up to C 64 H 130 based on the Free Volume Theory. *Fuel, 136*, 156-164.

Porte, J. J., Zimmerman, R. W., Kossack, C. A. (2014). Modelling Heavy Oil Viscosity during Thermal Stimulation using the Free Volume Theory. *SPE Annual Technical Conference and Exhibition*.

Powers, D., Sadeghi, H., Yarranton, H., Berg, F. V. (2016). Regular solution based approach to modeling asphaltene precipitation from native and reacted oils: Part 1, molecular weight, density, and solubility parameter distributions of asphaltenes. *Fuel, 178*, 218-233.

Quinones-Cisneros, S. E., Zeberg-Mikkelsen, C. K., Stenby, E. H. (2000). The friction theory (f-theory) for viscosity modeling. *Fluid Phase Equilibria, 169*(2), 249-276.

Quinones-Cisneros, S. E., Zeberg-Mikkelsen, C. K., Stenby, E. H. (2001). One parameter friction theory models for viscosity. *Fluid Phase Equilibria, 178*(1-2), 1-16.

Quinones-Cisneros, S. E., Zeberg-Mikkelsen, C. K., Stenby, E. H. (2001). The friction theory for viscosity modeling: Extension to crude oil systems. *Chem. Eng. Sci., 56*(24), 7007-7015.

Quinones-Cisneros, S. E., Zeberg-Mikkelsen, C. K., Stenby, E. H. (2003). Friction theory prediction of crude oil viscosity at reservoir conditions based on dead oil properties. *Fluid Phase Equilibria, 212*(1-2), 233-243.

Quinones-Cisneros, S. E., Zeberg-Mikkelsen, C. K., Baylaucq, A., Boned, C. (2004). Viscosity Modeling and Prediction of Reservoir Fluids: From Natural Gas to Heavy Oils. *Int. J. Therm.*, *25*(5), 1353-1366.

Rackett, H. G. (1970). Equation of state for saturated liquids. *J. Chem. Eng. Data.*, *15*(4), 514-517.

Ramos-Pallares, F., Schoeggl, F. F., Taylor, S. D., Satyro, M. A., Yarranton, H. W. (2015). Predicting the Viscosity of Hydrocarbon Mixtures and Diluted Heavy Oils Using the Expanded Fluid Model. *Energy & Fuels*, *30*(5), 3575-3595.

Ramos-Pallares, F., Taylor, S. D., Satyro, M. A., Marriott, R. A., & Yarranton, H. W. (2016). Prediction of viscosity for characterized oils and their fractions using the expanded fluid model. *Energy & Fuels*, *30*(9), 7134-7157.

Ramos-Pallares, F., Lin, H., Yarranton, H. W., Taylor, S. D. (2017). Prediction of the Liquid Viscosity of Characterized Crude Oils by Use of the Generalized Walther Model. *SPE Journal*, *22*(05), 1487-1505.

Rana, M. S., Sámano, V., Ancheyta, J., Diaz, J. (2007). A review of recent advances on process technologies for upgrading of heavy oils and residua. *Fuel*, *86*(9), 1216-1231.

Raseev, S. D. (2003). *Thermal and Catalytic Processes in Petroleum Refining*. New York: Marcel Dekker.

Riazi, M. R. (2005). *Characterization and Properties of Petroleum Fractions*. West Conshohocken, PA: ASTM International.

RIPP (SINOPEC Research Institute of Petroleum Processing). Personal Communication. Calgary, Canada, 2017.

Rodriguez-Leon, S. L. “The Stability of Visbroken Heavy Oil Against Asphaltene Precipitation”. MSc Thesis, 2018, University of Calgary, Calgary, Canada.

Rueda-Velásquez, R. I., Gray, M. R. (2017). A viscosity-conversion model for thermal cracking of heavy oils. *Fuel, 197,* 82-90.

Rueda-Velásquez, R. I. “Characterization of Asphaltene Molecular Structures by Cracking under Hydrogenation Conditions and Prediction of the Viscosity Reduction from Visbreaking of Heavy Oils.” PhD Thesis, 2013, University of Alberta, Edmonton, Canada.

Sanchez-Lemus, M. C. “Extender Distillation and Property Correlations for Heavy Oil.” University of Calgary. PhD Thesis, 2015, University of Calgary, Calgary, Canada.

Sánchez-Lemus, M., Schoeggl, F., Taylor, S., Yarranton, H. (2016). Physical properties of heavy oil distillation cuts. *Fuel, 180,* 457-472.

Saryazdi, F., Motahhari, H., Schoeggl, F. F., Taylor, S. D., Yarranton, H. W. (2013). Density of Hydrocarbon Mixtures and Bitumen Diluted with Solvents and Dissolved Gases. *Energy & Fuels*, *27*(7), 3666-3678.

Shu, W., Venkatesan, V. (1984). Kintetics Of Thermal Visbreaking Of A Cold Lake Bitumen. *J. Can. Pet. Tech.*, *23*(02).

Singh, I. D., Kothiyal, V., Kapoor, M. P., Ramaswamy, V., Aloopwan, M. K. (1993). Structural changes during visbreaking of light Arabian mix short residue: Comparison of feed and product asphaltenes. *Fuel, 72*(6), 751-754.

Singh, J., Kumar, S., Garg, M. O. (2012). Kinetic modelling of thermal cracking of petroleum residues: A critique. *Fuel Processing Technology*, *94*(1), 131-144.

Soto-Castruita, E., Ramirez-Gonzalez, P. V., Martinez-Cortes, U., Quinones-Cisneros, S. E. (2015). Effect of the Temperature on the Non-Newtonian Behavior of Heavy Oils. *Energy & Fuels*, *29*(5), 2883-2889.

Speight, J. (1986). Upgrading Heavy Feedstocks. *Ann. Rev. Energy. Env., 11*(1), 253-274.

Speight, J. G. (2007). *The Chemistry and Technology of Petroleum*. Boca Raton: CRC Press/Taylor & Francis.

Speight, J. (2012). Visbreaking: A technology of the past and the future. *Scientia Iranica, 19*(3), 569-573.

Svrcek, W. Y., Mehrotra, A. K. (1988). One parameter correlation for bitumen viscosity. *Chem. Eng. Res. Des., 66*(4), 323-327.

Tan, S. P., Adidharma, H., Towler, B. F., Radosz, M. (2005). Friction Theory and Free-Volume Theory Coupled with Statistical Associating Fluid Theory for Estimating the Viscosity of Pure n-Alkanes. *Ind. Eng. Chem. Res., 44*(22), 8409-8418.

Tham, M. J., Gubbins, K. E. (1970). Correspondence Principle for Transport Properties of Dense Fluids. Nonpolar Polyatomic Fluids. *Ind. Eng. Chem. Fund.,9* (1), 63-70.

Walther, C. (1931). The evaluation of viscosity data. *Erdol Teer, 7*, 382-384.

Wang, L., Zachariah, A., Yang, S., Prasad, V., Klerk, A. D. (2014). Visbreaking Oilsands-Derived Bitumen in the Temperature Range of 340–400 °C. *Energy & Fuels, 28*(8), 5014-5022.

Wiehe, I. A. (1992). A solvent-resid phase diagram for tracking resid conversion. *Ind. Eng. Chem. Res., 31*(2), 530-536.

Wiehe, I. A. (1993). A phase-separation kinetic model for coke formation. *Ind. Eng. Chem. Res.*, *32*(11), 2447-2454.

Wilke, C. R. (1950). A Viscosity Equation for Gas Mixtures. *The Journal of Chemical Physics*, *18*(4), 517-519.

Yan, T. (1990). Characterization of visbreaker feeds. *Fuel*, *69*(8), 1062-1064.

Yarranton, H.W., "SARA's Role in Oil Characterization: Should There be One?", *Petrophase 2009 10th International Conference on Petroleum Phase Behavior and Fouling*, Rio de Janeiro, June 14-19, 2009.

Yarranton, H. W., Satyro, M. A. (2009). Expanded Fluid-Based Viscosity Correlation for Hydrocarbons. *Ind. Eng. Chem. Res.*, *48*(7), 3640-3648.

Yarranton, H. W., Ortiz, D. P., Barrera, D. M., Baydak, E. N., Barré, L., Frot, D., Eyssautier, J., Zeng, H., Xu, Z., Dechaine, G., Becerra, M., Shaw, J., Mckenna, A., Mapolelo, M., Bohne, C., Yang, C., Oake, J. (2013). On the Size Distribution of Self-Associated Asphaltenes. *Energy & Fuels*, *27*(9), 5083-5106.

Yarranton, H., Dorp, J. V., Verlaan, M., Lastovka, V. (2013). Wanted Dead or Live: Crude-Cocktail Viscosity--A Pseudocomponent Method to Predict the Viscosity of Dead Oils, Live Oils, and Mixtures. *J. Can. Pet. Tech.*, *52*(03), 176-191.

Yarranton, H., Powers, D., Okafor, J., Berg, F. V. (2018). Regular solution based approach to modeling asphaltene precipitation from native and reacted oils: Part 2, molecular weight, density, and solubility parameter of saturates, aromatics, and resins. *Fuel*, *215*, 766-777.

Yaws, C. L. (2008). *Transport Properties of Hydrocarbons*. Norwich, NY: William Andrew Inc.

Zhao, S., Kotlyar, L., Woods, J., Sparks, B., Hardacre, K., Chung, K. (2001). Molecular transformation of Athabasca bitumen end-cuts during coking and hydrocracking. *Fuel*, *80*(8), 1155-1163.

Appendix A: Whole Oil Data

This appendix summarizes the density and viscosity data for all whole oils used in this thesis. The repeatability for all whole oils density and viscosity were ±0.5 kg/m^3 and ±3%, respectively.

Table A.1 Whole oil density and viscosity for WC-B-A3(1).

Pressure, MPa	**Temperature, °C**	**Density, kg/m^3**	**Viscosity, mPa·s**
0.1	50	988.0	4400
0.1	75	971.8	572
2.5	50	989.7	4930
2.5	75	973.3	631
2.5	100	957.1	153
2.5	125	941.2	54
2.5	150	925.0	25.3
5.0	50	991.1	5430
5.0	75	974.7	682
5.0	100	958.8	162
5.0	125	943.1	57.4
5.0	150	927.1	26.7
5.0	175	911.6	14.6
7.5	50	992.5	5970
7.5	75	976.5	741
7.5	100	960.5	173
7.5	125	944.9	60.6
7.5	150	929.2	27.9
7.5	175	913.9	15.2
10.0	75	977.8	801
10.0	100	962.1	184
10.0	125	946.8	63.9
10.0	150	931.3	29.1
10.0	175	915.9	15.9

Table A.2 Whole oil density and viscosity for WC-B-A3(2). All data measured at atmospheric pressure.

Temperature, °C	Density, kg/m³	Viscosity, mPa·s
40	995.1	16300
50	988.7	5350
60	982.4	2430
70	976.1	1110
80	969.7	586
90	963.4	347

Table A.3 Whole oil density and viscosity for WC-B-A3(1)-VIS5.1.

Pressure, MPa	Temperature, °C	Density, kg/m³	Viscosity, mPa·s
0.1	50	984.3	1730
0.1	75	968.2	296
0.1	100	952.0	94.6
2.5	50	985.3	1870
2.5	75	969.4	317
2.5	100	953.4	89.4
2.5	125	937.3	35.6
2.5	175	905.1	9.7
5.0	50	986.8	2040
5.0	75	971.0	337
5.0	100	955.3	94.7
5.0	125	939.0	37.3
5.0	150	923.2	18.3
5.0	175	907.1	10.2
7.5	50	988.2	2230
7.5	75	972.5	360
7.5	100	956.8	100
7.5	125	940.9	39.2
7.5	150	925.2	19.1
7.5	175	909.4	10.6
10.0	50	989.5	2420
10.0	75	974.0	384
10.0	100	958.5	106
10.0	125	942.7	41.2
10.0	150	927.1	20
10.0	175	911.5	11

Table A.4 Whole oil density and viscosity for WC-B-A3(2)-VIS4.9.

Pressure, MPa	Temperature, °C	Density, kg/m³	Viscosity, mPa·s
0.1	50	980.7	858
0.1	75	964.3	171
0.1	100	948.0	54.7
0.1	125	931.6	23.2
2.5	50	981.8	932
2.5	75	965.7	183
2.5	100	949.6	57.7
2.5	125	933.2	24.2
2.5	150	917.3	12.9
2.5	175	901.7	7.7
5.0	50	983.2	988
5.0	75	967.3	197
5.0	100	951.4	60.9
5.0	125	935.2	25.6
5.0	150	919.5	13.5
5.0	175	903.8	8.1
7.5	50	984.6	1075
7.5	75	969.1	209
7.5	100	953.2	64.4
7.5	125	937.1	26.8
7.5	150	921.6	14.1
7.5	175	906.2	8.3
10.0	50	986.1	1160
10.0	75	970.5	222
10.0	100	955.0	67.8
10.0	125	939.1	28
10.0	150	923.7	14.8
10.0	175	908.2	8.7

Table A.5 Whole oil density and viscosity for WC-B-A3(2)-VIS8.1.

Pressure, MPa	Temperature, °C	Density, kg/m³	Viscosity, mPa·s
0.1	50	980.4	613
0.1	75	964.2	130
0.1	100	948.0	43.8
2.5	50	981.5	665
2.5	75	965.4	139
2.5	100	949.5	46
2.5	125	933.3	20.4
2.5	150	917.1	10.8
2.5	175	901.2	6.7
5.0	50	982.9	705
5.0	75	967.0	147
5.0	100	951.2	48.4
5.0	125	935.1	21.3
5.0	150	919.3	11.3
5.0	175	903.3	6.9
7.5	50	984.4	759
7.5	75	968.5	156
7.5	100	952.9	51
7.5	125	937.0	22.3
7.5	150	921.2	11.8
7.5	175	905.6	7.2
10.0	50	985.9	821
10.0	75	969.9	166
10.0	100	954.6	53.7
10.0	125	938.8	23.3
10.0	150	923.3	12.4
10.0	175	907.7	7.5

Table A.6 Whole oil density and viscosity for WC-B-A3(2)-VIS19.3.

Pressure, MPa	Temperature, °C	Density, kg/m³	Viscosity, mPa·s
0.1	50	972.2	231
0.1	75	955.8	61.3
0.1	100	939.3	23.3
2.5	50	973.6	249
2.5	75	957.2	65.2
2.5	100	940.8	25
2.5	125	924.3	12.3
2.5	150	907.4	7
2.5	175	890.4	4.4
5.0	50	975.2	264
5.0	75	958.8	68.7
5.0	100	942.5	25.8
5.0	125	926.3	12.8
5.0	150	909.6	7.3
5.0	175	892.9	4.6
7.5	50	976.8	281
7.5	75	960.3	72.4
7.5	100	944.3	26.8
7.5	125	928.1	13.3
7.5	150	911.7	7.6
7.5	175	895.2	4.8
10.0	50	978.2	301
10.0	75	961.7	76.2
10.0	100	945.9	28.2
10.0	125	930	13.9
10.0	150	913.8	7.9
10.0	175	897.5	5

Table A.7 Whole oil density and viscosity for WC-B-A3(2)-VIS38.1.

Pressure, MPa	Temperature, °C	Density, kg/m³	Viscosity, mPa·s
0.1	50	977.1	123
0.1	75	960.2	35.8
0.1	100	943.3	15
2.5	50	978.5	132
2.5	75	961.3	37.7
2.5	100	945.2	15.7
2.5	125	928.4	8.2
2.5	150	911.5	4.9
2.5	175	895.0	3.3
5.0	50	979.9	139
5.0	75	963.0	39.3
5.0	100	946.8	16.4
5.0	125	930.3	8.5
5.0	150	913.7	5.1
5.0	175	897.4	3.4
7.5	50	981.4	148
7.5	75	964.6	41.3
7.5	100	948.5	17
7.5	125	932.3	8.8
7.5	150	915.8	5.3
7.5	175	900.0	3.5
10.0	50	982.9	157
10.0	75	966.3	43.6
10.0	100	950.1	17.9
10.0	125	934.4	9.2
10.0	150	918.0	5.5
10.0	175	902.3	3.6

Table A.8 Whole oil density and viscosity for WC-B-A4. Note: All measurements performed at atmospheric pressure.

Temperature, °C	Density, kg/m³	Viscosity, mPa·s
30	1003.9	150000
40	997.6	38500
50	991.4	12300
60	985.1	4670
70	978.9	2090
80	972.5	1030
90	966.1	555

Table A.9 Whole oil density and viscosity for WC-B-A4-VIS1. All measurements performed at atmospheric pressure.

Temperature, °C	Density, kg/m³	Viscosity, mPa·s
30	1002.8	91000
40	996.5	25200
50	990.2	8270
60	984.0	3420
70	977.7	1550
80	971.4	772
90	965.1	420

Table A.10 Whole residue density and viscosity for ME-VR-A1.

Pressure, MPa	Temperature, °C	Density, kg/m³	Viscosity, mPa·s
2.5	75	1018.4	414000
2.5	100	1003.8	22300
2.5	125	988.4	3090
2.5	150	973.4	702
2.5	175	959.1	227
5.0	75	1019.8	500000
5.0	100	1005.3	24700
5.0	125	990.0	3630
5.0	150	975.2	768
5.0	175	961.0	245
7.5	75	1021.2	578000
7.5	100	1006.9	29300
7.5	125	991.4	3747
7.5	150	976.9	823
7.5	175	962.9	258
10.0	75	1022.6	617000
10.0	100	1008.3	31300
10.0	125	992.8	3830
10.0	150	978.7	886
10.0	175	964.8	274

Table A.11 Whole residue density and viscosity for ME-VR-A1-VIS12.5.

Pressure, MPa	Temperature, °C	Density, kg/m³	Viscosity, mPa·s
0.1	50	1019.5	127000
0.1	75	1003.7	5610
2.5	50	1020.8	143000
2.5	75	1005.2	6230
2.5	100	989.7	810
2.5	125	973.4	195
2.5	150	957.6	67.2
2.5	175	941.8	30.7
5.0	50	1022.2	159000
5.0	75	1006.7	6670
5.0	100	991.3	867
5.0	125	975.2	203
5.0	150	959.7	71.3
5.0	175	944.1	31.8
7.5	50	1023.6	177000
7.5	75	1008.2	7220
7.5	100	992.9	929
7.5	125	977.1	215
7.5	150	961.7	74.8
7.5	175	946.4	33.3
10.0	50	1025.0	195000
10.0	75	1009.7	7940
10.0	100	994.6	988
10.0	125	979.0	229
10.0	150	963.7	78.7
10.0	175	948.6	34.9

Table A.12 Whole residue density and viscosity for ME-VR-A1-VIS18.8.

Pressure, MPa	Temperature, °C	Density, kg/m³	Viscosity, mPa·s
2.5	100	997.0	1310
2.5	125	979.9	220
2.5	150	966.0	68.5
2.5	175	945.6	30.2
5.0	100	998.6	1400
5.0	125	981.7	230
5.0	150	968.2	70.1
5.0	175	947.9	31.5
7.5	100	1000.3	1510
7.5	125	983.4	240
7.5	150	970.3	73.2
7.5	175	950.2	33.3
10.0	100	1001.9	1610
10.0	125	985.3	256
10.0	150	972.4	77.7
10.0	175	952.4	35.2

Appendix B: Distillation Data

This appendix provides all physical distillation and SimDist data collected for this study.

Table B.1 Spinning Band Distillation data for WC-B-A3(1) feedstock.

Cumulative Weight Fraction Distilled	Boiling Temperature °C
0.0161	206.6
0.0326	237
0.0495	258.2
0.0667	282.3
0.0841	300.6
0.1017	308.7
0.1193	322.2
0.1372	334.5
0.1551	345.8
0.1732	358.2
0.1913	363.5
0.2094	367.4
0.2276	372

Table B.2 Spinning Band Distillation data of WC-B-A3(2) feedstock.

Cumulative Weight Fraction Distilled	Boiling Temperature °C
0.0139	203
0.0280	226
0.0425	251
0.0573	272.5
0.0722	287
0.0870	294
0.1020	304
0.1170	314
0.1321	324
0.1398	333
0.1551	338
0.1706	346
0.1861	355
0.2018	365
0.2214	375

Table B.3 Spinning Band Distillation data of WC-B-A3(1)-VIS5.1.

Cumulative Weight Fraction Distilled	Boiling Temperature °C
0.0142	190
0.0288	221.4
0.0437	240.6
0.0589	261.4
0.0743	278.4
0.0899	294.8
0.1056	305.6
0.1214	318.4
0.1374	330.1
0.1534	338.2
0.1695	345
0.1856	353.1
0.2018	360
0.2181	368.9
0.2263	372

Table B.4 Spinning Band Distillation data of WC-B-A3(2)-VIS4.9.

Cumulative Weight Fraction Distilled	Boiling Temperature °C
0.01463	190.5
0.02976	223.5
0.04519	244.6
0.06079	258
0.07656	270.5
0.09242	279
0.10856	302
0.12483	314
0.14121	325
0.15767	333
0.17422	341
0.19084	349.5
0.20754	357
0.22434	369
0.24122	376
0.26659	379

Table B.5 Spinning Band Distillation data of WC-B-A3(2)-VIS8.1.

Cumulative Weight Fraction Distilled	**Boiling Temperature °C**
0.0122	121
0.0249	149
0.0387	218.6
0.0527	235
0.0671	257
0.0810	265
0.0950	274
0.1090	282
0.1197	289
0.1339	295
0.1482	303
0.1626	310
0.1771	325
0.1917	333
0.2064	341
0.2212	348
0.2360	355
0.2510	365
0.2660	374
0.2848	378

Table B.6 Spinning Band Distillation data of WC-B-A3(2)-VIS19.3.

Cumulative Weight Fraction Distilled	**Boiling Temperature °C**
0.0125	119
0.0255	145.4
0.0391	182.7
0.0531	207.4
0.0674	227
0.0815	242
0.0957	246
0.1102	268
0.1248	281
0.1395	288
0.1579	290
0.1727	295
0.1875	300
0.2025	309
0.2175	317.8
0.2326	327
0.2478	336
0.2632	343
0.2786	346
0.2940	356.6
0.3096	363
0.3252	373
0.3330	380

Table B.7 Spinning Band Distillation data of WC-B-A3(2)-VIS38.1.

Cumulative Weight Fraction Distilled	Boiling Temperature °C
0.0144	128
0.0296	163.2
0.0451	184
0.0609	201
0.0770	217
0.0933	231
0.1099	244
0.1265	252
0.1432	260
0.1601	273
0.1771	284
0.1942	291
0.2028	300
0.2201	306
0.2375	314
0.2551	326
0.2727	334
0.2904	338
0.3126	347
0.3306	358
0.3487	367
0.3669	377
0.3760	380

Table B.8 Spinning Band Distillation data of WC-B-A4.

Cumulative Weight Fraction Distilled	Boiling Temperature °C
0.0144	232
0.0294	276
0.0445	290
0.0597	306
0.0752	320
0.0907	331
0.1063	342
0.1220	354
0.1378	364
0.1616	374

Table B.9 Spinning Band Distillation data of WC-B-A4-VIS1.

Cumulative Weight Fraction Distilled	Boiling Temperature °C
0.0142	220
0.0288	257
0.0437	283
0.0588	300
0.0741	310
0.0894	322
0.1049	335
0.1204	350
0.1361	355
0.1676	372

Table B.10 Extended Simulated Distillation assays for WC-B-A3 and its visbroken products.

Cumulative Weight Fraction	WC-B-A3 °C	VIS5.1 °C	VIS4.9 °C	VIS8.1 °C	VIS19.3 °C	VIS38.1 °C
0.05	256	244.5	234	229	205	188
0.1	297.5	287.5	280	274	253	227
0.15	327	318.5	313	307	287	257
0.2	355	345.5	340	333	314	283
0.25	380	370.5	366	359	339	307
0.3	405	395	391	384	363	327
0.35	427.5	419	416	408	386	349
0.4	450	440.5	438	431	410	371
0.45	475	464	462	454	432	391
0.5	501.5	489.5	489	480	455	413
0.55	529	516	516	507	481	435
0.6	557.5	544	546	537	507	459
0.65	586	572.5	576	567	536	486
0.7	613.5	601	604	597	567	514
0.75	636.5	627.5	631	625	596	546
0.8	656.5	651	654	651	625	579
0.85	678.5	674	679	677	653	613

Table B.11 Extended Simulated Distillation assays for WC-B-A4 and its visbroken product.

Cumulative Weight Fraction	WC-B-A4 °C	VIS1 °C
0.01	208.1	219.2
0.02	237.4	242.8
0.03	257.5	260.1
0.04	272.8	274.2
0.05	285.6	286.0
0.10	329.8	320.7
0.15	364.3	351.5
0.20	394.6	385.9
0.25	422.0	416.5
0.30	447.4	443.8
0.31	452.8	449.4
0.32	458.4	455.2
0.33	464.2	461.2
0.34	469.8	467.1
0.35	475.4	472.7
0.40	504.5	501.9
0.45	535.2	531.9
0.50	567.4	564.0
0.55	597.6	596.1
0.60	625.1	626.8
0.65	647.9	653.4
0.70	669.8	676.2
0.75	693.4	696.2
0.80	716.6	723.6
0.85	-	751.9

Table B.12 Extended Simulated Distillation assays for ME-VR-A1 and its visbroken products.

Cumulative Weight Fraction	ME-VR-A1 °C	VIS12.5 °C	VIS18.8 °C
0.005	498.1	365.3	156.3
0.01	510	377.6	173.5
0.02	521.6	398.4	207.6
0.03	535	416.6	249.8
0.04	542.8	430.6	353.2
0.05	549.6	444.2	372
0.10	573.3	494.6	436.8
0.15	589.5	527.6	484.5
0.20	602.7	553	520.1
0.25	614	572.9	550.3
0.30	624.5	588.8	575.5
0.35	634	604.8	598
0.40	643.1	621.5	622.9
0.45	652.9	638.2	-
0.50	662.5	655.6	-
0.55	673.2	675.9	-
0.60	684.3	696.6	-
0.65	693.9	715.3	-
0.70	703.3	-	-
0.75	711.7	-	-
0.80	720.2	-	-
0.85	732.1	-	-

Appendix C: Measured Properties of Each Fraction

This appendix provides all of the measured properties for distillates, distillation residue, maltenes, saturates, aromatics, and resins. All the measurements were performed at atmospheric pressure. The repeatabilities of the measurements were ±0.0002 kg/m³ for density and ±10% for viscosity.

Table C.1 Distillate densities of the WC-B-A3 feed and products for the Development Dataset.

Temperature °C	**WC-B-A3 kg/m³**	**VIS5.1 kg/m³**	**VIS4.9 kg/m³**	**VIS8.1 kg/m³**	**VIS19.3 kg/m³**	**VIS38.1 kg/m³**
15.0	915.2	909.9	911.8	907.7	903.9	903.3
15.6	914.8	909.5	911.4	907.3	903.4	902.8
20.0	911.8	906.5	908.3	904.2	900.3	899.7
30.0	904.9	899.6	901.4	897.2	893.3	892.8
40.0	898.1	892.7	894.4	890.2	886.3	885.8
50.0	891.2	885.8	887.5	883.2	879.3	878.7

Table C.2 Distillate viscosities of the WC-B-A3 feed.

Temperature °C	**WC-B-A3 mPa·s**
10.0	23.7
15.0	18.2
20.0	14.2

Table C.3 Residue viscosities of the WC-B-A3 feed and products for the Development Dataset.

Temperature °C	WC-B-A3 mPa·s	VIS5.1 mPa·s	VIS4.9 mPa·s	VIS8.1 mPa·s	VIS19.3 mPa·s	VIS38.1 mPa·s
60.0	-	65800	53800	55500	60600	77300
70.0	40800	20400	17400	17500	18600	21790
80.0	14300	7480	6440	6420	6730	7010
90.0	5780	3310	2870	2840	2940	3140
100.0	2740	1590	1390	1370	1395	1430
110.0	1390	-	730	718	-	716
120.0	760	-	430	405	-	388

Table C.4 Maltene densities of the WC-B-A3 feed and products for the Development Dataset.

Temperature °C	WC-B-A3 kg/m³	VIS5.1 kg/m³	VIS4.9 kg/m³	VIS8.1 kg/m³	VIS19.3 kg/m³	VIS38.1 kg/m³
15.6	1004.1	1004.2	1006.5	1007.9	1007.5	1018.4
30.0	-	995.2	997.5	998.9	998.4	1009.1
40.0	989.0	989.0	991.3	992.7	992.1	1002.7
50.0	982.8	982.7	985.0	986.5	985.9	996.3
60.0	976.5	976.5	978.8	980.2	979.6	989.9
70.0	970.3	970.3	972.6	974.0	973.2	983.5
80.0	964.1	964.0	966.3	967.7	967.0	977.2
90.0	958.0	957.8	960.1	961.5	960.8	970.9

Table C.5 Maltene viscosities of the WC-B-A3 feed and products for the Development Dataset.

Temperature °C	WC-B-A3 mPa·s	VIS5.1 mPa·s	VIS4.9 mPa·s	VIS8.1 mPa·s	VIS19.3 mPa·s	VIS38.1 mPa·s
30.0	134000	73500	89900	71900	42900	25500
40.0	32800	19400	23100	18600	11600	6960
50.0	10000	6270	7410	5960	3980	2520
60.0	3700	2440	2780	2320	1610	1020
70.0	1580	1080	1220	1020	734	474
80.0	751	531	590	502	371	244

Table C.6 Saturate densities of the WC-B-A3 feed and products for the Development Dataset.

Temperature, °C	WC-B-A3 kg/m³	VIS5.1 kg/m³	VIS4.9 kg/m³	VIS8.1 kg/m³	VIS19.3 kg/m³	VIS38.1 kg/m³
15.0	903.3	900.0	900.5	899.5	898.2	891.7
15.6	903.0	899.6	900.2	899.1	897.8	891.5
20.0	900.3	896.9	897.5	896.4	895.1	888.7
30.0	894.1	890.7	891.3	890.2	888.9	882.6
40.0	888.1	884.7	885.3	884.2	882.8	876.5
50.0	882.0	878.6	879.2	878.1	876.7	870.5
60.0	-	872.5	873.2	872.0	870.6	864.3

Table C.7 Saturate viscosities of the WC-B-A3 feed and products for the Development Dataset.

Temperature °C	WC-B-A3 mPa·s	VIS5.1 mPa·s	VIS4.9 mPa·s	VIS8.1 mPa·s	VIS19.3 mPa·s	VIS38.1 mPa·s
15.0	1910	1420	1840	1600	1150	570
20.0	1200	903	1150	1020	748	387
30.0	518	404	505	449	345	191
40.0	251	201	247	221	176	106
50.0	135	110	133	122	99	62.9
60.0	79	65.7	78	72.1	61	40.1

Table C.8 Aromatic densities of the WC-B-A3 feed and products for the Development Dataset.

Temperature °C	WC-B-A3 kg/m³	VIS5.1 kg/m³	VIS4.9 kg/m³	VIS8.1 kg/m³	VIS19.3 kg/m³	VIS38.1 kg/m³
15.6	1011.0	1011.1	1013.9	1016.9	1020.4	1031.4
30.0	1001.9	1001.9	1004.8	1007.8	1011.1	1022.0
40.0	995.6	995.6	998.5	1001.4	1004.7	1015.6
50.0	989.4	989.3	992.2	995.1	998.4	1009.1
60.0	983.1	983.1	985.9	988.8	992.1	1002.7
70.0	976.9	976.8	979.7	982.5	985.7	996.3
80.0	970.6	970.6	973.3	976.2	979.4	990.0
90.0	964.2	964.2	967.0	970.0	973.1	983.6

Table C.9 Aromatic viscosities of the WC-B-A3 feed and products for the Development Dataset.

Temperature °C	WC-B-A3 mPa·s	VIS5.1 mPa·s	VIS4.9 mPa·s	VIS8.1 mPa·s	VIS19.3 mPa·s	VIS38.1 mPa·s
30.0	63500	41370	57900	49000	36800	24200
40.0	15600	10700	14500	12300	9690	6280
50.0	4890	3560	4670	3970	3170	2160
60.0	1880	1400	1850	1540	1260	864
70.0	817	631	829	682	566	395
80.0	399	316	417	337	284	202

Table C.10 Resin viscosities of the WC-B-A3 feed and products for the Development Dataset.

Temperature °C	WC-B-A3 mPa·s	VIS5.1 mPa·s	VIS4.9 mPa·s	VIS8.1 mPa·s	VIS19.3 mPa·s	VIS38.1 mPa·s
90.0	67800	63200	62400	36300	35100	49000
100.0	23000	21600	21100	12400	12100	15600
110.0	8760	8190	8030	5030	4840	5760
120.0	3870	3730	3590	2330	2210	2490
130.0	1910	1850	1760	1200	1100	1180

Table C.11 Distillate densities of the WC-B-A4 feedstock and product for the Test Dataset.

Temperature °C	WC-B-A4 kg/m³	VIS1 kg/m³
15.0	911.1	912.4
15.6	911.0	911.9
20.0	908.0	908.9
30.0	901.2	902.1
40.0	894.4	895.3
50.0	887.6	888.5

Table C.12 Residue viscosities of the WC-B-A4 feedstock and product for the Test Dataset.

Temperature °C	WC-B-A4 mPa·s	VIS1 mPa·s
60.0	97600	86800
70.0	30100	26800
80.0	10800	9700
90.0	4550	4170
100.0	2170	2000
110.0	1120	1033
120.0	622	580

Table C.13 Maltene densities of the WC-B-A4 feedstock and product for the Test Dataset.

Temperature °C	WC-B-A4 kg/m^3	VIS1 kg/m^3
15.6	1001.4	1001.9
30.0	992.4	992.9
40.0	986.1	986.6
50.0	980.0	980.4
60.0	973.7	974.1
70.0	967.4	967.9
80.0	961.2	961.7
90.0	955.0	955.5

Table C.14 Maltene viscosities of the WC-B-A4 feedstock and product for the Test Dataset.

Temperature °C	WC-B-A4 mPa·s	VIS1 mPa·s
30.0	146000	114000
40.0	35300	28800
50.0	10600	9000
60.0	3800	3380
70.0	1620	1460
80.0	770	700

Table C.15 Saturate densities of the WC-B-A4 feedstock and product for the Test Dataset.

Temperature °C	WC-B-A4 kg/m³	VIS1 kg/m³
15.0	901.1	901.3
15.6	900.7	900.9
20.0	898.0	898.3
30.0	891.9	892.1
40.0	885.8	886.1
50.0	879.8	880.0
60.0	873.7	873.9

Table C.16 Saturate viscosities of the WC-B-A4 feedstock and product for the Test Dataset.

Temperature °C	WC-B-A4 mPa·s	VIS1 mPa·s
15.0	1330	1355
20.0	851	867
30.0	384	391
40.0	194	197
50.0	107	110
60.0	64.7	65.5

Table C.17 Aromatic densities of the WC-B-A4 feedstock and product for the Test Dataset.

Temperature °C	WC-B-A4 kg/m³	VIS1 kg/m³
15.6	1003.9	1005.5
30.0	994.6	996.3
40.0	988.2	990.0
50.0	981.8	983.6
60.0	975.4	977.3
70.0	969.1	971.0
80.0	962.8	964.7
90.0	956.4	958.4

Table C.18 Aromatic viscosities of the WC-B-A4 feedstock and product for the Test Dataset.

Temperature °C	WC-B-A4 mPa·s	VIS1 mPa·s
30.0	33500	30000
40.0	8910	8150
50.0	3100	2890
60.0	1260	1190
70.0	578	544
80.0	293	280

Table C.19 Resin viscosities of the WC-B-A4 feedstock and product for the Test Dataset.

Temperature °C	WC-B-A4 mPa·s	VIS1 mPa·s
90.0	66000	63500
100.0	22700	21600
110.0	9010	8560
120.0	4070	3880
130.0	2020	1910

Table C.20 Maltene densities of the ME-VR-A1 feedstock and products for the Test Dataset.

Temperature °C	ME-VR-A1 kg/m³	VIS12.5 kg/m³	VIS18.8 kg/m³
15.6	1005.2	988.3	984.1
30.0	996.5	979.1	-
40.0	990.4	972.9	968.5
50.0	984.4	966.2	961.7
60.0	978.3	959.8	955.3
70.0	972.3	953.5	948.8
80.0	966.2	947.1	942.4
90.0	960.2	940.8	936.0

Table C.21 Maltene viscosities of the ME-VR-A1 feedstock and products for the Test Dataset.

Temperature °C	ME-VR-A1 mPa·s	VIS12.5 mPa·s	VIS18.8 mPa·s
30.0	-	4800	1950
40.0	235000	2280	796
50.0	59700	997	376
60.0	18100	489	202
70.0	7090	260	117
80.0	3150	150	73
90.0	1530	-	-

Table C.22 Saturate densities of the ME-VR-A1 feedstock and products for the Test Dataset.

Temperature °C	ME-VR-A1 kg/m³	VIS12.5 kg/m³	VIS18.8 kg/m³
15.0	890.2	867.7	856.0
15.6	889.8	867.3	855.6
20.0	886.9	864.2	852.7
30.0	880.6	857.6	846.3
40.0	874.5	851.1	839.9
50.0	868.2	844.5	833.6
60.0	862.2	837.8	827.2

Table C.23 Saturate viscosities of the ME-VR-A1 feedstock and products for the Test Dataset.

Temperature °C	ME-VR-A1 mPa·s	VIS12.5 mPa·s	VIS18.8 mPa·s
10.0	-	128	-
15.0	2340	92.6	68.0
20.0	1450	70.3	50.5
30.0	657	43.9	32.3
40.0	353	28.1	22.0
50.0	202	19.4	15.7
60.0	124	-	-

Table C.24 Aromatic densities of the ME-VR-A1 feedstock and products for the Test Dataset.

Temperature, °C	ME-VR-A1, kg/m^3	VIS12.5, kg/m^3	VIS18.8, kg/m^3
15.6	1006.0	1007.8	1019.3
30.0	997.3	997.9	1009.5
40.0	991.2	991.3	1003.0
50.0	985.2	984.8	996.4
60.0	979.0	978.4	990.0
70.0	973.0	972.1	983.6
80.0	966.9	965.7	977.1
90.0	960.8	959.3	970.7

Table C.25 Aromatic viscosities of the ME-VR-A1 feedstock and products for the Test Dataset.

Temperature °C	ME-VR-A1 mPa·s	VIS12.5 mPa·s	VIS18.8 mPa·s
30.0	168000	16700	3680
40.0	43500	5120	1390
50.0	13600	1960	613
60.0	5200	862	303
70.0	2300	422	166
80.0	1120	227	96.6

Table C.26 Resin viscosities of the ME-VR-A1 feedstock and products for the Test Dataset.

Temperature °C	ME-VR-A1 mPa·s	VIS12.5 mPa·s	VIS18.8 mPa·s
90.0	133000	22150	30000
100.0	44000	8190	10500
110.0	16500	3600	4170
120.0	7020	1730	1870
130.0	3380	894	930

Appendix D: Density and Viscosity Parameters of Oil Fractions

This appendix provides all fitted density and viscosity parameters for distillates, saturates, aromatics, resins and asphaltenes. The density parameters are the extrapolated reference density at 0°C, ρ_{REF}, and the temperature dependence, b. The EF viscosity parameters are C_2 and $\rho_s°$ and $\Delta a_{Dist\text{-}Asph}$ is the distillate-asphaltene EF binary interaction parameter increment for visbroken products.

Table D.1 Distillate parameters of the WC-B-A3 feed and products for the Development Dataset.

Parameter	WC-B-A3	VIS5.1	VIS4.9	VIS8.1	VIS19.3	VIS38.1
ρ_{REF}, kg/m³	925.5	920.3	922.2	918.2	914.37	914.0
b, kg/m³°C	-0.6850	-0.6890	-0.6947	-0.7004	-0.7018	-0.7165
C_2	0.2326	0.2318	0.2342	0.2289	0.2277	0.2265
$\rho_s°$, kg/m³	983.97	980.18	981.56	981.51	980.77	982.95

Table D.2 Saturate parameters of the WC-B-A3 feed and products for the Development Dataset.

Parameter	WC-B-A3	VIS5.1	VIS4.9	VIS8.1	VIS19.3	VIS38.1
ρ_{REF}, kg/m³	912.5	909.1	909.6	908.6	907.4	900.9
b, kg/m³°C	-0.6097	-0.6105	-0.6081	-0.6105	-0.6132	-0.6097
C_2	0.4054	0.3977	0.4076	0.4061	0.4037	0.3835
$\rho_s°$, kg/m³	962.81	959.98	960.40	959.94	960.4	955.53

Table D.3 Aromatic parameters of the WC-B-A3 feed and products for Development Dataset.

Parameter	WC-B-A3	VIS5.1	VIS4.9	VIS8.1	VIS19.3	VIS38.1
ρ_{REF}, kg/m³	1020.7	1020.8	1023.7	1026.7	1030.2	1041.3
b, kg/m³°C	-0.6276	-0.6291	-0.6298	-0.6310	-0.63511	-0.6422
C_2	0.4490	0.4408	0.4393	0.4407	0.43053	0.4040
ρ_s°, kg/m³	1055.19	1056.00	1055.83	1061.47	1064.91	1074.9

Table D.4 Resin parameters of the WC-B-A3 feed and products for Development Dataset.

Parameter	WC-B-A3	VIS5.1	VIS4.9	VIS8.1	VIS19.3	VIS38.1
ρ_{REF}, kg/m³	1065.7	1071.9	1066.4	1068.9	1074.8	1100.4
b, kg/m³°C	-0.6134	-0.6207	-0.6199	-0.6170	-0.6231	-0.6505
C_2	0.6020	0.6090	0.6002	0.5690	0.5635	0.5515
ρ_s°, kg/m³	1082.16	1088.95	1082.51	1084.73	1090.00	1111.34

Table D.5 Asphaltene parameters of the WC-B-A3 feed and products for the Development Dataset.

Parameter	WC-B-A3	VIS5.1	VIS4.9	VIS8.1	VIS19.3	VIS38.1
ρ_{REF}, kg/m³	1181.0	1183.4	1181.8	1189.2	1192.9	1209.3
b, kg/m³°C	-0.6202	-0.6709	-0.7058	-0.64487	-0.6674	-0.6873
C_2	0.9879	0.9788	0.8983	0.82563	0.8695	0.7685
ρ_s°, kg/m³	1164.40	1166.32	1167.95	1167.59	1165.31	1177.05
$\Delta a_{Dist\text{-}Asph}$	-	0.0787	0.0865	0.05985	0.0883	0.0693

Table D.6 Distillate parameters of the WC-B-A4 feed and products for the Test Dataset.

Parameter	WC-B-A4	VIS1
ρ_{REF}, kg/m³	921.6	922.6
b, kg/m³°C	-0.6801	-0.6814
C_2	0.3181	0.2348
ρ_s°, kg/m³	1000.77	976.93

Table D.7 Saturate parameters of the WC-B-A4 feed and products for the Test Dataset.

Parameter	WC-B-A4	VIS1
ρ_{REF}, kg/m³	910.2	910.4
b, kg/m³°C	-0.6083	-0.6086
C_2	0.3950	0.3965
ρ_s°, kg/m³	961.18	961.52

Table D.8 Aromatic parameters of the WC-B-A4 feed and products for the Test Dataset.

Parameter	WC-B-A4	VIS1
ρ_{REF}, kg/m³	1013.8	1015.3
b, kg/m³°C	-0.6338	-0.6331
C_2	0.4547	0.4502
ρ_s°, kg/m³	1051.03	1052.78

Table D.9 Resin parameters of the WC-B-A4 feed and products for the Test Dataset.

Parameter	WC-B-A4	VIS1
ρ_{REF}, kg/m³	1052.5	1052.4
b, kg/m³°C	-0.6027	-0.6139
C_2	0.6185	0.6115
ρ_s°, kg/m³	1071.09	1069.17

Table D.10 Asphaltene parameters of the WC-B-A4 feed and products for the Test Dataset.

Parameter	WC-B-A4	VIS1
ρ_{REF}, kg/m³	1181.8	1182.7
b, kg/m³°C	-0.5978	-0.6500
C_2	0.8986	0.9485
ρ_s°, kg/m³	1141.62	1152.85
$\Delta a_{Dist\text{-}Asph}$	-	0.0467

Table D.11 Saturate parameters of the ME-VR-A1 feed and products for the Test Dataset.

Parameter	ME-VR-A1	VIS12.5	VIS18.8
ρ_{REF}, kg/m³	899.4	877.6	865.5
b, kg/m³°C	-0.6228	-0.6624	-0.6394
C_2	0.5129	0.3920	0.3841
ρ_s°, kg/m³	963.04	949.10	939.40

Table D.12 Aromatic parameters of the ME-VR-A1 feed and products for the Test Dataset.

Parameter	ME-VR-A1	VIS12.5	VIS18.8
ρ_{REF}, kg/m³	1015.5	1017.6	1029.3
b, kg/m³°C	-0.6079	-0.6503	-0.6527
C_2	0.5471	0.4610	0.4248
ρ_s°, kg/m³	1057.40	1065.83	1075.08

Table D.13 Resin parameters of the ME-VR-A1 feed and products for the Test Dataset.

Parameter	ME-VR-A1	VIS12.5	VIS18.8
ρ_{REF}, kg/m³	1053.8	1057.8	1062.3
b, kg/m³°C	-0.5953	-0.6007	-0.6468
C_2	0.6429	0.5686	0.5776
ρ_s°, kg/m³	1072.17	1077.41	1076.92

Table D.14 Asphaltene parameters of the ME-VR-A1 feed and products for the Test Dataset.

Parameter	ME-VR-A1	VIS12.5	VIS18.8
ρ_{REF}, kg/m³	1186.9	-	-
b, kg/m³°C	-0.5937	-	-
C_2	0.9690	-	-
ρ_s°, kg/m³	1183.55	-	-